Two-Parameter Kinematic Approach for the Shear Behavior of Deep Beams Made of Fiber-Reinforced Concrete

Author: Karolína Tvrzníková

Supervisor: Prof. Boyan Mihaylov

University: University of Liège

European Commission
ERASMUS MUNDUS

University: University of Liège

Date: 9.1.2017

ABSTRACT

Deep concrete beams are characterized by small shear-span-to-depth ratios and high shear resistance. Owing to their high strength, they are used as transfer girders in buildings, cap beams in bridges, and pile caps in foundations. It is also characteristic of deep beams that they develop complex deformation patterns and cannot be modelled based on the plane-sections-remain-plane hypothesis. This thesis focuses on modelling the complex shear behavior of fiber-reinforced concrete (FRC) deep beams. While deep beams are typically reinforced only with steel bars in the form of flexural and shear reinforcement, experimental studies have shown that the addition of steel fibers in the concrete can enhance their shear behavior.

The main aim of this thesis is to study a five-spring model for deep beams with conventional reinforcement proposed by Mihaylov et al. (2015), and to extend this model to deep beams with FRC. The five-spring model uses only two kinematic parameters to describe the deformations in deep beams. The extended model captures the complete load-displacement response of FRC beams by accounting for three effects associated with the steel fibers: 1) tension in the fibers crossing the shear cracks; 2) enhanced ductility of the critical compressed zones in deep beams; and 3) tension stiffening effect on the flexural reinforcement. To account for these three local effects, existing models from the literature are studied, compared, and validated. Each of the models is implemented in a Matlab code and is validated with relevant material tests. It is shown that the most suitable models for the modelling of the three effects were proposed by Lee et al. (2013), Ou et al. (2012) and Lee et al. (2013). Once these models were validated, they were implemented in the global framework provided by the five-spring model for deep beams.

The extended five-spring model is validated against a database of tests of FRC deep beams collected from the literature. It is shown that the predicted shear strengths are in good agreement with the measured values. The validated model is then used to perform a parametric study focused on the effects of the shear-span-to-depth (*a/d*) ratio, shear and longitudinal reinforcement ratios, as well as fiber volumetric ratio on the shear behavior of deep beams. Increased shear resistance was observed for increasing the shear and longitudinal reinforcements, as well as increasing the fiber volumetric ratio. By increasing *a/d* ratio, the shear strength decreased. At last, the effectiveness of shear reinforcement was compared with the fiber reinforcement for different *a/d* ratios. It is concluded that the fiber reinforcement is more effective only for *a/d* ratios lower than 0.8, while the shear reinforcement is more effective for higher *a/d* ratios.

ACKNOWLEDGEMENTS

Firstly, I would like to thank all the members of the jury and everyone who will take time to read this thesis.

Most of all, I would like to thank Professor Boyan Mihaylov, for his great guidance and help provided throughout the development of this thesis. All the time he devoted to our consultations, his patience and knowledge he shared with me throughout the semester are the main reasons behind the completion of this thesis. Thank you for pushing me to work harder and question myself. Working with him was a truly rewarding experience.

Special thanks to my office colleagues Jian Liu, Nikola Tatar and Renaud Franssen. They would always answer my questions and provide help anytime I asked. It was a pleasure to work in such a friendly environment.

I would also like to thank the whole SUSCOS team. All the coordinators and professors from all the partner universities and in particular Professor František Wald, for all the effort and dedication which makes SUSCOS such a unique learning experience. Special thanks also to my classmates that have made this past year and half really great.

At last, I am thankful to my family, Abram and friends for their support no matter the distance that separated us.

TABLE OF CONTENTS

Abstract 1
Acknowledgements 2
Table of Contents 3
List of Figures 5
List of Tables 8
List of Annotations 9
1 Introduction 14
1.1 General 14
1.2 Scope and Objectives of the Thesis 15
1.3 Thesis Outline 16
2 Background 17
2.1 Fiber-Reinforced Concrete (FRC) 17
2.1.1 Properties and Classification of FRC 17
2.1.2 Factors Affecting Behavior of FRC 19
2.2 Tests on FRC Deep Beams 20
2.2.1 Mansur and Ong (1991) 20
2.2.2 Mansur and Alwist (1984) 22
2.3 Two-Parameter Kinematic Theory and Five-Spring Model for Deep Beams 24
3 Extended Five-Spring Model for FRC Deep Beams 33
3.1 Introduction 33
3.2 Tension in Fibers across the Critical Diagonal crack 33
3.2.1 Introduction 33
3.2.2 Formulation of the SDEM 35
3.2.3 Validation of the SDEM 38
3.2.4 Implementation of the SDEM into the Five-Spring Model 41
3.3 Tension-Stiffening of the Bottom Flexural Reinforcement 45
3.3.1 Introduction 45
3.3.2 Formulation of Tension-Stiffening Model for R/FRC 46
3.3.3 Validation of the Tension-Stiffening Model for R/FRC 48
3.3.4 Implementation of the Tension-Stiffening Model into the Five-Spring Model . 51
3.4 Compressive Behavior of the Critical Loading Zone 53

3.4.1 Introduction 53
3.4.2 Stress-Strain Curves for FRC 54
3.4.3 Implementation of the Stress-Strain Curve into the Five-Spring Model 61
3.5 Deflections 64
3.5.1 Introduction 64
3.5.2 Definition of the Additional Deflection 64
3.5.3 Implementation of the Additional Deflection into the Five-Spring Model 65
4 Validation of the Extended Five-Spring Model 66
4.1 Introduction 66
4.2 Sample Specimen Evaluation 66
4.3 Effect of Fiber Volumetric Ratio 70
4.4 Effect of *a/d* Ratio 70
4.5 Discussion 72
5 Parametric Study 75
5.1 Introduction 75
5.2 Parametric Study 75
5.2.1 *a/d* Ratio 75
5.2.2 Longitudinal Reinforcement 77
5.2.3 Fiber Volumetric Ratio 79
5.2.4 Shear Reinforcement 80
5.2.5 Comparison of Effectiveness of Fibers vs. Shear Reinforcement 83
5.2.6 Size Effect 85
5.3 Discussion 87
6 Summary and Conclusions 89
References 91
Appendix A: Test Database 94
Appendix B: SDEM - Matlab Code 95
Appendix C: Tension-Stiffening - Matlab Code 96
Appendix D: Average Diagonal Stress in the Critical Loading Zone - Matlab Code 97
Appendix E: Extended Five-Spring Model - Matlab Code 98

LIST OF FIGURES

Figure 1.1 Application of deep beam in a building (Mihaylov et al.,2013) 14

Figure 2.1 Softening (a) and hardening (b) post-cracking behavior of SFRC - adapted from fib MC2010 (2013) 18

Figure 2.2 Typical load-CMOD curve from fib MC2010 (2013) 18

Figure 2.3 Experimental setup by Mansur and Ong (1991) 21

Figure 2.4 Experimental results by Mansur and Ong (1991) 21

Figure 2.5 Cracking pattern of the beam B4 by Mansur and Ong (1991) 22

Figure 2.6 Experimental setup by Mansur and Alwist (1984) 23

Figure 2.7 Failure mode of control specimen by Mansur and Alwist (1984) 23

Figure 2.8 Main assumptions of kinematic model (Mihaylov et al.,2013) 24

Figure 2.9 Degrees of freedom of kinematic model (Mihaylov et al.,2013) 25

Figure 2.10 Variation of the angle α_1 during transition from deep to slender beams (Mihaylov et al.,2013) 25

Figure 2.11 Five-spring model (Mihaylov, 2015) 27

Figure 2.12 Free-body diagram of the rigid block (Mihaylov, 2015) 27

Figure 2.13 Critical loading zone (Mihaylov, 2015) 28

Figure 2.14 Shear forces in five-spring model at 5 mm imposed distortion of the CLZ 31

Figure 2.15 Equilibrium of forces in five-spring model for imposed displacement Δ 32

Figure 3.1 Tensile behavior of FRC (Lee et al., 2013) 34

Figure 3.2 Illustration of additional force provided by fibers in the extended five-spring model 35

Figure 3.3 Fiber types used in the study by Lim et al. (1987) 35

Figure 3.4 Comparison of proposed model and test results for members with straight fibers tested by Lim et al. (1987) 39

Figure 3.5 Comparison of proposed model and test results for members with end-hooked fibers tested by Lim et al. (1987) 39

Figure 3.6 Comparison of proposed model and test results for members with end-hooked fibers tested by Susetyo (2009) 40

Figure 3.7 Definition of angle β 41

Figure 3.8 Variation of the angle β given different a/d ratios 42

Figure 3.9 Variation of the angle β given different fiber volume ratios 42

Figure 3.10 Equilibrium of forces in extended five-spring model with fiber contribution at Δ_c=5 mm 43

Figure 3.11 Predicted V-Δ response with addition of fibers 44

Figure 3.12 Tensile behavior of RC and R/FRC members by Lee et al. (2013) 45

Figure 3.13 Illustration of implemented modification due to tension-stiffening effect 46

Figure 3.14 Comparison of proposed models and test results by Bischoff (2003) 49

Figure 3.15 Comparison of proposed models and test results by Deluce and Vecchio (2013) 50

Figure 3.16 Separate evaluation of contribution of tensile forces in Tension-stiffening model 51

Figure 3.17 Equilibrium of forces in extended five-spring model with tension-stiffening model at Δ_c=5 mm..... 52

Figure 3.18 Predicted V-Δ response with implementation of tension-stiffening model..... 52

Figure 3.19 Illustration of modification due to change of stress-strain curve of concrete in compression 53

Figure 3.20 Analytical proposal of stress-strain compression curve by Barros and Figueiras (1999) 56

Figure 3.21 Analytical proposal of stress-strain compression curve by Lee et al. (2015) 57

Figure 3.22 Analytical proposal of stress-strain compression curve by Ou et al. (2012) 59

Figure 3.23 Analytical proposal of stress-strain compression for high-strength concrete by Mansur et al. (1999) 60

Figure 3.24 Equilibrium of forces in extended 5sm with adjusted stress-strain curve at Δ_c=5 mm 62

Figure 3.25 Predicted V-Δ response with modified stress-strain curve 63

Figure 4.1 Cracking pattern and mode of failure of beam B4 by Mansur and Ong (1991) 67

Figure 4.2 Comparison of load-deflection curves for beam B4 obtained from five-spring method and experimental results by Mansur and Ong (1991) 68

Figure 4.3 Comparison of load-deflection curves for beam B4 obtained from finite element model, five-spring method and experimental results by Mansur and Ong (1991) 69

Figure 4.4 Cracking pattern of the beam B4 obtained by the FE analysis 69

Figure 4.5 Effect of fiber volume ratio on ultimate shear strength 70

Figure 4.6 Effect a/d ratio on ultimate shear strength 71

Figure 4.7 Comparison of results obtained by FEM and five-spring model for different fiber volumetric ratios 73

Figure 5.1 Effect of a/d ratio for different fiber volume ratios 76

Figure 5.2 Breakdown of effect of a/d ratio for V_f = 1% 76

Figure 5.3 Effect of longitudinal reinforcement for different fiber volume ratios 77

Figure 5.4 Breakdown of effect of longitudinal reinforcement for V_f = 1% 78

Figure 5.5 Effect of fiber volumetric ratio for different shear reinforcement ratios 79

Figure 5.6 Breakdown of effect of fiber volumetric ratio for ρ_v = 0.5% 80

Figure 5.7 Effect of shear reinforcement for different fiber volume ratios 81

Figure 5.8 Breakdown of effect of shear reinforcement for V_f = 1% 81

Figure 5.9 Results for B10 obtained with the extended five-spring model 82

Figure 5.10 Average tensile strain at deflection equal to zero for different shear reinforcement ratios 83

Figure 5.11 Results for B10 obtained with the extended five-spring model with completed curve 83

Figure 5.12 Variation of V_{max} for different a/d ratios with ρ_v = 0.2% 84

Figure 5.13 Fiber volume ratio equivalent to 0.2% shear reinforcement ratio 84

Figure 5.14 Size effect for different fiber volume ratios 85

Figure 5.15 Size effect breakdown for 0% fiber volume ratio 86

Figure 5.16 Size effect breakdown for 2% fiber volume ratio 87

LIST OF TABLES

Table 2.1 Sample beam properties 30

Table 3.1 Pullout strength of single fiber by Voo and Foster (2003)..... 37

Table 4.1 Standard deviation and coefficient of variation of results obtained with extended five-spring model 74

Table 5.1 Properties of a sample beam for parametric study 75

LIST OF ANNOTATIONS

$\varnothing_h$	= Diameter of web reinforcement
$\varnothing_l$	= Diameter of bottom longitudinal reinforcement bars
$\varnothing_v$	= Diameter of stirrups
2PKT	= Two-parameter kinematic theory
5sm	= Five-spring model
a	= Shear span
a/d	= Shear-span-to-depth ratio
a_{c1}	= Distance between facing edges of loading and support plate
a_{eff}	= Effective shear span
a_g	= Maximum size of coarse aggregate
A_s	= Area of longitudinal bars on flexural tension side
$A_{c,eff}$	= Area of concrete providing tension stiffening for bottom reinforcement
b	= Width of cross section
c	= Coefficient for tension-softening effect of concrete or mortar
C	= Compression force in section with maximum moment
c_f	= Coefficient to consider effect of steel fibers on tension-stiffening
CLZ	= Critical loading zone
CMOD	= Crack mouth opening displacement
CTOD	= Crack top opening displacement
d	= Effective depth of section
d_b	= Diameter of bottom longitudinal bars
d_{bv}	= Stirrups bar diameter
d_f	= Fiber diameter
DOF	= Degree of freedom
E_c	= Elastic modulus of concrete
E_s	= Elastic modulus of steel
E_v	= Elastic modulus of stirrups
f'_c	= Concrete cylinder strength

f_c	= Local stress of concrete
$f_{c,\,TS}$	= Tensile stress due to tension-stiffening
$f_{c.soft}$	= Tensile stress in concrete due to tension-softening
f_{con}	= Tensile stress in concrete
F_{con}	= Tensile force of concrete
f_{cr}	= Cracking strength of concrete of mortar matrix
f_{ct}	= Tensile stress by concrete/mortar tension-softening at given crack width
f_{eh}	= Tensile stress due to mechanical anchorage effect of end-hooked steel fibers
FEM	= Finite Element Model
F_f	= Force provided by fibers
f_f	= Tensile stress at crack due to steel fibers
f_{fib}	= Tensile stress in fibers
F_{fib}	= Tensile force of fibers
f_{R1k}	= Stress at serviceability limit state
f_{R3k}	= Stress at ultimate limit state
FRC	= Fiber-reinforced concrete
F_{reb}	= Tensile force of reinforcing bar
f_{reb}	= Tensile stress in reinforcing bar
f_{SFRC}	= Total tensile stresses of SFRC member
f_{st}	= Tensile stress due to frictional bond behavior of steel fibers
f_y	= Yield strength of bottom longitudinal bars
f_{yv}	= Yield strength of stirrups
h	= Height of member
I_{cr}	= Moment of inertia of cracked section
I_g	= Moment of inertia of un-cracked section
k	= Factor influencing post-peak decay in stress
l_0	= Length of heavily cracked zone at bottom of critical diagonal crack
l_{b1}	= Width of loading plate parallel to longitudinal axis of member
l_{b1e}	= Effective width of loading plate parallel to longitudinal axis of member

l_{b2}	= Width of support plate parallel to longitudinal axis of member
l_f	= Fiber length
l_i	= Distance between mechanical anchorages for end-hooked fibers
l_k	= Length of dowels provided by bottom longitudinal reinforcement
l_s	= Distance between loading points
l_t	= Length of bottom reinforcement within the cracked part of shear span
M	= Bond parameter
n	= Curve fitting factor
n_b	= Number of bottom longitudinal bars
P	= Applied concentrated load
P_{cr}	= Applied load at moment of formation of crack
RI_v	= Fiber reinforcing index based on fiber volumetric ratio
RI_w	= Fiber reinforcing index based on fiber weight ratio
s	= Slip and displacement in critical diagonal crack
s_b	= Maximum spacing between reinforcing bars
s_{cr}	= Distance between the radial cracks along bottom longitudinal reinforcement
$SDEM$	= Simplified diverse embedment method
s_{eh}	= Slip at maximum tensile force due to mechanical anchorage of an end-hooked fiber
s_f	= Slip at frictional bond strength for straight fiber
$SFRC$	= Steel fiber reinforced concrete
T	= Tensile force in bottom reinforcement
T_f	= Tensile force in bottom reinforcement including action of fibers
V	= Shear force
V_{ci}	= Shear resisted by aggregate interlock
V_{CLZ}	= Shear carried by critical loading zone
V_d	= Shear resisted by dowel action
V_{exp}	= Measured shear strength
V_F	= Shear resisted by fibers
V_f	= Fiber volumetric ratio

v_f	= Vertical component of stress resisted by fibers
V_{pred}	= Predicted shear strength
V_s	= Shear resisted by stirrups
w	= Width of critical diagonal crack halfway along the crack
w_{cr}	= Average crack width
$w_{cr.T}$	= Width of the crack applied in SDEM to define tensile stress in fibers
W_f	= Fiber weight percentage in the mixture
α	= Angle of the line extending from inner edge of support plate to far edge of tributary area of loading plate responsible for shear force V
α_1	= Angle of critical diagonal crack
α_f	= Fiber orientation factor
β	= Angle between the force provided by the fibers F_f and the vertical component of the force V_F
β_{eh}	= Coefficient to consider effect of fiber slip on longer embedment side on frictional behavior
β_f	= Coefficient to consider effect of fiber slip on longer embedment side on mechanical anchorage effect
Δ	= Midspan deflection of beam
Δ_1	= Additional deflection to account for four-point loading
Δ_c	= Transverse displacement of critical loading zone
Δ_t	= Deflection of shear span due to elongation of bottom longitudinal reinforcement
δ_x	= Displacement along x axis
δ_y	= Displacement along z axis
ε	= Diagonal compressive strains in critical loading zone
ε'_c	= Strain at peak strength
ε_{c0}	= Strain at peak for plain concrete
ε_{cf}	= Strain at peak for FRC
ε_{max}	= Maximum diagonal compressive strain in critical loading zone
$\varepsilon_{t,\,avg}$	= Average strain in the bottom longitudinal reinforcement
ε_v	= Strain in transverse reinforcement in critical diagonal crack halfway along the crack
θ	= Angle of diagonal cracks in uniform stress field

ρ_h = Ratio of longitudinal web reinforcement

ρ_l = Ratio of bottom longitudinal reinforcement

ρ_v = Ratio of transverse reinforcement

σ = Diagonal compressive stress in critical loading zone

σ_{avg} = Average diagonal stress in critical loading zone

σ_v = Stress in transverse reinforcement

$\tau_{eh,\,max}$ = Pullout strength due to mechanical anchorage of hooked-end fiber

$\tau_{f,\,max}$ = Frictional bond strength

υ_{ci} = Aggregate interlock shear stress

Ω = Area under stress-strain curve

1 INTRODUCTION

1.1 GENERAL

Deep beams are characterized by relatively small shear-span-to-depth (*a/d*) ratios. Maximum value of ratio for deep beams is around 2.5. Because of their proportions, they develop mechanisms of load resistance that are quite different from those in slender beams, and their strengths are likely to be governed by shear rather than flexure (Mansur and Ong, 1991). Thanks to their high shear strengths deep beams are used for example as transfer girders in buildings, where they carry heavy loads from discontinuous columns, as shown in Figure 1.1. Structural safety of a building with deep beam highly depends on the resistance of the girder as its failure could result in a partial or complete collapse of the building. When subjected to vertical ground accelerations due to strong earthquakes, the ability of structure to redistribute forces from damaged girders to other structural members is crucial. The extent of such force redistribution depends on displacement capacity and post-peak behavior of the transfer beam (Mihaylov, 2015).

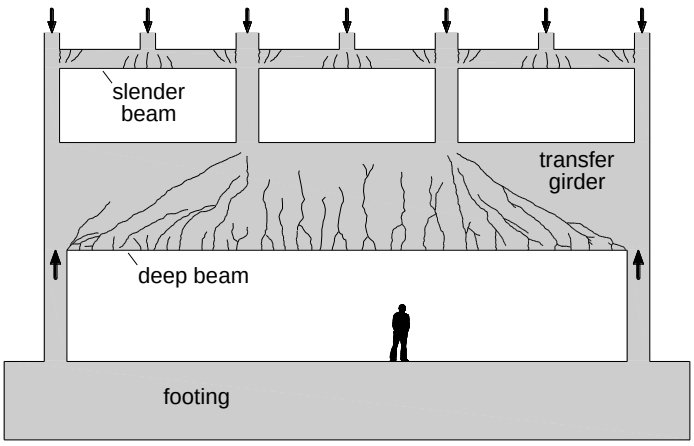

Figure 1.1 Application of deep beam in a building (Mihaylov et al.,2013)

The load-deformation response of slender beams can be modelled based on the hypothesis that "plane sections remain plane" first proposed by Robert Hook in 1678. However, for deep beams such as transfer girders, plane sections do not remain plane and shear strains become dominant. The deformation patterns of such beams become more complex and a different modelling approach is required.

In deep beams, a significant portion of the shear is carried by strut action, where compressive stresses flow directly from the load to the support (Mihaylov et al.,2013). Due to this, strut-and-tie models are recommended when designing deep beams. However, strut-and-tie method is not always capable of predicting the shear behavior of deep beams due to the large number of parameters that influence the shear behavior. A model that takes into account the number of parameters that influence the shear behavior has been proposed by Mihaylov et al. (2013). The model uses equations with two degrees of freedom and predicts the shear behavior of deep beams through equilibrium, compatibility and stress-strain relationships.

A two-parameter kinematic theory (2PKT) for deep beams has been introduced by Mihaylov et al. (2013) and is capable of describing the deformed shape of deep beams and the ultimate shear strength of such members. Later the model has been extended to non-linear five-spring model, which is able to predict the complete load-displacement response of shear-critical deep beams. Four springs of the model represent the shear resistance mechanisms of the beam, and the fifth spring represents the flexural behavior. The five-spring model has shown to predict the post-peak shear behavior effectively, which is important for the analysis of structures under extreme loading.

To enhance the post-peak capacity and displacement capacity, the addition of fibers to concrete matrix has shown to significantly improve brittle behavior of concrete. The post-peak behavior of fiber reinforced beams improves compared to regular concrete and provides higher ductility of the members. Some of the observed enhancements include higher tensile strength of concrete, increased post-cracking ductility, higher toughness and reduced crack width and crack spacing. Fibers are produced from materials such as steel, carbon, glass, plastic or cotton. For the reinforcement of deep beams used within this study, steel fibers were considered. Steel fibers can be found in various profiles including straight, hooked-end, crimped and flattened-end. The effectiveness of steel fibers in improving the behavior depends on several factors like fiber volume ratio, fiber length and fiber aspect ratio.

1.2 Scope and Objectives of the Thesis

This thesis is a continuation of work developed by Mihaylov et al. (2013). His two-parameter kinematic theory for shear behavior of deep beams is capable of describing the shear strength and deformation patterns for deep beams in shear failure. The kinematic theory as proposed by Mihaylov et al. (2013) is applicable to reinforced concrete deep beams with possible transverse reinforcement. Later, an extension of 2PKT allowed a complete prediction of pre- and post-peak shear behavior of deep beams. Both of the methods showed to predict the results effectively when compared to experimental results.

As it has been previously researched by Narayan and Darwish (1989) and Mansur and Ong (1991), inclusion of fibers in concrete can increase the ductility and displacement capacity of deep beams. The effect of fibers was, however, not considered in the five-spring model developed by Mihaylov (2015). The main objective of this thesis is to extend the five-spring model, to be able to capture the behavior of reinforced concrete deep beams with inclusion of steel fibers.

First, the original five-spring model is analyzed. After a thorough analysis, changes caused by the fibers, such as additional tensile forces from fibers bridging the cracks, are evaluated. Appropriate models are proposed based on previous research and validated against experimental data. Such models are then implemented into the original five-spring model to create an extended five-spring model that captures the behavior of fiber reinforced concrete deep beams. Proposed extended five-spring model is then validated against experimental studies done by other researchers, and the accuracy of the model is evaluated. Additionally, a

parametric study is performed to study the effects of vertical and longitudinal reinforcement, fiber volume ratio, size effect and *a/d* ratio on the shear strength of the beam.

1.3 THESIS OUTLINE

This thesis consists of six chapters, including Chapter 1 with some general information and scope of the thesis.

Chapter 2 provides background information about topics relevant for the thesis. It includes a brief overview of state-of-arts of design with fibers, including an overview of code provisions. Selected experimental studies from other researchers are described, including the properties of the specimen, experimental setup and obtained results with observations. It also consists of description of two-parameter kinematic theory and five-spring model by Mihaylov (2015). The theory behind the model is briefly explained, and the original model that served as a starting point for the thesis is introduced.

Chapter 3 describes all the modifications introduced into the original model in order to capture the behavior with inclusion of steel fibers. First, simplified diverse embedment model to model the tension resisted by the fibers bridging the crack is introduced. Then, the created Matlab code is validated against experimental and analytical results, and the version of the code as it enters the five-spring model is explained. Secondly, tension-stiffening model is introduced. A Matlab code is then created and a code to model the tension force provided by bottom longitudinal reinforcement of the beam is validated against experimental and analytical results. The obtained Matlab code is then explained as it enters the five-spring model. Later, the stress-strain behavior of fiber-reinforced concrete under uniaxial compression is evaluated. Proposals by several researchers are introduced and the most suitable ones are selected to enter into the extended five-spring model. At last, additional formula to account for additional deflections in the mid-span of deep beams under four-point loading is introduced.

Chapter 4 presents a validation of the proposed extended five-spring model. A sample specimen is described and experimental results are compared with results obtained using extended five-spring model and finite element model results. The effect of fiber volume ratio is analyzed and a comparison between experimental results, analytical results and numerical results is provided. Also the effect of *a/d* ratio is evaluated and experimental results are compared with analytical ones. At last, results of other load-deflection curves based on other experimental results are provided. Discussion is carried out to summarize the effectiveness of the model, and an issue encountered during the validation process for deep beams with high shear reinforcement is addressed and explained.

Chapter 5 consists of a parametric study. The effect of *a/d* ratio is analyzed, as well as the effect of bottom longitudinal reinforcement. Fiber volume ratio and its influence on shear strength is analyzed along with the effect of shear reinforcement and size effect. Finally, the amount of fibers or shear reinforcement that is needed to obtain a given shear strength is calculated and the effectiveness of each type of reinforcement is analyzed.

Chapter 6 contains a summary with conclusions and limitations of the proposed model.

2 BACKGROUND

2.1 FIBER-REINFORCED CONCRETE (FRC)

Fiber-reinforced concrete is a composite material consisting of cement matrix and discrete fibers. The material of the fibers can vary from steel, polymers and carbon to glass or natural materials. The main difference between regular concrete and FRC is an enhanced post-cracking residual tensile resistance due to fibers capacity to bridge the cracks. Research regarding FRC has started in the USA almost 50 years ago, however the research focused on structural response of FRC has mainly developed only over last 15 years as described by Di Prisco et al. (2013). As a consequence, international building codes for structural design are lacking guidelines for design with FRC and due to the lack of guidelines practitioners are generally unwilling to use FRC just based on voluntary guidelines or research papers.

2.1.1 Properties and Classification of FRC

In the *fib* Model Code 2010, FRC is recognized as a new material for structures (Di Prisco et al., 2013). The code is divided in two sections, one devoted to material behavior and the other to structural behavior. It mainly addresses steel fibers, however can be considered for other types of fibers with limitations. The code also introduces classification of FRC to standardize performance-based production.

Unless high volume of fibers is used, the addition of fibers does not significantly affect elastic properties of concrete or compressive strength. However, for fiber volumes higher than 1% the ascending branch of compressive stress-strain curve changes depending on the amount of fibers and with increasing fiber volume ratio becomes less steep. Such results suggest higher ductility and toughness of FRC and have been previously investigated. However, *fib* Model Code 2010 does not describe the compressive behavior of FRC unless experimental results are available, and so the most recent research and analytical approach to describe the stress-strain relationship is discussed later in this thesis.

Behavior in tension is the most important aspect of FRC. The fibers are able to bridge the crack and transmit stresses across the crack. With increasing fiber content, the post-peak behavior is characterized by increased toughness, becoming ductile for very high fiber contents as described by Di Prisco et al. (2013). Depending on the orientation of the member and fibers, steel fiber reinforced concrete (SFRC) members in uniaxial tension can have softening or hardening post-cracking behavior as shown in Figure 2.1. Susetyo (2009) explains that tension hardening effects occur in concrete containing higher fiber volume content than the critical fiber volume content. The critical fiber volume is the volume of fibers which after matrix cracking will carry the load which the composite maintained before cracking (Newman and Choo, 2013). If there are very few fibers present, the stress on the composite may be high enough to break the fibers thus causing the tensile-softening effect as described by Shah et al. (2012). When the volume of fibers is lower than the minimum fiber volume fraction the fibers weaken the material rather than strengthen it, and the failure is controlled by the matrix. The reinforcing action of

fibers and tensile-hardening is only observed once the fiber volume fraction exceeds the critical fiber volume fraction (Shah et al, 2012).

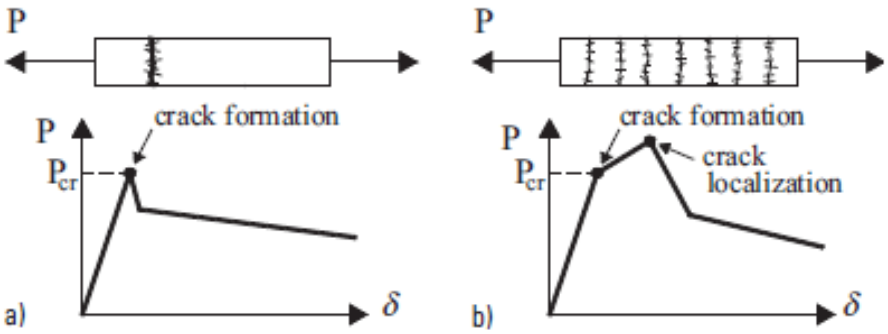

Figure 2.1 Softening (a) and hardening (b) post-cracking behavior of SFRC - adapted from *fib* MC2010 (2013)

To determine tension behavior of FRC, uniaxial tests are not advised for standard testing due to difficulty to carry out the tests. Instead, the relationship between tensile stress and crack width is typically derived by inverse analysis from the results from two- or three- point bending tests. Typical results from a bending test are presented in Figure 2.2 (fib Model Code 2010). On the vertical axis of the plot is the applied load, and on the horizontal axis is the crack mouth opening displacement (CMOD) measured at a notch cut in the test specimen (beam). CMOD is defined as the opening of the notch at the bottom face of the beam for three-point bending tests. For four-point loading tests the measured parameter is the crack top opening displacement (CTOD).

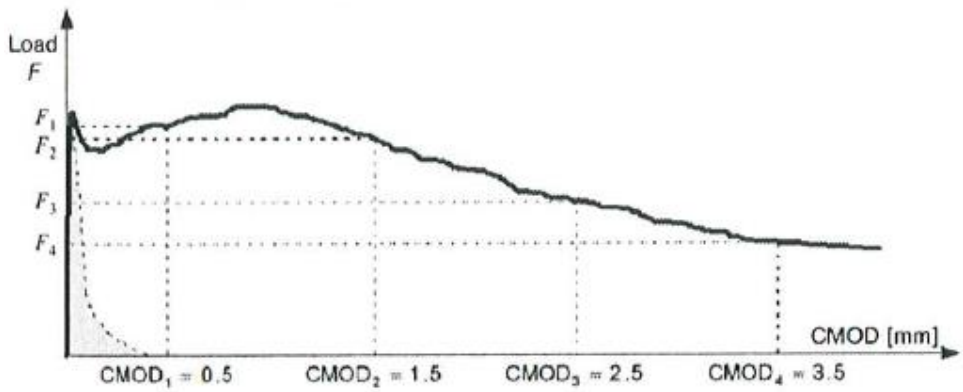

Figure 2.2 Typical load-CMOD curve from *fib* MC2010 (2013)

According to fib Model Code 2010, fiber-reinforced concrete can be classified to five different classes based on the results from two- or three- point bending tests. Two important stresses from the measured post-cracking behavior are used: the first corresponding to CMOD of 0.5 mm (f_{R1k}) and the second to CMOD of 2.5 mm (f_{R3k}). Stress f_{R1k} is significant for serviceability limit states while f_{R3k} for ultimate limit state design. The classification has two parameters where one corresponds to f_{R1k} and represents a strength interval between consecutive

strength values (1, 1.5, 2, 2.5, 3, 4, 5, 6, …MPa), and a letter *a, b, c, d* or *e*, where each letter represents different residual strength ratio as follows:

$$a\ if\ 0.5 < \frac{f_{R3k}}{f_{R1k}} < 0.7$$

$$b\ if\ 0.7 \leq \frac{f_{R3k}}{f_{R1k}} < 0.9$$

$$c\ if\ 0.9 \leq \frac{f_{R3k}}{f_{R1k}} < 1.1$$

$$d\ if\ 1.1 \leq \frac{f_{R3k}}{f_{R1k}} < 1.3$$

$$e\ if\ 1.3 \leq \frac{f_{R3k}}{f_{R1k}}$$

For example, material labeled as 2*d* would have f_{R1k} equal to 2 – 3 MPa and f_{R3k}/f_{R1k} ratio from 1.1 to 1.3.

2.1.2 Factors Affecting Behavior of FRC

The impact of fibers on behavior of concrete depends on several factors which include fiber volume ratio, fiber length, fiber aspect ratio, fiber tensile strength and the strength of concrete matrix (ACI Committee 544, 2008).

Fiber length does not play a significant role in post-cracking behavior of SFRC containing reinforcing bars (Deluce and Vecchio, 2013). However, the longer the fiber is, the more cracks it can bridge. Short fibers should not be smaller than crack spacing in order to be able to transfer stresses between the cracks.

Fiber volume ratio influences the properties of hardened concrete and also the workability of freshly mixed concrete. The higher the fiber volume ratio, the more significant the effect becomes. The flexural strength increases, however concrete workability decreases with high fiber concentration and special mixing and placing methods are needed (Zollo, 1997). ACI Committee 544 (1993) suggests a range of fiber volume ratio from 0.25% to 2% for conventional steel fiber reinforced concrete.

Fiber aspect ratio is defined as the ratio of the fiber length to the fiber diameter and indicates the slenderness of the fiber (Johnston, 2001). Higher aspect ratio means higher surface area of fibers and higher surface area of fiber improves bond between the fibers and the concrete which leads to better performance of the composite. Higher aspect ratio also improves the residual post-cracking tensile strength and toughness of the concrete as described by Johnson (2001), however reduced workability applies in cases with high aspect ratio.

Tensile strength of fibers is the tensile stress that results in the rupture of the fiber. Tensile strengths of fibers can be up to 2000 MPa. The more stress the fiber is able to resist the more ductile behavior the member experiences. When fibers with high tensile strengths are used, the fiber will be pulled out of the matrix without rupturing, and the residual tensile strength of the FRC will depend of the bond strength between the fibers and the concrete matrix (Susetyo, 2009).

2.2 TESTS ON FRC DEEP BEAMS

Four studies of the effect of steel fibers on behavior of deep beams were evaluated. Mansur and Alwist (1984) tested 12 fiber-reinforced deep beams with openings and analyzed the effect of volume fiber ratio, opening location and *a/d* ratio. Narayan and Darwish (1988) tested 12 reinforced concrete deep beams including 11 with steel fiber reinforcement. The main focus of their study was the effect of fiber volume ratio, *a/d* ratio and concrete strength. Mansur and Ong (1991) analyzed 10 reinforced concrete deep beams including 9 with steel fibers, observing mainly the influence of fiber volume ratio, *a/d* ratio and transversal and longitudinal reinforcement. One of the newest research studies focused on deep beams was carried out by Campione (2012) and consists of 4 reinforced concrete deep beams from which 2 of them included steel fibers.

Numerous other tests were conducted, however only two of the previously mentioned ones were considered suitable for the validation of the extended five-spring model. When selecting studies relevant for the validation of the extended five-spring model, only members with height over 500 mm were to be considered. Such restriction is due to the behavior of deep beams, which cannot be captured correctly if the size of the tested specimen is smaller than 500 mm. Also tests where cylinders were used to apply load, without presence of loading plates transferring the load, were discarded from the tests used for the validation. This was due to the unrealistic concentration of stresses under the loading point and thus invalid results obtained from the test. The experimental results by Campione (2012) were discarded due to the lack of information about the specimen.

Given all of the limitations mentioned above, only two of the studies were considered relevant for the validation of the five-spring model. The tests of Mansur and Alwist (1984) and the experiments conducted by Mansur and Ong (1991) were considered and a database with provided beam properties which can be seen in Appendix A was created. Both of the studies will be described in detail in the following sections.

2.2.1 Mansur and Ong (1991)

Mansur and Ong (1991) conducted a study including 9 fiber reinforced deep beams and one control specimen without fibers. The major parameters observed in the study were *a/d* ratio, volume fraction of fibers and ratios of longitudinal and transversal reinforcement.

All of the specimens had height of 500 mm, width of 90 mm, maximum aggregate size of 10 mm, yield strength of bottom longitudinal and web reinforcement of 440 MPa and 375 MPa, respectively. Bottom longitudinal reinforcement consisted of 4 reinforcement bars, with 16 mm diameter, placed in two layers. The rebars were welded to a 15 mm thick steel plate at each end. Web reinforcement had diameter of 6 mm and the number of bars varied depending on the length and cross section of the member. Bottom longitudinal reinforcement ratio was 1.93% while the transversal ratio varied from 0.42% to 1.26%. The layout of the reinforcement and experimental setup is shown in Figure 2.3. Fibers used in the experiment were straight, slightly twisted with 0.5 mm square in cross section and length of 30 mm. Concrete strength was

determined for each specimen individually and is specified in table in Appendix A. Further details regarding the test setup and properties of the specimen are shown in the table in Appendix A with reference number 1. Data highlighted in purple was not directly specified by the authors, but obtained by an assumption or calculation based on provided data. The beams were tested in four-point loading, where the loads and reactions were applied through rollers and bearing blocks. Load was applied in 50 kN increments until the failure which was noted after the collapse.

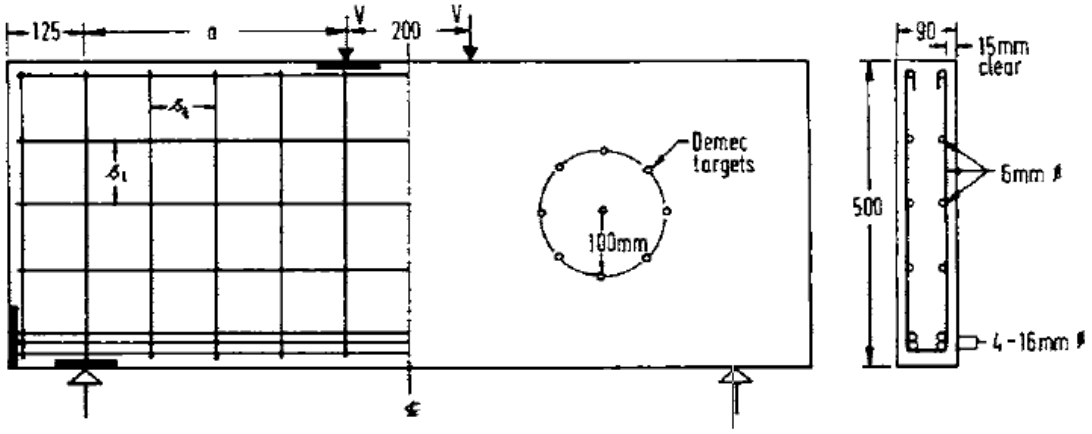

Figure 2.3 Experimental setup by Mansur and Ong (1991)

Results showed that the reduction of the shear span resulted in lower occurrence of flexural cracking. While for beams with *a/d* ratio of 1.85 the flexural cracks occurred first, for *a/d* ratio of 1.23 flexural and diagonal cracks propagated simultaneously. For shorter shear spans diagonal cracks propagated first with little or no occurrence of flexural failure. It was also observed that increase in *a/d* ratio results in lower stiffness of the member as shown in Figure 2.4a.

The effect of increasing fiber volume was most significant in cracking behavior of the beam. While in the beam with no fibers the cracks formed suddenly and then propagated rapidly, in beams with fibers the crack propagation and widening was significantly slower. Increasing fiber volume ratio resulted in higher ultimate strength as shown in Figure 2.4b.

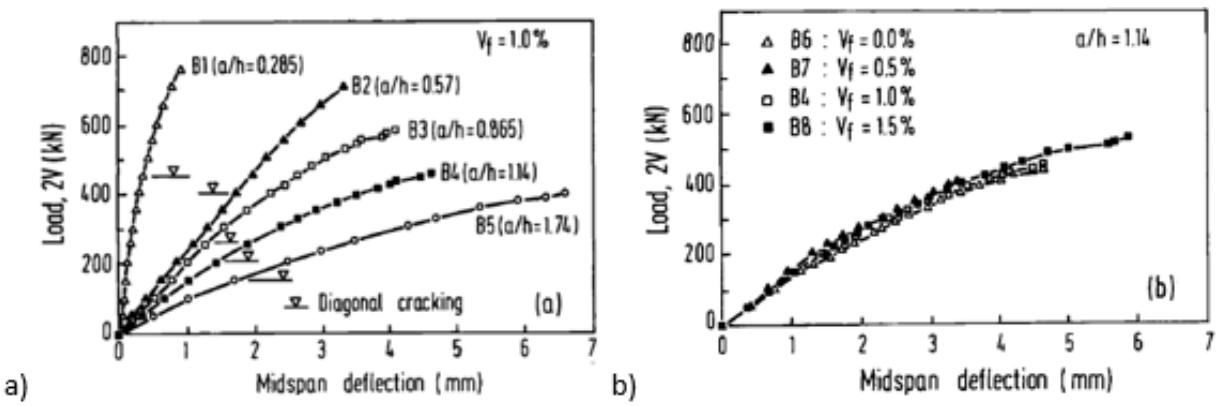

Figure 2.4 Experimental results by Mansur and Ong (1991)

The tests also included two beams designated to study the effect of vertical and longitudinal web reinforcement. It was concluded that the longitudinal reinforcement has almost no influence on the shear strength of the beams. However, increasing the ratio of vertical reinforcement proved to significantly increase the shear resistance of the member.

To describe the shear failure in detail, beam B4 from the study was selected as a sample. The beam had 1% of fiber volume ratio, and vertical reinforcement of 0.42% and *a/d* ratio of 1.23. In the test the shear cracks propagated at the same time as flexural cracks. However, it was the propagation of shear cracks that lead to the final failure of the beam. As described in the experiment, at 80 to 90 percent of the ultimate load, one of the diagonal cracks began to grow excessively. This critical diagonal crack was described to originate at the mid-depth of the beam and with increasing load to extend to the support and to the loading point. A crushing of the concrete was observed between the loading point and the tip of the inclined crack. The size of the critical loading zone which is susceptible to compression introduced by the loading plate is also one of the parameters influencing the overall shear resistance of the beam. The cracking pattern of the beam can be observed in Figure 2.5.

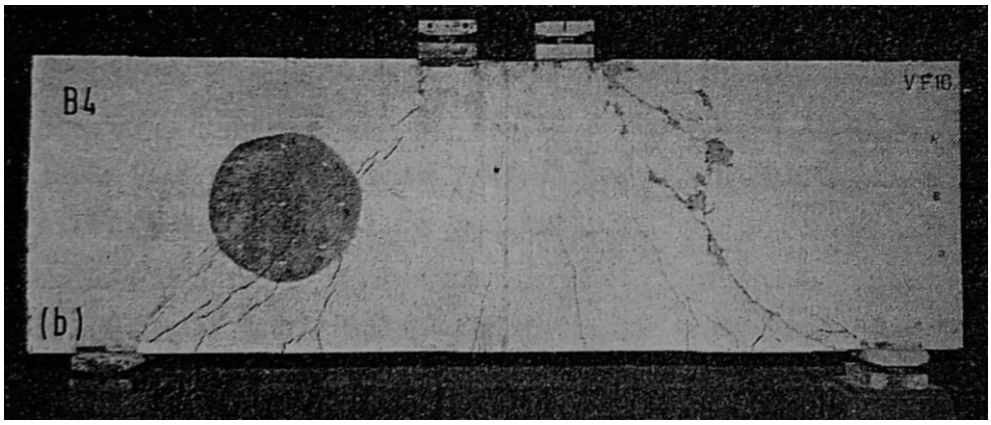

Figure 2.5 Cracking pattern of the beam B4 by Mansur and Ong (1991)

2.2.2 Mansur and Alwist (1984)

Mansur and Alwist (1984) tested 12 fiber reinforced concrete deep beams with openings. Such beams are not relevant for the validation of the extended five-spring model, however one of the tested beams was a control beam for comparison, and did not include any openings. The control specimen had height of 850 mm and width of 80 mm, maximum aggregate size of 10 mm, yield strength of bottom longitudinal and web reinforcement of 418 MPa and 304 MPa, respectively. Bottom longitudinal reinforcement consisted of 2 reinforcement bars, with 16 mm diameter. The rebars were welded to a 20 mm thick steel plate at each end. Web reinforcement had diameter of 3.3 mm with 12 bars in longitudinal direction and 31 in vertical direction. Bottom longitudinal reinforcement ratio was 0.81% and transversal ratio 0.43%. The specimen setup is illustrated in Figure 2.6. Fibers used in the experiment were hook-ended fibers, glued together in bundles. Length of the fibers was 30 mm and diameter 0.4 mm. Concrete strength of the

specimen was 40 MPa. Further details regarding the test setup and properties of the specimen are shown in the table in Appendix A with reference number 2. The beam was tested in four-point loading where the loads and reactions were applied through rollers and bearing blocks. The beam was loaded with 20 kN increments until the failure.

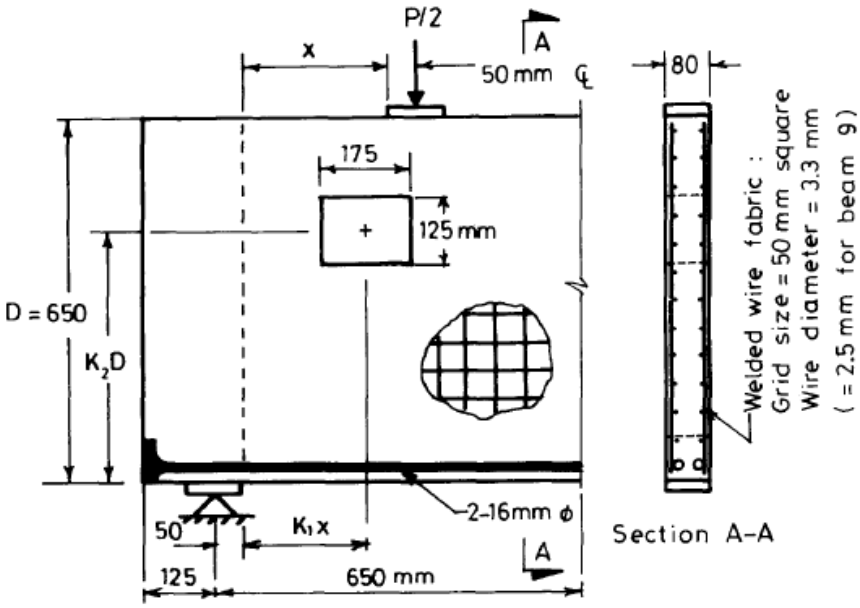

Figure 2.6 Experimental setup by Mansur and Alwist (1984)

The results showed that the beam behaved linearly at the beginning. Diagonal cracks appeared first and with increasing load started propagating and widening. Flexural cracks appeared later in the loading but did not affect the final failure. Final failure occurred by rapid propagation and widening of one of the diagonal cracks as illustrated in Figure 2.7.

Figure 2.7 Failure mode of control specimen by Mansur and Alwist (1984)

2.3 Two-Parameter Kinematic Theory and Five-Spring Model for Deep Beams

The two-parameter kinematic theory is based on a simple kinematic description of the deformation patterns of deep beams. The theory has been introduced by Mihaylov et al. (2013) and is capable to predict the shear strength and deformation patterns of deep beams at shear failure. Later the method has been expanded to a five-spring model (5sm) which is capable of predicting the complete pre-peak and post-peak behavior of deep beams (Mihaylov, 2015). The 5sm allows engineers to evaluate the safety and assess the deformations and crack widths of deep reinforced concrete beams such as transfer girders (Mihaylov et al., 2013). However, the theory does not account for the action of fibers.

Based on results from tests on the behavior of deep reinforced concrete beams under monotonic and cyclic loading by Mihaylov (2008), observations made were used as a background for the 2PKT. The main assumptions of the kinematic approach are illustrated in Figure 2.8. It is assumed that the shear failure of deep beams occurs along a straight critical shear crack that extends from the support to the load. The concrete above the critical crack is modeled as a rigid block with a critical loading zone (CLZ) located under the loading plate. The concrete below the crack is modeled with a series of rigid radial struts that connect the loading point with the bottom longitudinal reinforcement. The two regions are connected by the stirrups and longitudinal reinforcement.

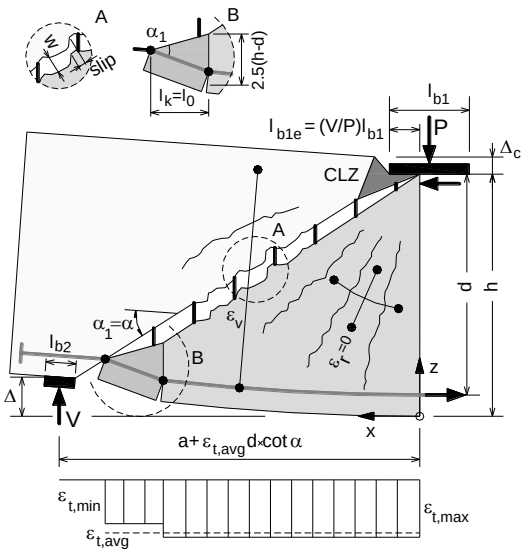

Figure 2.8 Main assumptions of kinematic model (Mihaylov et al.,2013)

The two-parameter kinematic theory assumes that with respect to the loading plate, the motion of the concrete block above the critical crack can be described as a rotation around the loading point and a vertical translation of the rigid block, see Figure 2.9. The rotation is proportional to the average strain in the bottom longitudinal reinforcement $\varepsilon_{t,avg}$, while the translation equals the vertical displacement Δ_c of the critical loading zone (Mihaylov et al., 2013). The two degrees of freedom (DOFs) as described are the two parameters of the kinematic theory. The elongation

of the bottom reinforcement causes the rigid radial struts to rotate around the loading point and the cracks between them to widen. The transverse displacement in the critical loading zone causes the critical diagonal crack to widen and a slip displacement to occur along the crack. As illustrated in Figure 2.9, both degrees of freedom contribute to the increase of tensile strains in transverse reinforcement (stirrups).

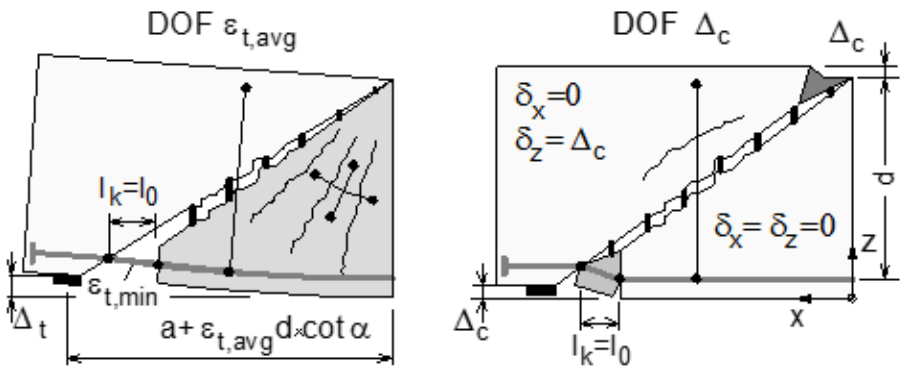

Figure 2.9 Degrees of freedom of kinematic model (Mihaylov et al.,2013)

The angle of the critical crack depends on the shear-span-to-depth (*a/d)* ratio and is defined as α_1. Angle α_1 is determined as the smallest value of two other angles α and θ, see Figure 2.10. Angle α is the angle of the line connecting the inner edge of the support plate with the outer edge of the effective width of the loading plate. The effective width of the loading plate is the portion of the loading plate participating in the transfer of the applied load to the support. Angle α governs for deep beams while angle θ captures the transition to slender beams when the shear span *a* becomes relatively large as compared to the effective depth *d*. Angle θ can be obtained from sectional shear models for slender beams, however, for simplification, its value will be assumed equal to 35°.

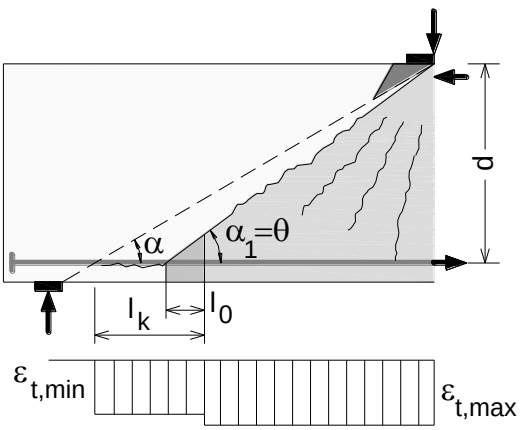

Figure 2.10 Variation of the angle α_1 during transition from deep to slender beams (Mihaylov et al.,2013)

Based on the assumptions for the kinematics of deep beams, and assuming that the two degrees of freedom $\varepsilon_{t,avg}$ and Δ_c are known, the two-parameter kinematic theory is able to provide the complete displacement field of the shear span of deep beams. In other words, the horizontal and

vertical displacement of each point from the shear span can be expressed with DOFs $\varepsilon_{t,avg}$ and Δ_c. As shown by Mihaylov et al. (2013), these expressions are as follows:

- for points below the critical diagonal crack

$$\delta_x(x,z) = \varepsilon_{t,avg} x \tag{1}$$

$$\delta_z(x,z) = \frac{\varepsilon_{t,avg} x^2}{h-z} \tag{2}$$

- for points above the critical diagonal crack

$$\delta_x(x,z) = \varepsilon_{t,avg}(h-z)\cot\alpha \tag{3}$$

$$\delta_z(x,z) = \varepsilon_{t,avg} x\cot\alpha + \Delta_c \tag{4}$$

These equations can be used to derive important deformations in the shear span, again as a function of $\varepsilon_{t,avg}$ and Δ_c. Such important deformation for example is the width of the critical diagonal crack halfway along the crack. This width is expressed as follows:

$$l_k = l_0 + d(cot\alpha - cot\alpha_1) \leq 2l_0 \tag{5}$$

$$l_0 = 1.5(h-d)cot\alpha_1 \geq s_{cr} \tag{6}$$

$$w = \Delta_c cos\alpha_1 + \frac{\varepsilon_{t,avg} l_k}{2sin\alpha_1} \tag{7}$$

$$s_{cr} = \frac{0.28 d_b}{\rho_l}\frac{2.5(h-d)}{d} \tag{8}$$

Where l_k is the length of dowels provided by the bottom longitudinal reinforcement, l_0 is the length of heavily cracked zone at bottom of critical diagonal crack, and s_{cr} is the distance between the cracks along bottom longitudinal reinforcement (see Figure 2.8).

Using the two degrees of freedom, the kinematic model can be used to evaluate the overall deflection of the member. The deflection is defined as the relative displacement between the support and the section with maximum bending moment, assuming that the latter section remains vertical (Mihaylov, 2015). The deflection is defined as follows:

$$\Delta = \frac{\varepsilon_{t,avg} l_t}{d} a + \Delta_c \tag{9}$$

Where the first term of the equation describes the deflection of shear span Δ_t due to elongation of bottom longitudinal reinforcement. The variable l_t is the length of bottom reinforcement within the cracked part of shear span, as illustrated in the free-body diagram in Figure 2.12, and is defined as:

$$l_t = d\,cot(\alpha_1) + l_k - l_0 \tag{10}$$

Given the two deflections Δ_t and Δ_c, the five-spring model represents the shear span using two sets of springs connected in series and loaded by shear force *V*. As shown in Figure 2.11, a set of four parallel springs elongates by the value of deflection Δ_c, while the fifth spring elongates by Δ_t. The four parallel springs represent the shear behavior of the beam, while the fifth spring represents the flexural behavior.

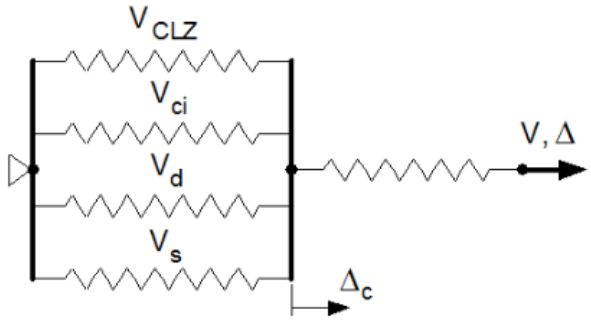

Figure 2.11 Five-spring model (Mihaylov, 2015)

The forces of the five-spring model, and their definition within the shear span of the beam, are illustrated in Figure 2.12. The force V_{CLZ} is the shear carried by the critical loading zone, V_{ci} is the shear resisted by aggregate interlock along the critical crack, V_d is the shear resisted by the dowel action of the bottom flexural reinforcement, and V_s is the shear resisted by the stirrups. The sum of these forces is the shear force V obtained from the equilibrium of the vertical forces acting on the rigid block. The force in the flexural spring is the shear force derived from the moment equilibrium of the shear span taken about the point of application of the compression force C in the section with maximum moment. The equilibrium equation is as follows:

$$V = \frac{T(0.9)d}{a} \tag{11}$$

Where *T* is the tension force in the flexural reinforcement and 0.9*d* is the assumed lever arm between the compression force *C* and the tension force *T*.

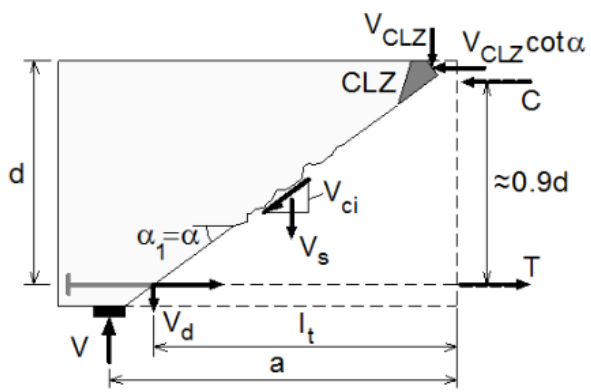

Figure 2.12 Free-body diagram of the rigid block (Mihaylov, 2015)

Therefore, given that the shear force can be expressed in two different ways, the equilibrium of the spring forces requires that:

$$\frac{T(0.9)d}{a} = V_{CLZ} + V_{ci} + V_s + V_d \tag{12}$$

Shear failure is predicted if the set of four parallel springs fails first, and failure due to yielding of the flexural reinforcement occurs if the flexural spring fails first. The force in flexural reinforcement is expressed as:

$$T = E_s A_s \varepsilon_{t,avg} + \frac{0.33\sqrt{f'_c}}{1+\sqrt{200\varepsilon_{t,avg}}} A_{c,eff} \leq A_s f_y \tag{13}$$

Where the first term of the equation models the resistance of bare steel reinforcement. The second term of the equation models the tension stiffening effect of the concrete, where the area of concrete involved in the tension stiffening effect is taken as:

$$A_{c,eff} = \min\left[2.5(h-d), \frac{h}{2}\right] b \tag{14}$$

The last part of the equation for the force T is the yield force of the bottom longitudinal reinforcement.

The shear carried by the critical loading zone is derived using the degree of freedom Δ_c. The critical loading zone has a triangular shape that depends on the effective width of the loading plate and the angle of the critical crack. The concrete in the critical loading zone is subjected to diagonal compressive stresses σ and strains ε, where the strain at the bottom plane of the critical loading zone is ε_{max}. The strain ε_{max} can be expressed using DOF Δ_c as shown in Figure 2.13. The diagonal compressive stress is obtained through appropriate stress-strain relationships for concrete under uniaxial compression, which is in this case Popovics (1970) curve for stress-strain relationship. The average stress σ_{avg} is multiplied by the area of the section passing through the edge of the loading plate and perpendicular to the bottom face of the critical loading zone.

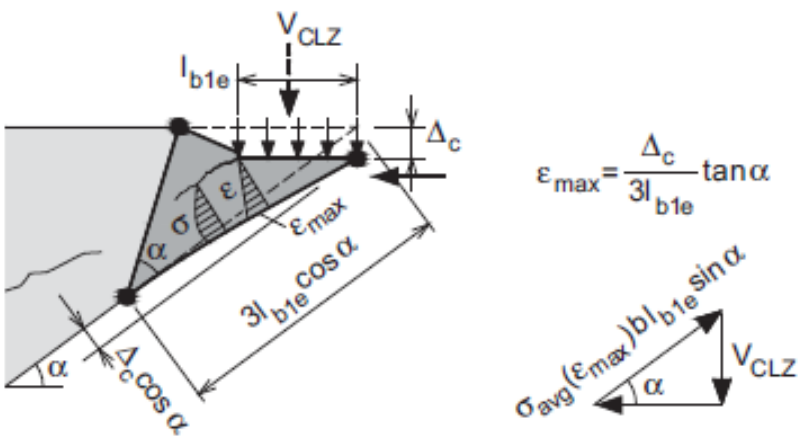

Figure 2.13 Critical loading zone (Mihaylov, 2015)

The shear carried by the critical loading zone is then expressed as:

$$V_{CLZ} = \sigma_{avg}[\varepsilon_{max}(\Delta_c)]bl_{b1e}sin^2\alpha \quad (15)$$

The shear force resisted by the aggregate interlock is expressed using the average shear stress v_{ci} transferred across the critical crack by interlocking of the rough crack surfaces:

$$V_{ci} = 0.18v_{ci}bd \quad (16)$$

The value of v_{ci} is evaluated halfway along the critical crack as a function of crack width w and slip s. Where the crack slip is defined as follows:

$$s = \Delta_c \sin(\alpha_1) \quad (17)$$

In order to compute the value of $v_{ci,}$ contact density model (CDM) developed by Li et al. in 1989 is used. The model represents the crack surface using series of planes at different angles, where the planes with the same angle on each side of the crack are connected by contact springs. The springs have an elastic-perfectly-plastic behavior in compression and zero resistance in tension. The CDM also accounts for clamping stresses, which are not taken into account in the five-spring model and thus a factor 0.18 is adopted to reduce the shear resistance v_{ci}.

The shear carried by the stirrups across the critical diagonal crack is expressed using both degrees of freedom of the kinematic approach. Firstly, the strain in the stirrups is evaluated as:

$$\varepsilon_v = 2\frac{\Delta_c + 0.25\varepsilon_{t,avg}dcot^2\alpha_1}{0.9d} \quad (18)$$

The stress in the stirrups is then expressed as:

$$\sigma_v = \min(\varepsilon_v E_v, f_{yv}) \quad (19)$$

And the shear carried by the stirrups can be then taken as the stress in the stirrups multiplied by the effective area of stirrups that are providing shear resistance:

$$V_s = \sigma_v \rho_v b(dcot\alpha_1 - l_0 - 1.5l_{b1e}) \quad (20)$$

Where ρ_v is the transverse reinforcement ratio which should not be larger than $0.15f'_c/f_y$. The value in brackets should not be smaller than $0.5dcot(\alpha_1)$. For beams without stirrups, the five-spring model becomes a four-spring model as the value of V_s is 0.

The last component of the equilibrium equations represents the shear force resisted by the dowel action of the bottom longitudinal reinforcement. The resistance depends on the number of bottom flexural bars, diameter of the bars, and the length of the dowels l_k. The equation is then as follows:

$$V_d = n_b\frac{12E_s\pi d_b^4}{64l_k^3}\Delta_c \leq n_b f_y\frac{d_b^3}{3l_k}\left[1-\left(\frac{T}{A_s f_y}\right)^2\right] \quad (21)$$

Where the first term of the equations represents the behavior of the elastic fixed-fixed dowels subjected to relative transverse support displacement Δ_c. The second part corresponds to the

formation of plastic hinges at the ends of the dowels, where the moment capacity of the plastic hinges is reduced due to the tension force *T* acting on the bars.

The five-spring model is then solved for increasing deflection Δ_c at a step of 0.1 mm. The final load-deflection curve is then created by calculating the shear force at each step for the given shear distortion of the CLZ and plotted for the consecutively calculated overall deformation. Given that the elongation of the flexural spring is $\Delta_t = \Delta - \Delta_c$, the only unknown kinematic parameter is the Δ_c. The deformation can be obtained solving the equilibrium equation (12). Figure 2.14 illustrates the shear forces in the five-spring model for a sample beam with properties described in Table 2.1 for imposed shear distortion of the CLZ of 5 mm. The figure describes how only one point of many that create the final load-deflection curve is obtained.

Table 2.1 Sample beam properties

a/d	b (mm)	d (mm)	h (mm)	l (mm)	ρ_l (%)	A_s (mm^2)	$\varnothing_l$ (mm)	No. $bars_l$	f_y (MPa)	a_g (mm)	f_c' (MPa)	f_{yv} (MPa)	ρ_v (%)	$\varnothing_v$ (mm)	No. $bars_v$
1,55	400	1095	1200	3900	1,27	5541,8	28	9	550	20	40	490	0,1	10	10

The horizontal axis of Figure 2.14 shows the range of tensile strain in the bottom longitudinal reinforcement. The vertical axis represents the shear forces obtained from all the springs of the five-spring model. Thick red line represents the sum of shear forces resisted by the critical loading zone, aggregate interlock, stirrups and dowel action. As the shear force resistance of the CLZ is only dependent on the Δ_c parameter, the shear force does not depend on the strain in the bottom longitudinal reinforcement, the line representing V_{CLZ} is a constant. The shear force resisted by the stirrups is also a constant, since in this part of the loading the stirrups are considered to have yielded. At the moment of shear distortion of the CLZ that is considered in this case, the stress in the stirrups is dependent on the yield strength of the bottom longitudinal reinforcement rather than on the strain and modulus of elasticity of the reinforcement. The shear force resisted by the aggregate interlock is dependent on the strain in the dowels provided by the reinforcement. Therefore, the curve representing the aggregate interlock decreases with increasing strain. The last force contributing to the sum of shear forces is the dowel action which is dependent on both of the parameters. The shear force resisted by the dowels decreases as the strain in the bottom longitudinal reinforcement increases until the point where the reinforcement has yielded and is no longer able to transfer any stresses.

The thick black line represents the shear obtained from the moment equilibrium. The orientation of this bilinear curve depends on the properties of the concrete matrix and bottom longitudinal reinforcement. First part of the curve is the contribution of tensile resistance of the concrete matrix and second part represents the contribution of the reinforcement. The intersection of the two thick lines highlighted with red dot, marks the solution of the equilibrium equation. Consecutively, the value of the shear force at the intersection is the shear resistance of the beam at 5 mm distortion of the critical loading zone. The intersection is found iteratively using the bisection method.

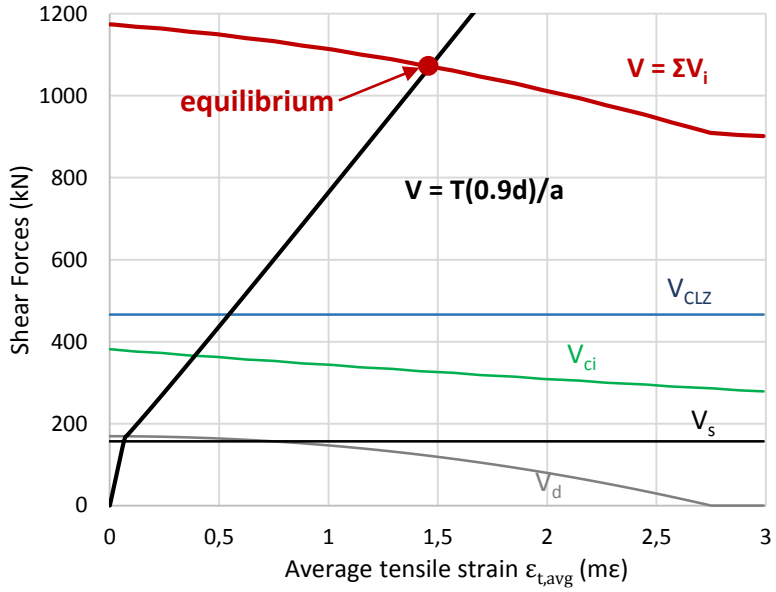

Figure 2.14 Shear forces in five-spring model at 5 mm imposed distortion of the CLZ

The final curve of the model is then generated by gradually increasing the distortion of the CLZ from 0 to 15 mm, and repeating the calculations illustrated in Figure 2.14. For each step, which represents a certain value of the distortion of the CLZ, the solution (red dot) is found using equilibrium equations and bisection method. Obtained intersections then create a load-displacement curve as shown in red in Figure 2.15, where the overall deflection Δ is calculated for given Δ_c. Horizontal axis of the Figure 2.15 represents the imposed displacement Δ with range from 0 to 15 mm in this case. Vertical axis represents the values of shear forces obtained from the equilibrium equations, which can be described as the path of the red dot for different imposed distortions of the CLZ. Thick red curve corresponds to the solutions of the equilibrium equations for increasing displacement and is described as a sum of the shear forces provided by each of the parameters described in the 5sm. Thinner curves of the graph each represent one of the four parallel springs of the five-spring model. These curves are obtained also using the Figure 2.14 and generating the intersections of each of the curves with the thick black curve describing the moment equilibrium equation.

As it can be seen in the Figure 2.15 the CLZ provides the most shear force resistance of the model. The value of the shear force provided by the critical loading zone increases until deflection of about 6 mm where crushing of the CLZ occurs. The peak of the V_{CLZ} occurs at the same deflection as the maximum shear force resisted by the beam is achieved. The aggregate interlock, which reaches its maximum right after the beam reaches its peak shear strength and then starts decreasing, also greatly contributes to the overall shear resistance of the beam. The shear force provided by the dowel action of the bottom longitudinal reinforcement does not vary much throughout the loading. The amount of shear resistance is in this case comparable with shear force provided by the stirrups. The contribution of stirrups is increasing until the yield strength is reached, after that the curve becomes constant since it is no longer dependent on any of the degrees of freedom considered within the model.

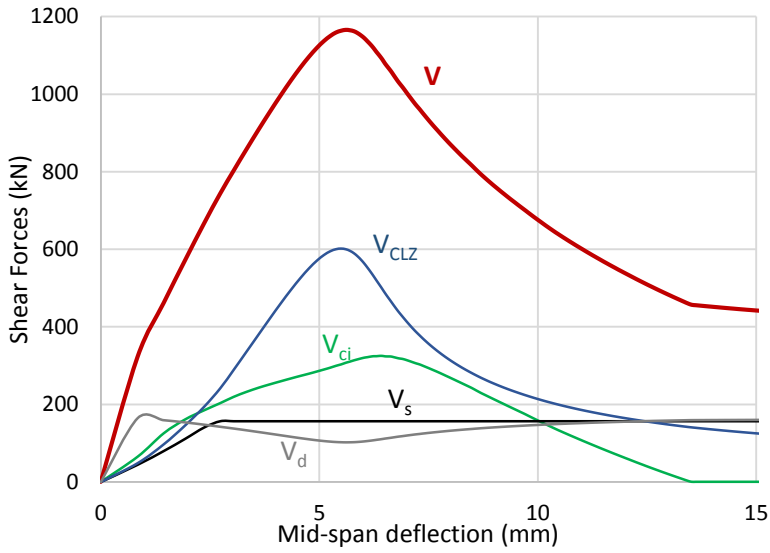

Figure 2.15 Equilibrium of forces in five-spring model for imposed displacement Δ

As it has been already mentioned previously, the 5sm proposed by Mihaylov (2015) is only applicable to deep beams with conventional reinforcement and with or without stirrups. The model does not account for the action of fibers. Based on described experiments on deep beams reinforced with fibers carried out by various researchers it has been concluded that inclusion of fibers can enhance the behavior of the deep beams and their post-peak response. The main objective of this thesis is to introduce the fiber action into the existing five-spring model. The aim of the next chapter is to extend the 5sm to deep beams with conventional and fiber reinforcement.

3 EXTENDED FIVE-SPRING MODEL FOR FRC DEEP BEAMS

3.1 INTRODUCTION

The extension of the five-spring model is divided into several subchapters, each of which is focused on a different part of the model that is affected by the addition of fibers into the concrete mixture. An extension of the model is made by adding another spring to the spring model to represent the shear resistance of fibers along the diagonal crack of the beam. This extension provides a fifth spring to the set of parallel springs by using the Simplified Diverse Embedment Model by Lee et al. (2013). Following the already existing model, two adjustments are made to account for the effect of the fibers on the properties of the concrete.

The first adjustment is implemented in the flexural spring which now also accounts for tension stiffening behavior of the beam caused by the addition of fibers using the Tension-Stiffening Model by Lee et al. (2013). The second adjustment is made in the stress-strain relationship for fiber-reinforced concrete under uniaxial compression, that now includes the impact of fibers on the resistance of the critical loading zone under uniaxial compression. The last adjustment does not deal with the effect of fibers, but rather extends the model to be able to represent not only three-point loading cases by giving the deflection under the loading point, but also four-point loading cases by introducing additional equations that enable the calculation of deflection in the middle of the beam.

In this chapter all of these extensions and modifications are described as given in the literature, including their limitations and formulations. Each of the implemented models is firstly developed as a separate code in Matlab and its results are validated against information and graphs provided in the literature. Secondly a description of the modified formulation of the code as it enters the five-spring model is provided and justified with description of its function within the model.

3.2 TENSION IN FIBERS ACROSS THE CRITICAL DIAGONAL CRACK

3.2.1 Introduction

One of the most crucial and beneficial aspects of adding steel fibers into the concrete structures is the non-brittle behavior after concrete cracking, that is achieved through fibers bridging the cracks. Whilst in normal concrete the tensile stress quickly decreases as soon as the crack starts propagating, in fiber-reinforced concrete we can observe the action of fibers that transfer the tensile stresses and contribute to the total response. Such behavior provides considerable tensile resistance to the structure even after the propagation of the crack.

Figure 3.1 illustrates the tensile behavior of FRC. The behavior of regular concrete with tension-softening effect is illustrated with dash-dotted line. The maximum value of stress depends on the tensile strength of the concrete. For FRC members the effect of fibers is included into the overall response of the member. As it can be seen in Figure 3.1, the fibers start acting as soon

as the crack starts propagating and provide additional resistance to the member even after the concrete matrix has lost its ability to transfer stresses. The solid line in the figure represents the response of FRC member, which consists of the sum of the tension softening effect and the action of fibers. Based on these observations it can be concluded, that in order to accurately predict the post-cracking response of FRC, the tensile stress behavior attainable with fibers should be evaluated.

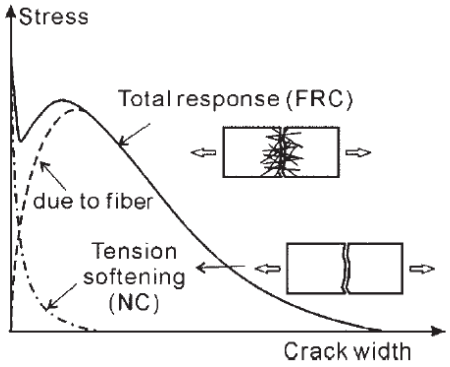

Figure 3.1 Tensile behavior of FRC (Lee et al., 2013)

Figure 3.2 illustrates the additional force F_f that will be implemented within the extended five-spring model to represent the actions of fibers across the critical diagonal crack. The action of fibers while bridging the crack results in additional vertical force V_F that will enter the parallel set of springs and provide higher shear resistance to the member.

Figure 3.2a shows the additional stress f_f representing the tensile stress at crack due to steel fibers. The stress can be calculated using the SDEM by Lee et al. (2013) which describes the stress transfer through the crack taking into account the concrete matrix and steel fibers (hooked or straight). However, to obtain the stress f_f transferred through the crack only the contribution of fibers, without the resistance provided by the concrete matrix will be considered. The stress v_f represents the vertical component of the force f_f acting along the critical crack of the member. For a given width b of the cross section and the length of critical diagonal crack, the shear force resistance F_f provided by the fibers bridging the crack can be calculated. The vertical component V_F of the force F_f is then calculated using the angle α_1 of the critical crack.

Figure 3.2b shows the tensile stresses f_f resisted by the fibers for a given crack width. The figure represents a sample beam with fiber volume of 1%, fiber length of 30 mm, diameter of fibers of 0.5 mm and straight fibers. Horizontal axis of the figure describes different crack widths varying from 0 mm to 10 mm. Vertical axis shows the stresses transferred by the fibers along the area of the critical crack. The curve then represents the stress transferred through the steel fibers for increasing width of the crack.

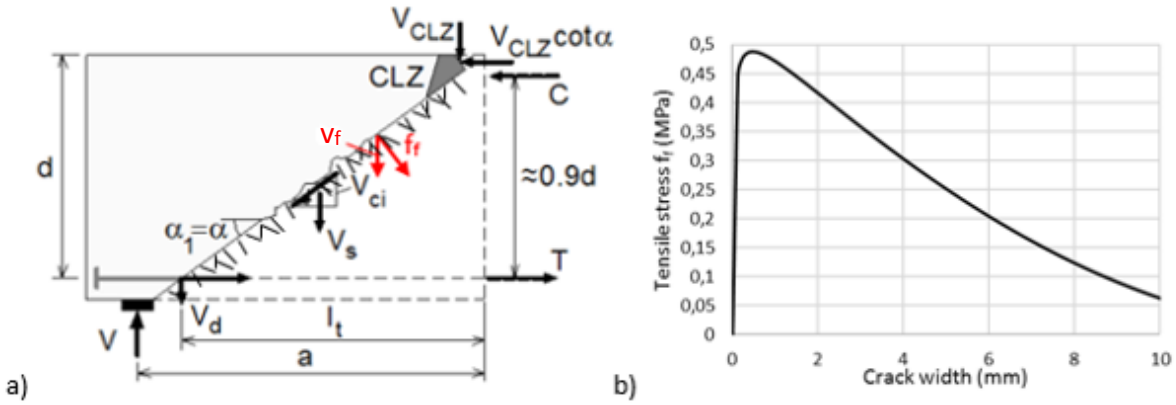

Figure 3.2 Illustration of additional force provided by fibers in the extended five-spring model

Several researchers have tried to describe the tensile stress behavior of fibers but so far the most realistic method is the Diverse Embedment Model (DEM) by Lee et al. (2011) that predicts tensile stress in fibers across a given crack. In this model the pullout strength of fibers is analyzed taking into account embedment on both sides and considering both frictional bond behavior and mechanical anchorage effects. Given such circumstances, the DEM can be applied to end-hooked fibers as well as straight fibers. The DEM method also takes into consideration all possible fiber orientations and embedment lengths.

Due to the complicated calculation of the tensile strength of the fibers using the DEM, which includes double numerical integration, Lee et al. (2013) proposed a Simplified DEM (SDEM). SDEM is derived from the DEM by eliminating the integration and by neglecting the slip on the longer embedded side. The frictional bond behavior and mechanical anchorage effects are incorporated in the model as coefficients preventing an overestimation of the tensile stress attained by fibers. The tensile stress behavior of the fibers obtained using the SDEM has shown a good agreement with the results obtained using the DEM and thus it can be concluded that despite the simplification the accuracy of the model remained.

3.2.2 Formulation of the SDEM

In order to be able to perform the SDEM it is necessary to know the compressive strength of concrete that will be considered in the calculation and the fiber volumetric ratio included in the concrete. Regarding the properties of the fibers, the length of the fibers and its diameter are necessary. In case of using hook-ended fibers, the length of the straight part between the mechanical anchorages should be specified, see Figure 3.3.

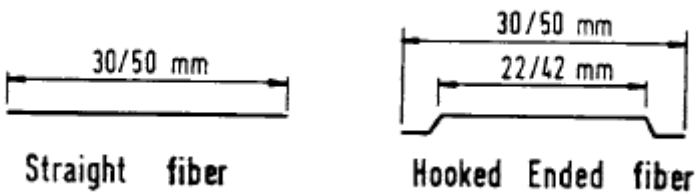

Figure 3.3 Fiber types used in the study by Lim et al. (1987)

The tensile stress in steel fiber-reinforced concrete without conventional reinforcement can be described with the following equation:

$$f_{SFRC} = f_f + f_{c,soft} \tag{22}$$

Where f_f is the tensile stress at crack due to steel fibers and $f_{c,soft}$ stands for the tensile stress in concrete due to tension softening effect described by Voo and Foster (2003) as follows:

$$f_{c,soft} = f_{cr} e^{-cw_{cr}} \tag{23}$$

Where f_{cr} is the cracking stress of the concrete estimated as $f_{cr} = 0.33\sqrt{f'_c}$ (Ramaswamy et al. 1994). The coefficient c is either 15 or 30 for concrete or mortar, respectively, and w_{cr} is the given average crack width.

Due to the simplification in the SDEM, the bond mechanism for the pullout behavior of steel fibers and the mechanical anchorage effect due to end-hooks are evaluated separately. The total tensile stress at a crack due to the fibers can be described as:

$$f_f = f_{st} + f_{eh} \tag{24}$$

Where f_{st} is the tensile stress due to frictional bond behavior of steel fibers and f_{eh} is the tensile stress due to mechanical anchorage effect of end-hooked steel fibers. These tensile stresses are expressed as follows:

$$f_{st} = \alpha_f V_f K_{st} \tau_{f,max} \frac{l_f}{d_f} \left(1 - \frac{2w_{cr}}{l_f}\right)^2 \tag{25}$$

$$f_{eh} = \alpha_f V_f K_{eh} \tau_{eh,max} 2 \left(\frac{l_i - 2w_{cr}}{d_f}\right) \tag{26}$$

Where V_f stands for fiber volumetric ratio, l_f is the fiber length, d_f is the diameter of the fiber, α_f is the fiber orientation factor that can be assumed to be 0.5 for cases where the dimensions of the structural member are much larger than the fiber length (Lee et al., 2013), and τ is the pullout strength of a single fiber taken from Table 3.1 (Voo and Foster, 2003).

Table 3.1 Pullout strength of single fiber by Voo and Foster (2003)

Fiber type	Matrix	Pullout strength
Straight	Concrete	$\tau_{f,max} = 0.396\sqrt{f_c'}$ (MPa) $[4.77\sqrt{f_c'}$ (ksi)]
	Mortar	$\tau_{f,max} = 0.330\sqrt{f_c'}$ (MPa) $[3.97\sqrt{f_c'}$ (ksi)]
End-hooked	Concrete	$\tau_{eh,max} = 0.825\sqrt{f_c'}$ (MPa) $[9.94\sqrt{f_c'}$ (ksi)]
	Mortar	$\tau_{eh,max} = 0.660\sqrt{f_c'}$ (MPa) $[7.95\sqrt{f_c'}$ (ksi)]

The parameters K_{eh} and K_{st} are defined as follows:

$$K_{st} = \frac{\beta_f}{3}\frac{w_{cr}}{s_f} \quad for\ w_{cr} < s_f \tag{27}$$

$$K_{st} = 1 - \sqrt{\frac{s_f}{w_{cr}}} + \frac{\beta_f}{3}\sqrt{\frac{w_{cr}}{s_f}} \quad for\ w_{cr} \geq s_f \tag{28}$$

$$K_{eh} = \beta_{eh}\left[\frac{2}{3}\frac{w_{cr}}{s_{eh}} - \frac{1}{5}\left(\frac{w_{cr}}{s_{eh}}\right)^2\right] \quad for\ w_{cr} < s_{eh} \tag{29}$$

$$K_{eh} = 1 + \left(\frac{7\beta_{eh}}{15} - 1\right)\sqrt{\frac{s_{eh}}{w_{cr}}} - \frac{2\left(\sqrt{w_{cr}} - \sqrt{s_{eh}}\right)^2}{l_f - l_i} \quad for\ s_{eh} \leq w_{cr} < \frac{l_f - l_i}{2} \tag{30}$$

$$K_{eh} = \left(\frac{l_i - 2w_{cr}}{2l_i - l_f}\right)^2 K_{eh,i} \quad for\ \frac{l_f - l_i}{2} \leq w_{cr} < \frac{l_i}{2} \tag{31}$$

Where β_f, is a coefficient reflecting the effect of fiber slip on the longer embedded side and has been analytically determined as 0.67. In the same way as the determination of β_f, the value of coefficient β_{eh} has been defined as 0.76 where this coefficient prevents the tensile force by mechanical anchorage from being overestimated due to the effect of a fiber slip on the longer embedded side as defined by Lee et al. (2013).

The length l_i is the length of the straight part of the fiber between the mechanical anchorages for end-hooked fibers, and can be obtained by subtracting 8 mm from the overall length of the fiber l_f based on the assumption shown in the Figure 3.3.

The value of s_f, which refers to a slip at maximum tensile force due to mechanical anchorage of fiber with inclination angle of 0 degrees with respect to the crack surface, can be assumed as 0.01 mm based on the experiments provided by Naaman and Najm (1991). Equally, the value of s_{eh}, which describes the slip at maximum tensile force due to mechanical anchorage of an end-hooked fiber, has been derived from the same experiments and is considered to be equal to 0.1 mm.

The last unknown value in the equations of K_{eh} is the variable $K_{eh.i}$ which is the value of K_{eh} at $w_{cr} = (l_f - l_i)/2$. An important point that should be taken into account while applying the SDEM is that only the DEM is suitable for SFRC in which fiber rupture is expected. Fiber rupture is not considered in the SDEM.

3.2.3 Validation of the SDEM

To perform calculations of tensile stresses in steel fibers across cracks, a code in Matlab was developed using the formulation of the SDEM as described in the previous chapter. The code is verified and the SDEM is validated by performing comparisons with SDEM simulations and test results from the literature (Lee et al. 2013, Lim et al. 1987, Susetyo 2009). The Matlab code itself as it enters the five-spring model is included in Appendix B.

3.2.3.1 Experimental results by Lim et al. (1987)

Lim et al. (1987) tested members with straight and hook-ended fibers subjected to uniaxial tension. These specimens had a rectangular cross section of 70 mm width and 100 mm thickness. The input value of concrete cylinder strength was not specified and thus is just assumed to be 40 MPa. It should be taken into consideration that such value might have a big impact on the accuracy of the results.

For the comparison, test results for straight fibers tested by Lim et al. (1987) and SDEM results by Lee et al. (2013) were used. In the experimental study the fiber volumetric ratio used has been considered to be 1% and 1.5% respectively. Fiber length used was 30 mm and the diameter of the fibers was 0.565 mm. As displayed in the Figure 3.4, we can observe that the proposed Matlab code is slightly more conservative than results by Lee and the experimental results. It can be assumed that the main cause of this difference is the assumed cylinder strength of the concrete. The strength was selected with the intention to match as closely as possible all the analytical results provided by Lee et al. (2013). Several cylinder strengths were considered and the one that showed the best agreement with the analytical curve generated by Lee et al. (2013) was used.

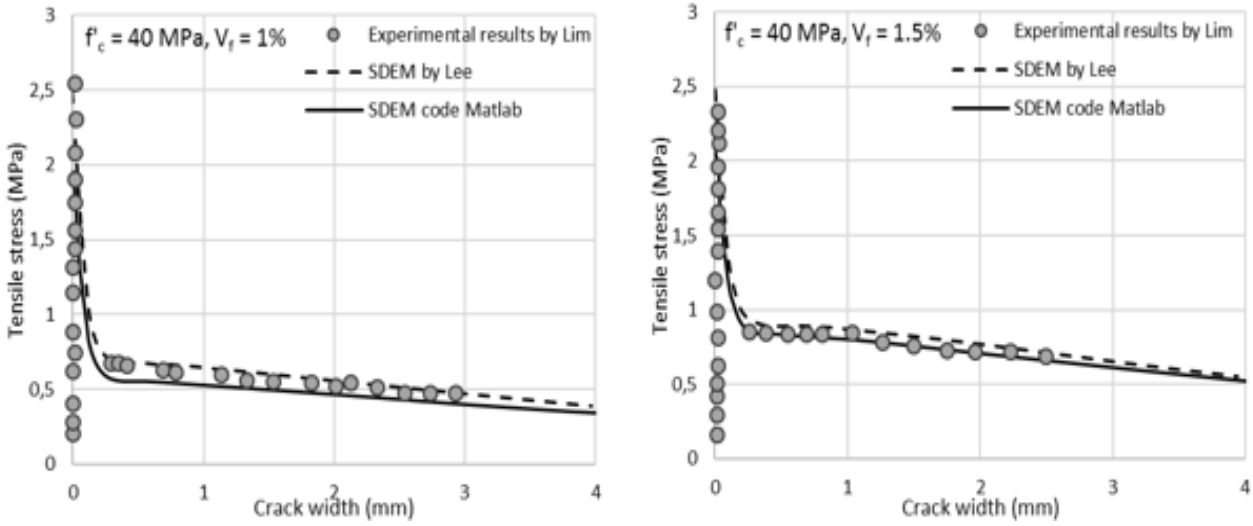

Figure 3.4 Comparison of proposed model and test results for members with straight fibers tested by Lim et al. (1987)

Another validation has been performed using the data from the tests by Lim et al. (1987) performed with end-hooked fibers, see Figure 3.5. In this experiment two types of fibers were used. The graph on the left corresponds to a fiber volume ratio 0.5%, fiber length 30 mm and diameter of the fiber 0.5 mm. The graph on the right represents fiber volume ratio of 1%, fiber length 50 mm and diameter of the fiber 0.5 mm. The results show again good agreement with the SDEM by Lee considering the shape of the curve. The curve generated using the created Matlab code proves to be more conservative but it can be assumed that the main reason for such difference is again the assumed concrete strength.

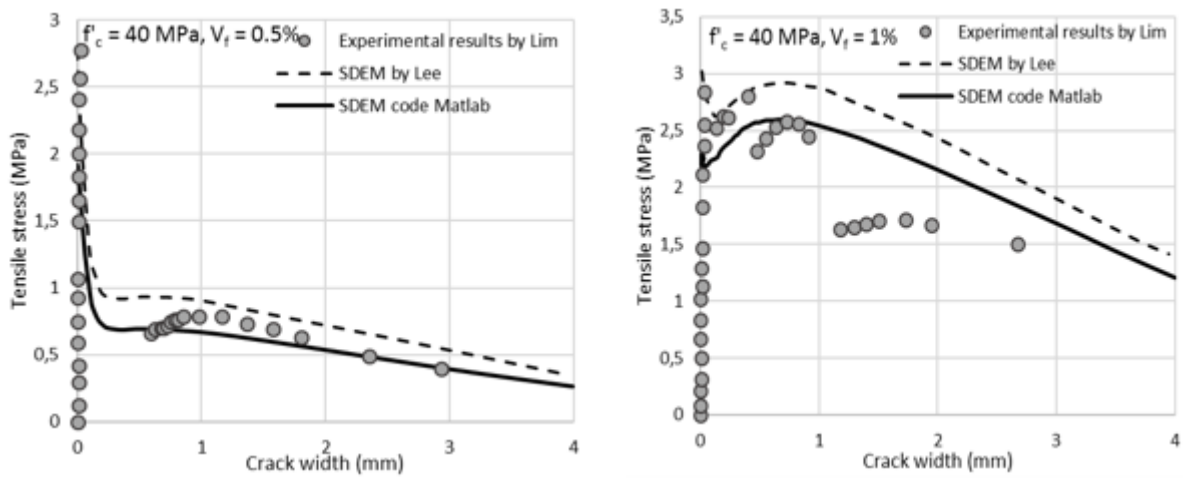

Figure 3.5 Comparison of proposed model and test results for members with end-hooked fibers tested by Lim et al. (1987)

3.2.3.2 Experimental results by Susetyo (2009)

Susetyo (2009) performed direct tension tests using specimens with cross section of 70x100 mm^2 and concrete compressive stress varying of 80 MPa and 50 MPa. In his experiments Susetyo tested steel FRC members with hook-ended fibers with overall fiber length 50 mm and

fiber diameter 0.62 mm. Two examples shown in the Figure 3.6 refer to concrete strength of 50 MPa and fiber volume ratio of 0.5%, and 1% respectively. The frictional bond strength $\tau_{f,\,max}$ and $\tau_{eh,max}$ was considered to be 0.396 f'_c and 0.429 f'_c respectively, based on previous research of Voo and Foster (2003) and Lee et al. (2011). The input value of l_i was not specified in this case and thus was based on the data provided by Lim et al. (1987). It should be taken into consideration that such assumption might slightly affect the accuracy of results.

During the data validation it was discovered that the formula for cracking strength based on the work of Ramaswamy et al. (1994) greatly underestimates the initial value of concrete strength. In order to match the results closer, a different formula was used for the value of cracking strength of concrete, in this case the most suitable formulation was one provided in the European Code (EN 1992-1-1:2004, EC2 Section 3.1) which defines cracking strength for concrete cylinder strength of 50 MPa as $f_{cr} = 0.3f'^{\frac{2}{3}}_c$.

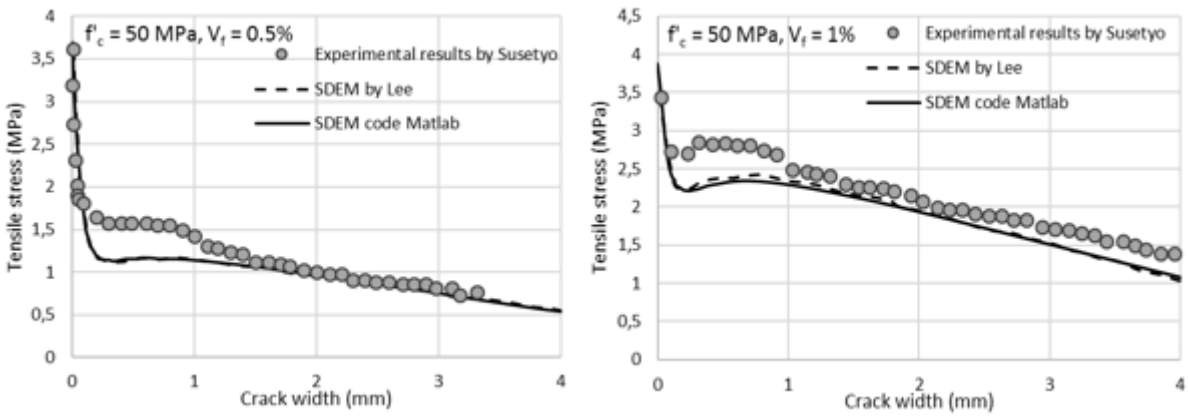

Figure 3.6 Comparison of proposed model and test results for members with end-hooked fibers tested by Susetyo (2009)

As can be seen in the Figure 3.6 the results obtained using the Matlab code almost perfectly match the results provided by Lee et al. (2013). Overall the experimental results show slightly higher tensile stress in the beginning of crack width propagation than the tensile stress obtained using the SDEM, after reaching crack width of 1 mm the SDEM results show good agreement with the experimental results.

3.2.3.3 Conclusion

Based on the results obtained using the experimental results from Susetyo (2009) and Lim et al. (1987) it can be concluded that the developed code correctly simulates the tensile stress behavior of the fibers.

3.2.4 Implementation of the SDEM into the Five-Spring Model

The SDEM was included in the model as a sixth spring that represents the shear strength provided by the action of fibers and in the model is referred to with a symbol V_F. The contribution of the tensile stress in concrete due to tension softening effect has been neglected in order to only account for the fiber action and thus the final tensile stress in the fibers is described as $f_f = f_{st} + f_{eh}$.

The shear strength provided by the action of fibers across the critical diagonal cracks is described as follows:

$$V_F = \frac{f_f bd}{\sin(\alpha_1)} \cos(\beta) \tag{32}$$

Where the angle β represents the angle between the force provided by fibers F_f and the vertical component of the force V_F as illustrated in Figure 3.7. The maximum possible value for the angle is α_1 and the minimum is 0. A study has been conducted in order to define the most suitable value of the angle β, where three different values have been considered.

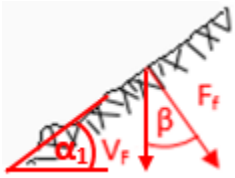

Figure 3.7 Definition of angle β

The first assumption was the most conservative one and considered the angle β equal to α_1. This scenario assumes that the angle of the fibers stays the same throughout the whole process of widening of the crack and thus only the vertical component of the force is being accounted for. This consideration does not take into account the fact that as the diagonal crack keeps on widening the part of the beam below the diagonal crack is sliding along the crack and the angle β of the fibers gets lower the wider the crack gets. This is the reason that another scenario has been taken into consideration. In this case the angle β is defined as follows:

$$\beta = \operatorname{atan}\left(\frac{s}{w}\right) \tag{33}$$

Where s is the slip and w is the width of the crack and are defined as follows:

$$s = \Delta_c \sin \alpha_1 \tag{34}$$

$$w = \varepsilon_{t,avg} \frac{l_k}{2 \sin \alpha_1} + \Delta_c \cos \alpha_1 \tag{35}$$

This scenario assumes that the force F_f is parallel to the relative displacement between the crack faces. The last option taken into account is when the angle β is equal to zero, and thus the

resulting force consists only of the vertical component. An analysis was carried out to define the most suitable scenario to include in the five-spring mode. Properties of the beam B4 from the experimental study of Mansur and Ong (1991) were used for the analysis of the impact of the changing angle. Predicted shear strength was obtained for changing *a/d* ratios and a curve was generated. Same process was repeated for three different assumptions of angle β, resulting in three different curves. Figure 3.8 shows the results of the analysis. The results obtained using angle β equal to α_1, and definition of the angle from equation (33), are overlapping, while β equal to 0 provides slightly higher shear resistance.

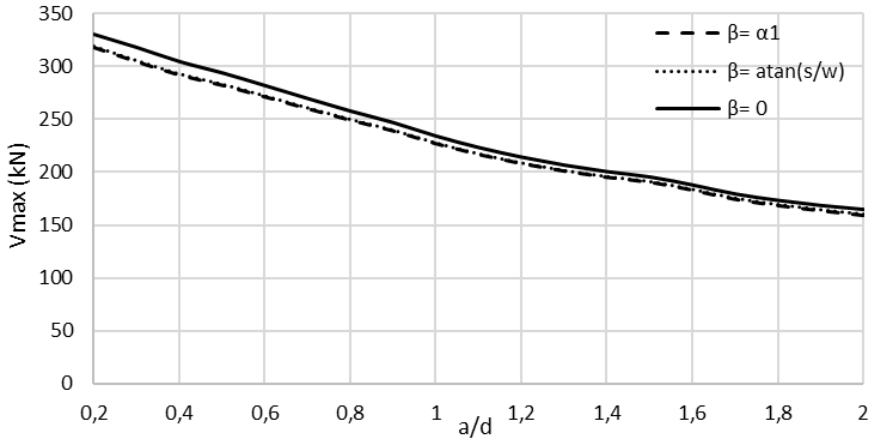

Figure 3.8 Variation of the angle β given different *a/d* ratios

Figure 3.9 shows the results of the analysis performed on the beam B4 for different fiber volume ratios. The process was same as for the Figure 3.8, where three different curves were created to analyze the impact of changing angle β. Two of the curves are again overlapping, while the one with β equal to 0 results in slightly higher predicted shear strength. From the results it can be concluded, that the impact on the shear strength of the beam by using different angle β is insignificant. The scenario with the simplest assumption, where β is equal to zero has been implemented within the final model.

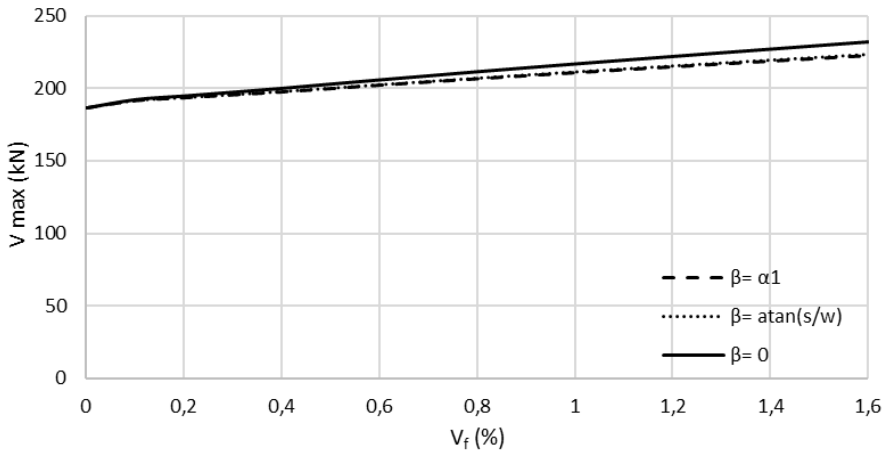

Figure 3.9 Variation of the angle β given different fiber volume ratios

In order to illustrate the additional force introduced into the five-spring model Figure 3.10 highlights effect of the 0.5% volume of fibers introduced into the sample beam previously chosen to describe the five-spring model in the Chapter 2.3 of this thesis. The figure represents the equilibrium of forces for Δ_c equal to 5 mm. The force V_F is indicated with the bold yellow curve and the increased shear strength is depicted in red. It can be seen, that the main difference caused by the addition of fibers is in the sum of shear forces $V = \sum V_i$ whose value has increased by the shear force provided by the fibers. The value indicated by the dotted line represents the value of the shear force before the fibers were added. The shear strength provided by fibers shows a decreasing tendency for increasing tensile strain. Such phenomenon is caused by the dependency of the shear strength on the width of the crack, where the width of the crack increases with increasing average tensile strain.

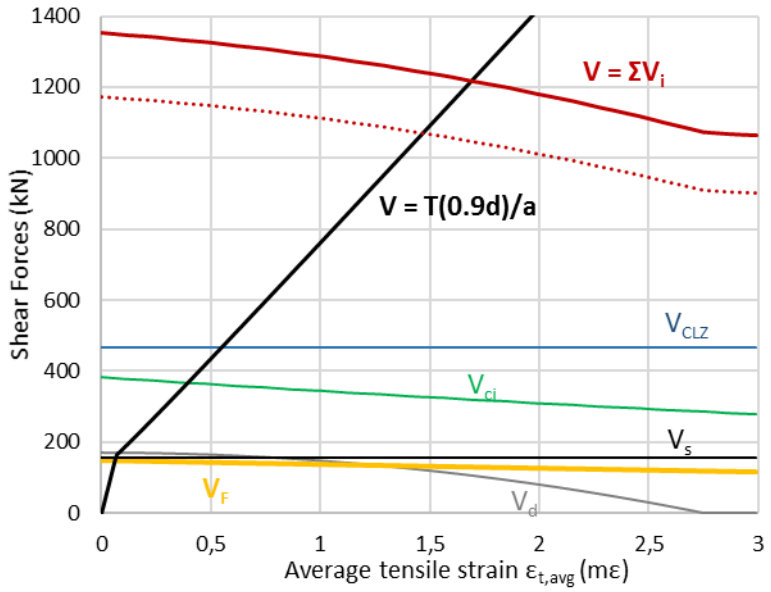

Figure 3.10 Equilibrium of forces in extended five-spring model with fiber contribution at Δ_c=5 mm

Figure 3.11 shows the effect of fibers on the overall V-Δ response of the member. Thick yellow curve represents the contribution of fibers and the red curve the overall response. The response of the member before adding fibers is represented with red dotted line to highlight the difference caused by addition of fibers. As it can be observed from the figure, the fibers start acting as soon as the deformation begins. The biggest contribution of the fibers occurs at the deformation of about 3 mm from which the curve starts slowly decreasing. The addition of 0.5% of fibers provides the beam with an increase of about 200 kN in shear resistance and also higher post-peak resistance.

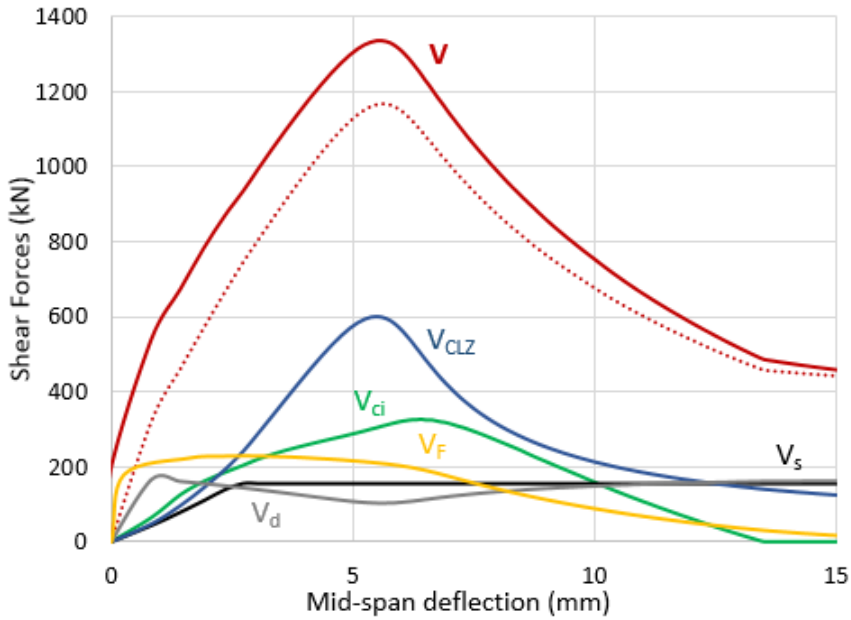

Figure 3.11 Predicted V-Δ response with addition of fibers

3.3 TENSION-STIFFENING OF THE BOTTOM FLEXURAL REINFORCEMENT

3.3.1 Introduction

As it was described before, steel fibers are used in concrete members to compensate for the low tensile strength and brittle response of the material. Given the constitutive equations for the springs in the five-spring model, it is necessary to consider the effect of fibers on the tensile force in the bottom reinforcement which is described in the original five-spring model by Mihaylov (2015) for the cracked stage of the behavior of the member as:

$$T = E_s A_s \varepsilon_{t,avg} + \frac{0.33\sqrt{f'_c}}{\sqrt{1+200\varepsilon_{t,avg}}} A_{c,eff} \leq A_s f_y \tag{36}$$

Where the first term of this equation describes the behavior of bare elastic reinforcement and the second term describes the tension stiffening effect of the concrete around the reinforcement. However, the tension behavior of FRC members with conventional reinforcement (R/FRC) is significantly different from the behavior of members without fibers. As described in a study by Lee et al. (2013) the contribution of fibers to the tensile stress is considerable as illustrated in Figure 3.12.

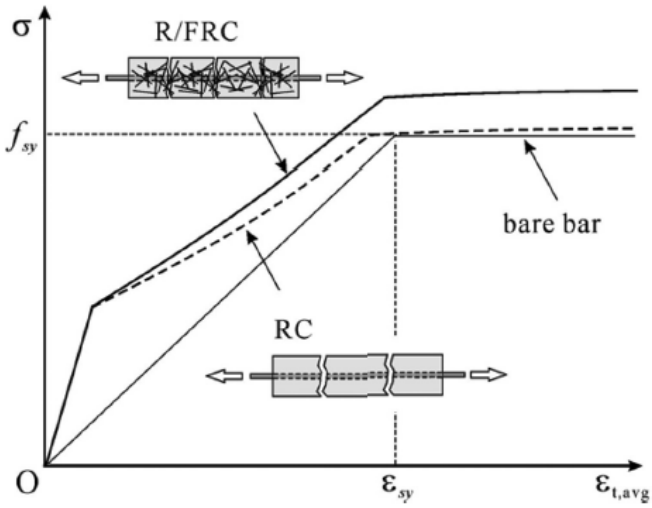

Figure 3.12 Tensile behavior of RC and R/FRC members by Lee et al. (2013)

As we can see in the Figure 3.12, R/FRC is able to resist higher tensile stresses not only after initial cracking, but also after yielding of the bar. Due to this additional resistance the equation for the tensile force in the bottom reinforcement will be modified based on the model proposed by Lee et al. (2013) on tension-stiffening for steel fiber-reinforced concrete containing conventional reinforcement. The model proposed by Lee et al. (2013) reflects the effect of steel fibers on the tensile behavior of R/FRC member and is based on the DEM model whose simplified version has been already described in the previous chapter of this thesis. Other researchers have also researched the tension-stiffening behavior of R/FRC members, but such

models proposed by Bischoff (2003) or Deluce and Vecchio (2013) evaluate only the total tensile stresses. The tensile stresses due to fiber and the bond mechanism between the concrete matrix and the reinforcing bar cannot be separately evaluated in their models, while the model developed by Lee et al. (2013) allows us to do so. In the model proposed by Lee et al. (2013) the tensile resistance of the R/FRC member is divided into three different components which are summed up in the end. The effect of concrete matrix, fibers and tension-stiffening or softening are all evaluated separately, while in the other models only the total tensile resistance is evaluated.

Figure 3.13a highlights tensile force T which is going to be affected by the addition of fibers. Figure 3.13b illustrates the difference between the tensile force of the original five-spring model, that does not include the effect of fibers, and the resulting tensile force with fibers included in the concrete mixture causing tension-stiffening effect.

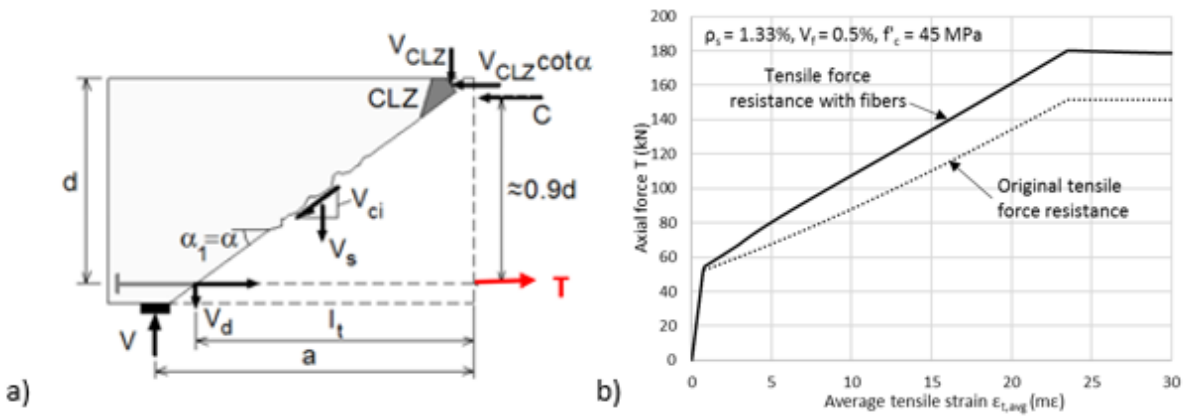

Figure 3.13 Illustration of implemented modification due to tension-stiffening effect

3.3.2 Formulation of Tension-Stiffening Model for R/FRC

The tensile stress resistance of R/FRC consists of three terms: tensile stress resistance of the reinforcing bar, tensile stress resistance of the steel fibers, and tensile stress from tension-stiffening or tension-softening effect, whichever is larger. The final formulation of the tensile force in the bottom reinforcement including fibers can be described as follows:

$$T_f = F_{reb} + F_{fib} + F_{con} \tag{37}$$

Where F_{reb} is the tensile force of the reinforcing bar, F_{fib} is the tensile force of the fibers, and F_{con} the tensile force from tension-stiffening or tension-softening effect. In this chapter all of these expressions will be described and analyzed in detail, and then T_f will be used to calculate the shear force derived from moment equilibrium in the five-spring model.

The first term of the equation describes the tensile force resisted by the bare bar, this force is evaluated the same way it was described in the original five-spring model and thus can be defined as:

$$F_{reb} = E_s A_s \varepsilon_{t,avg} \leq A_s f_y \tag{38}$$

The second term refers to the tensile force resisted by steel fibers and is expressed as follows:

$$F_{fib} = f_f A_{c,eff} \tag{39}$$

Where $A_{c,\,eff}$ is the area of concrete around the bottom reinforcement that contributes to the tension-stiffening effect and can be calculated as:

$$A_{c,eff} = 2.5b(h-d) \leq bh/2 \tag{40}$$

Because the tensile stresses sustained by the steel fibers are calculated for a given crack width while the tensile stress due to tension stiffening is calculated for given average tensile strain, it is necessary to define the relationship between the crack width and the average tensile strain. Average crack spacing model has been defined based on the model proposed by Deluce (2011) where average crack spacing is defined as:

$$s_{cr} = 2\left(c + \frac{s_b}{10}\right)k_3 + \frac{k_1 k_2}{s_{mi}} \tag{41}$$

Where s_b is the maximum spacing between reinforcing bars and the rest of the variables are expressed as follows: $c = 1.5a_g$ $k_1 = 0.4$ $k_2 = 0.25$

Where a_g is the maximum aggregate size.

$$s_{mi} = \frac{\rho_s}{d_b} + \frac{\alpha_f V_f}{d_f} max\left(\frac{\frac{l_f}{d_f}}{50}, 1\right) \tag{42}$$

$$k_3 = 1 - \frac{\min(V_f, 0.015)}{0.015}\left[1 - \min\left(\frac{50}{\frac{l_f}{d_f}}, 1\right)\right] \tag{43}$$

Where d_b is the diameter of the reinforcing bar and ρ_s is the ratio of the reinforcement within the concrete area $A_{c,eff}$. Having estimated the crack spacing, the width of the crack that will be applied within the SDEM to define the tensile stress f_f is defined as:

$$w_{cr,T} = s_{cr}\varepsilon_{t,avg}$$

The last term of the equation (37), to define the tensile force in the bottom reinforcement, describes the tension-stiffening/tension-softening provided by the concrete and is expressed as follows:

$$F_{con} = f_{ct} A_{c,eff} \tag{44}$$

Where f_{ct} is the tension response due to bond mechanism of the reinforcing bar and is described as:

$$f_{ct} = \max(f_{c,soft}, f_{c,TS}) \leq E_c \varepsilon_{t,avg} \tag{45}$$

Where the elastic modulus of concrete matrix E_c for fiber reinforced concrete is defined as $E_c = 3300\sqrt{f'_c} + 6900$, as presented in the CSA A23.3-04 (2004) and $f_{c,TS}$ is the tension-stiffening effect that reflects the effect of steel fibers and was derived by Lee et al. (2013). The model is based on the conventional tension-stiffening model for reinforced concrete members by Bentz (2005) and is modified to take into account the effect of steel fibers as follows:

$$f_{c,TS} = \frac{f_{cr}}{1 + \sqrt{3.6 c_f M \varepsilon_{t,avg}}} \tag{46}$$

Where M is the bond parameter defined as $M = \frac{A_{c,eff}}{\sum d_b \pi}$ and c_f is the coefficient to consider the effect of steel fibers which was defined based on a parametric study performed by Lee et al (2013). Only the variables with significant influence on the tension-stiffening response have been taken into account such as percentage of conventional reinforcement, fiber volumetric ratio and fiber type. Based on the parametric study the following values for c_f were proposed:

- for straight fibers

$$c_f = 0.6 + \frac{1}{0.058}\left(\frac{l_f}{d_f}\right)^{0.9} \frac{100 V_f}{M^{0.8}} \tag{47}$$

- for hook-ended fibers

$$c_f = 0.6 + \frac{1}{0.034}\left(\frac{l_f}{d_f}\right) \frac{(100 V_f)^{1.5}}{M^{0.8}} \tag{48}$$

3.3.3 Validation of the Tension-Stiffening Model for R/FRC

Based on the Tension-Stiffening model a code in Matlab was developed using the formulation described in the previous section. The code to account for tension-stiffening within the five-spring model can be found in Appendix C. The developed model will be validated against data provided by Lee et al. (2013) and experimental results. The validation includes results from application of the Tension-Stiffening model by Lee et al. (2013) and provided experimental data by Bischoff (2003) and Deluce and Vecchio (2013).

3.3.3.1 Experimental results by Bischoff (2003)

In the test eight axially loaded tension specimens were tested. Each specimen had a cross-section size of 100x100 mm. Two ratios of reinforcement were tested using either single 15 M bar or 20 M bar with final reinforcement ratios of 2% and 3.1%, respectively. Members were divided into two groups of four where for each reinforcement ratio were produced four

members. Three out of those four members were additionally reinforced with 0.78% fiber volumetric ratio and one of the three specimens contained an un-bonded reinforcing bar.

Conclusion of the experiment by Bischoff (2003) is that after cracking, fiber reinforced members experience more tension-stiffening than plain concrete. The difference becomes more obvious once a sufficient number of cracks have developed. It has been also observed that while plain concrete does not exhibit any tension-stiffening once the reinforcement yields, fiber reinforced concrete continues to exhibit tension-stiffening after yielding since the fibers are able to transmit additional tensile forces across the crack where the steel rebar has yielded.

For the validation only two fiber reinforced specimens were considered, each with different amount of reinforcement ratio and both with bonded reinforcing bar. The fibers used in this experiment were end-hooked fibers, 50 mm long with diameter of 0.5 mm. Shrinkage of the member has been measured within the experiment and implemented into the code to reflect the real behavior of the member.

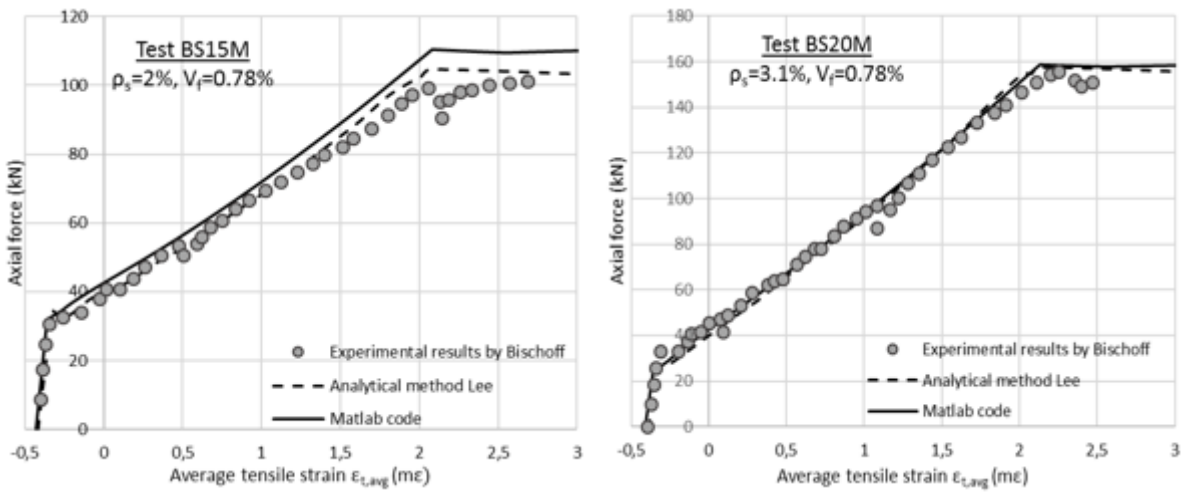

Figure 3.14 Comparison of proposed models and test results by Bischoff (2003)

Figure 3.14 compares results of the experiment carried out by Bischoff (2003), results obtained by Lee et al. using proposed tension-stiffening model and results obtained with the created Matlab code. It can be observed that both models copy the behavior of the experiment quite well. Slight difference in test BS15M between the analytical results by Lee et al. (2013) and created code is most likely due to the simplification of the DEM used in the code. While Lee et al. (2013) have applied the DEM within their method, the Matlab code defines stress attainable by fibers using the SDEM, which does not account for fiber rupture as it has been explained before. Thus it is possible that in the experiment with 2% reinforcement ratio some fiber rupture already appears that the Matlab code cannot capture, while in the test BS20M thanks to the 3.1% reinforcement ratio no fiber rupture appears.

3.3.3.2 Experimental results by Deluce and Vecchio (2013)

Experimental investigation carried out by Deluce and Vecchio consisted of tests on total of 12 uniaxial tension reinforced concrete specimens and 48 uniaxial tension R/FRC specimens. In

this case, parameters studied within the experiment were the fiber volumetric ratio, fiber length, fiber aspect ratio, conventional reinforcement ratio and reinforcing bar diameter. In his thesis Deluce (2011) describes the tests in detail including numerous material tests. However, for the purpose of validation only two tests were selected. Selected specimen had cross section of 150x150 mm, and concrete strength of 45 MPa and 80 MPa. Two different fiber volumetric ratios were considered, 0.5% and 1% of fibers in the concrete matrix. Fibers used in this experiment were end-hooked with length of 30 mm, diameter of fibers 0.38 mm and conventional reinforcement with diameter 19.5 mm and reinforcement ratio of 1.33%.

Based on the experimental results Deluce and Vecchio (2013) concluded that steel fiber added to the concrete mixture with conventional reinforcing bar improves the cracking characteristics and tension-stiffening behavior and that they can increase the post-yield load-carrying capacity to levels significantly higher than the bare-bar yield load. They also came to a conclusion that fiber length does not appear to play a significant role in the post-cracking behavior of SFRC containing conventional reinforcing bars, provided that the crack spacing is not so short that a fiber bridges multiple cracks.

Due to the unclear definition of cracking strength of concrete, an assumption has been made in order to match the curve of the proposed model. In this experiment the effect of shrinkage has not been included within the final graph. As presented in Figure 3.15 the proposed model by Lee et al. (2013) agrees very well with the results of Deluce and Vecchio and also with the proposed Matlab code.

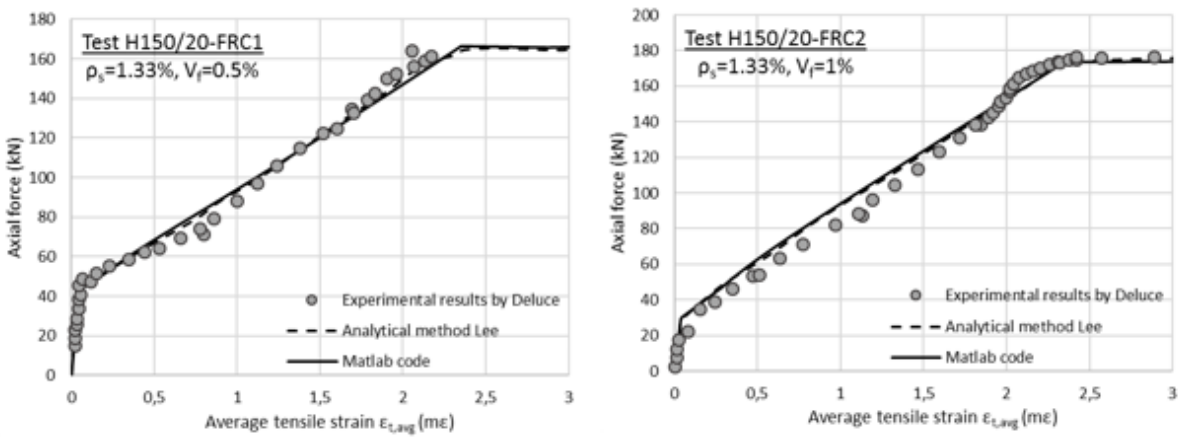

Figure 3.15 Comparison of proposed models and test results by Deluce and Vecchio (2013)

3.3.3.3 Conclusion

Given the experimental results of Bischoff (2003) and Deluce and Vecchio (2013) it can be concluded that developed model simulates correctly the tension-stiffening behavior of R/FRC members. Thanks to the Tension-Stiffening model derived by Lee et al. (2013) it is possible to evaluate the tension force resistance of each of the considered parts of the member and thus the impact of fibers, concrete matrix and conventional reinforcement can be evaluated separately as shown in the Figure 3.16. A limitation that should be considered while implementing the

code is the same as for the SDEM and thus that fiber rupture should not occur and is not being accounted for in the model.

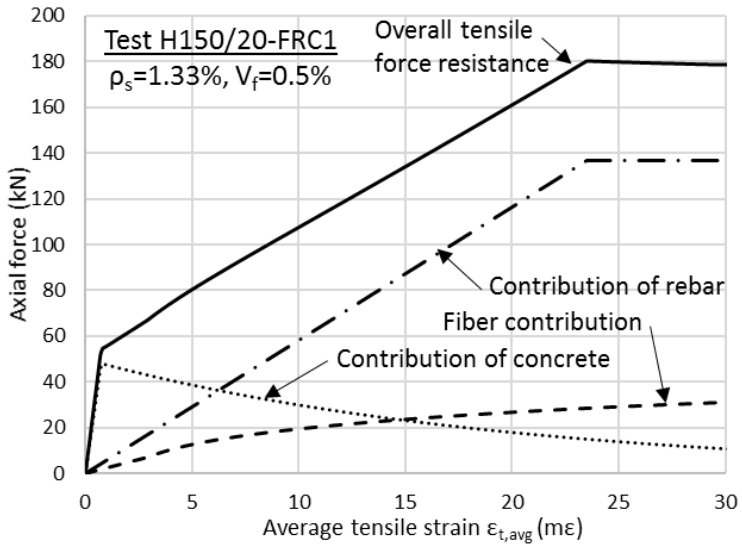

Figure 3.16 Separate evaluation of contribution of tensile forces in Tension-stiffening model

3.3.4 Implementation of the Tension-Stiffening Model into the Five-Spring Model

Within the five-spring model, the Tension-Stiffening model has been included just as it has been described in the formulation of the model. The only change concerns the definition of tensile force contribution from the rebar, where the yielding of the bar was neglected in order to focus on shear failures of deep beams.

After obtaining the tension force in the bottom flexural reinforcement using tension-stiffening model, moment equilibrium equation of the shear span is used to define the shear force. The equilibrium is calculated about the point of application of the compression force in the section with maximum moment as presented by Mihaylov (2015), and the final equation to determine the shear force can be described as follows:

$$V = \frac{T_f(0.9d)}{a} \tag{49}$$

Where d is the effective depth and a is the shear span of the member, and V in this case represents the force in the flexural spring of the five-spring model.

In order to illustrate the modification introduced into the five-spring model, the tension-stiffening model was implemented into the sample beam example previously used in sections 2.3 and 3.2.4. In the Figure 3.17 the thick black curve represents the shear force derived from the moment equilibrium, which is influenced by the tension stiffening model. The dotted curve represents the original shear force derived from moment equilibrium. As it can be observed from the figure, the tension-stiffening does not influence the result significantly. However, the transition of the curve results in a change of equilibrium points obtained through intersection of the thick black curve with the rest of the curves.

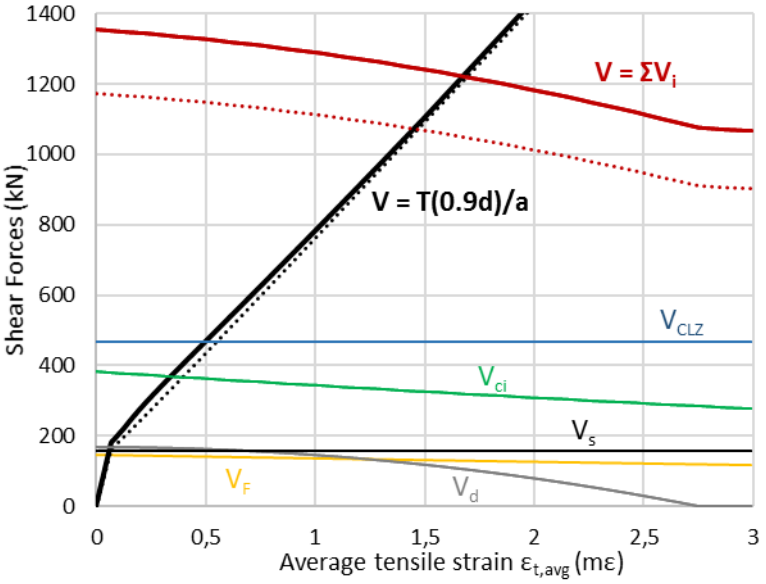

Figure 3.17 Equilibrium of forces in extended five-spring model with tension-stiffening model at Δ_c=5 mm

Figure 3.18 illustrates the effect that tension-stiffening has on the load displacement curve. Slightly steeper orientation of the curve causes that forces influenced by strain in bottom reinforcement change their values from the original model due to the transition of the equilibrium points. The original values are depicted with dotted lines within the graph, while the values corresponding to the tension-stiffening model and addition of fibers are illustrated with solid lines. The tension-stiffening effect influences very slightly the values of most of the shear forces. The only forces that are not affected are the critical loading zone, whose value is consistent and does not depend on the strain in bottom flexural reinforcement, and the effect of fibers. Overall, the effect of tension stiffening does not significantly influence the resistance of the member unless a very high volume of fibers is included in the mixture.

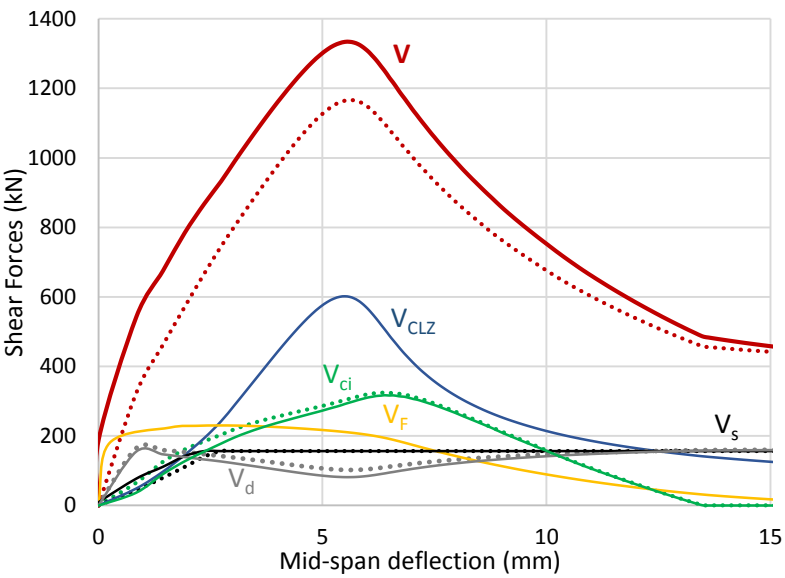

Figure 3.18 Predicted V-Δ response with implementation of tension-stiffening model

3.4 COMPRESSIVE BEHAVIOR OF THE CRITICAL LOADING ZONE

3.4.1 Introduction

Apart from enhanced tensile strength that the addition of fibers provides significant increase in toughness, in compression has been observed in fiber reinforced concrete members. Traditionally, transverse reinforcement is adopted to improve the toughness of concrete in compression. However, the use of steel fibers has advantages over transverse reinforcement, namely less labor cost and shorter construction time. Steel fibers bridge longitudinal cracks caused by the lateral expansion of concrete in compression. As the cracks widen, the pull-out strength of fibers increases the toughness of the member as described by Ou et al. (2012).

Figure 3.19a illustrates the effect of fibers on compression behavior of the member within the five-spring model. The resistance of the critical loading zone is increased due to the inclusion of fibers and the ultimate shear strength increases. Figure 3.19b describes shear resisted by critical loading based on transverse displacement of the critical loading zone, the solid line describes behavior with fibers and the dotted line without fibers.

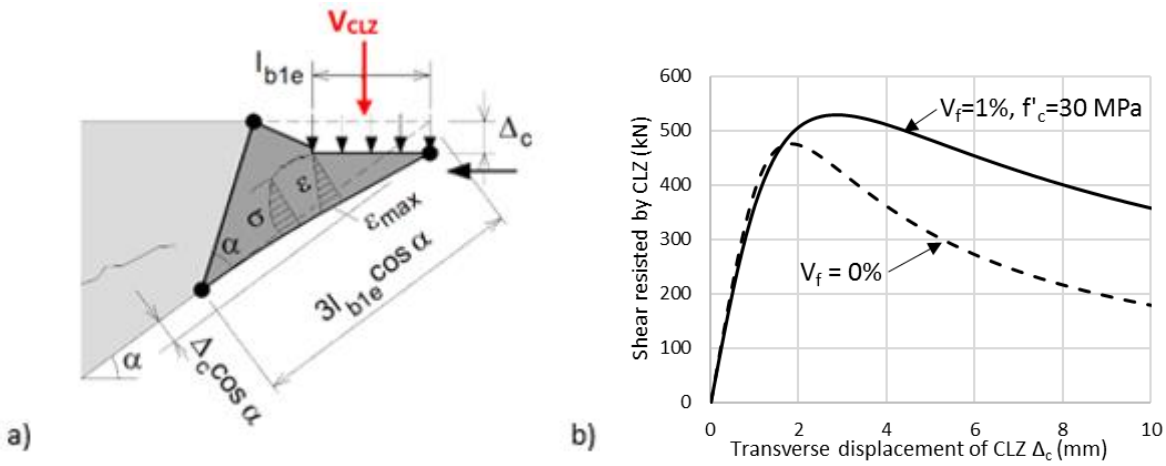

Figure 3.19 Illustration of modification due to change of stress-strain curve of concrete in compression

Many researchers have performed experiments in order to describe the compressive stress-strain response of FRC. The most recognized formulation is by Di Prisco et al. (2013) where it is concluded that when using FRC, compressive strength is not particularly influenced by the presence of fibers up to 1% of content by volume. However, in the extended five-spring model, fiber volumetric ratios higher than 1% are taken into account as well. It is necessary to adjust the stress-strain curve to reflect the effect of fibers on the concrete under uniaxial compression using a different model suitable for fiber volumes higher than 1%.

In the original model, the compressive behavior of concrete is described using Popovics (1970) definition of stress-strain relationships for concrete as follows:

$$f_c = f'_c \frac{n\left(\frac{\varepsilon_{cf}}{\varepsilon'_c}\right)}{n - 1 + \left(\frac{\varepsilon_{cf}}{\varepsilon'_c}\right)^{nk}} \tag{50}$$

Where f'_c is the peak stress obtained from a cylinder test, ε'_c is the strain when the stress f_c reaches f'_c and is described as:

$$\varepsilon'_c = \frac{f'_c}{E_c}\frac{n}{n-1} \tag{51}$$

Factor k increases the post-peak decay in stress, for $\frac{\varepsilon_{cf}}{\varepsilon'_c} < 1$ k is taken as 1, and for $\frac{\varepsilon_{cf}}{\varepsilon'_c} > 1$ as:

$$k = 0.67 + \frac{f'_c}{62} \tag{52}$$

However, k must not be taken less than unity.

Curve fitting factor n is defined as:

$$n = 0.8 + \frac{f'_c}{17} \tag{53}$$

Tangent stiffness E_c, when ε_{cf} equals zero and described as:

- for normal strength concrete

$$E_c = 4730\sqrt{f'_c} \tag{54}$$

- for concrete strength higher than 40 MPa

$$E_c = 3320\sqrt{f'_c} + 6900 \tag{55}$$

3.4.2 Stress-Strain Curves for FRC

The next section evaluated the effect of steel fibers with fiber volumes higher than 1% on the compressive behavior of FRC. Several proposals from various researchers are presented and analyzed in order to choose the most adequate model that is to be used within the five-spring model. As a comparison Popovics (1970) stress-strain curve was used to ensure correct behavior of concrete in the pre-peak branch of the curve.

3.4.2.1 Barros and Figueiras (1999)

In the experimental study of Barros and Figueiras (1999) five series were manufactured where fiber percentage, fiber aspect ratio and water-to-cement ratio were the parameters whose influence was of the main focus. Cylinder specimens, 150 mm in diameter and 300 mm in height with concrete strength varying from 30 – 60 MPa, were tested under displacement control. Only two of the series were used to determine the compression behavior from which each series consisted of four specimens. In those two series end-hooked fibers were used with length of 60 mm, diameter equal to 0.8 mm and strength of 1100 MPa.

The analytical approach suggested by Barros and Figueiras is similar to Ezeldin and Balaguru (1992) where only one parameter is proposed and the whole expression is based on the following stress-strain relationship:

$$f_c = f'_c \frac{\frac{\varepsilon_{cf}}{\varepsilon'_c}}{(1-p-q) + q\left(\frac{\varepsilon_{cf}}{\varepsilon'_c}\right) + p\left(\frac{\varepsilon_{cf}}{\varepsilon'_c}\right)^{(1-q)/p}} \tag{56}$$

$$q = 1 - p - \frac{E_c}{E_{cf}} \qquad p + q \in \,]0,1[\qquad \frac{1-q}{p} > 0 \tag{57}$$

$$E_{cf} = \frac{f'_c}{\varepsilon_{cf}} \tag{58}$$

$$E_c = 21500\left(\frac{f'_c}{10}\right)^{1/3} \tag{59}$$

Where for fibers with length of 30 mm and diameter 0.5 mm:

$$\varepsilon'_c = \varepsilon_{c0} + 0.0002W_f \tag{60}$$

$$p = 1 - 0.919e^{-0.394W_f} \tag{61}$$

$$\varepsilon_{c0} = 0.0022 \tag{62}$$

$$W_f = 325V_f \tag{63}$$

And for fibers with length of 60 mm and diameter 0.8 mm:

$$\varepsilon'_c = \varepsilon_{c0} + 0.00026W_f \tag{64}$$

$$p = 1 - 0.722e^{-0.144W_f} \tag{65}$$

Where ε_{c0} is the strain at peak for plain concrete and W_f is the fiber weight percentage in the mixture. Proposed analytical approach has been validated against experimental results and showed a good agreement. In order to evaluate the model, the model was applied on an example specimen with concrete strength of 40 MPa, fiber volumetric ratio 1%, fiber length of 30 mm and fiber diameter 0.5 mm and compared to results with curve proposed by Popovics (1970). As it can be seen in the Figure 3.20 the strain at maximum concrete strength is higher which is one of the effects that prove that fibers have influence on the compression behavior of concrete.

The effect of fibers on the post peak behavior is significant and instead of brittle failure which appears in case of regular concrete, FRC exhibits more ductile behavior.

It can be concluded that model by Barros and Figueiras (1999) represents the stress-strain compression behavior quite well, however it should be taken into account that only one fiber aspect ratio was considered in the study, so it is questionable whether proposed model reasonably represents the effect of aspect ratio of steel fibers on compressive behavior.

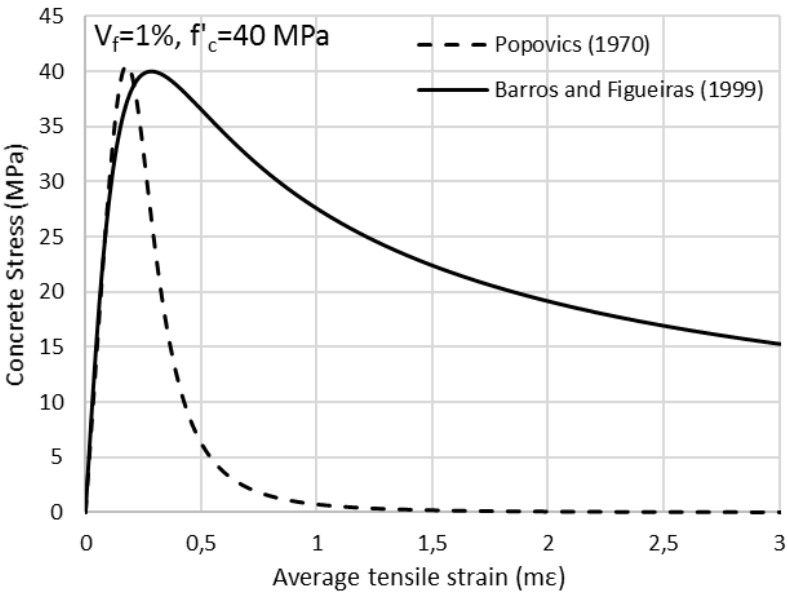

Figure 3.20 Analytical proposal of stress-strain compression curve by Barros and Figueiras (1999)

3.4.2.2 Lee, Oh and Cho (2015)

Experimental study of Lee et al. (2015) consisted of tests on 48 cylinder specimens subjected to uniaxial compression. Specimens had a size of 150 mm in diameter and 300 mm in height. Several variables were investigated including concrete compressive strength, fiber volumetric ratio, and fiber aspect ratio. Fiber volumetric ratio was ranging from 0.5% to 2% and end-hooked steel fibers of three different fiber aspect ratios (47%, 65%, 79%) were used. Concrete strength varied from 40 MPa to 90 MPa.

Results of the experiments showed that the compressive strength increased slightly with increasing fiber volumetric ratio up until 1.5% of fiber volume while with 2% of fiber volume the compressive strength slightly decreased. This phenomenon has been previously described by Ezeldin and Balaguru (1992) and is assumed to be caused by the transverse confinement effect of the steel fibers which restrain the lateral expansion of SFRC specimens. Due to observed changes in slump effect while changing the aspect ratio and fiber volumetric ratio it was concluded that the compressive strength of SFRC can be affected by the fiber aspect ratio as well as the fiber volumetric ratio.

In the analytical model the effect of steel fibers was represented by employing the fiber reinforcing index $RI_v = V_f l_f / d_f$ which has been previously introduced by several researchers

such as Ezeldin and Balaguru (1992) and Mansur et al. (1999) and is implemented in the model as follows:

$$f_c = f'_c \frac{A\frac{\varepsilon_{cf}}{\varepsilon'_c}}{A - 1 + \left(\frac{\varepsilon_{cf}}{\varepsilon'_c}\right)^B} \tag{66}$$

$$\varepsilon'_c = (0.0003RI_w + 0.0018)f'^{\,0.12}_c \tag{67}$$

$$E_c = (-367RI_w + 5520)f'^{\,0.41}_c \tag{68}$$

$$RI_w = 3.25RI_v \tag{69}$$

Where A and B are parameters to reflect the effect of the steel fibers on compressive behavior and are defined as:

$$A = B = \frac{1}{1-\frac{f'_c}{\varepsilon'_c E_c}} \quad \text{for} \quad \frac{\varepsilon_{cf}}{\varepsilon'_c} \leq 1 \tag{70}$$

$$A = 1 + 0.723(RI_w)^{-0.957} \tag{71}$$

$$B = \left(\frac{f'_c}{50}\right)^{0.064}[1 + 0.882(RI_w)^{-0.882}] \geq A \text{ for } \frac{\varepsilon_{cf}}{\varepsilon'_c} > 1 \tag{72}$$

Analytical model by Lee et al. (2015) has been implemented on hypothetical specimen previously considered for Barros and Figueiras (1999) example and compared with Popovics (1970) curve. As it can be seen on the Figure 3.21 the pre-peak behavior agrees well with all the models but there is a considerable difference between the post-peak behavior of the curve obtained by Barros and Figueiras (1999) which assumes much higher stresses in concrete than Lee et al. (2015).

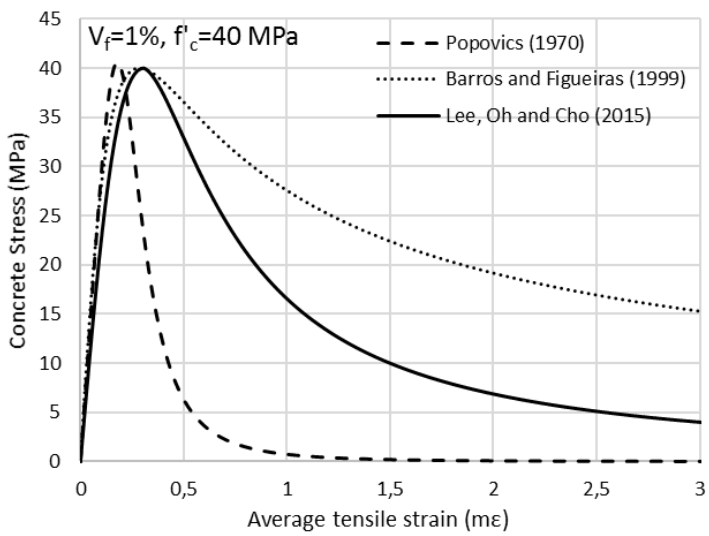

Figure 3.21 Analytical proposal of stress-strain compression curve by Lee et al. (2015)

3.4.2.3 Ou, Tsai, Liu and Chang (2012)

In the experimental study 40 specimens were tested with variation of diameter of the fiber, fiber length and fiber volumetric ratio. Compressive strength of concrete was 40 MPa. Steel fibers used in the study were end-hooked and had tensile strength of 1000 MPa. Maximum reinforcing index taken under consideration was 1.7 due to reduced workability of the concrete mixture that has been observed with higher reinforcing index. All the specimens had diameter of 150 mm and height of 300 mm.

Based on the experiment it was concluded that since the modulus of elasticity fluctuated as the reinforcing index increased, the reinforcing index has low impact on the value of modulus of elasticity. For the compressive strength, little correlation with the reinforcing index was observed in the pre-peak branch but for the post-peak it was confirmed that fibers significantly contribute to the ductility of the material. Strain at the peak stress tends to increase with reinforcing index based on the obtained results. It was also observed that the toughness limit of the material was reached at a fiber volume fraction of approximately 2% for all steel fibers and that long fibers (50 – 60 mm) outperformed short fibers (30 mm).

An analytical model developed by Ou et al. (2012) is based on a model proposed by Carreira and Chu (1985) and predicts a slightly steeper descending branch at a reinforcing index of 1.7 than at a reinforcing index of 1.3. The proposal, given that $\varepsilon_{c0} = 0.002$ is following:

$$\varepsilon'_c = \varepsilon_{c0} + 0.0007(RI_v) \tag{73}$$

$$\beta = 0.71(RI_v)^2 - 2(RI_v) + 3.05 \tag{74}$$

$$f'_{cf} = f'_c + 2.35(RI_v) \tag{75}$$

$$f_c = f'_{cf} \frac{\beta\left(\frac{\varepsilon_{cf}}{\varepsilon'_c}\right)}{\beta - 1 + \left(\frac{\varepsilon_{cf}}{\varepsilon'_c}\right)^{\beta}} \tag{76}$$

Proposed model has been also implemented on the same hypothetical specimen as previous models and Figure 3.22 shows obtained results. It can be observed that model proposed by Ou et al. (2012) shows very good agreement with model by Lee et al. (2015) however the concrete compressive peak strength is assumed to be slightly higher and strain at peak a bit lower.

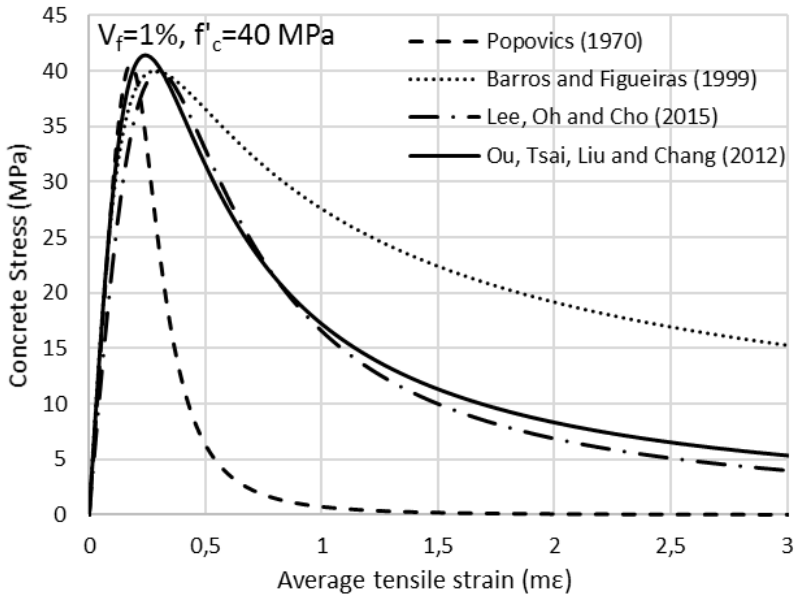

Figure 3.22 Analytical proposal of stress-strain compression curve by Ou et al. (2012)

3.4.2.4 Mansur, Chin and Wee (1999)

Experimental study of Mansur et al. (1999) investigated high-strength concrete members with end-hooked fibers with 0.5 mm diameter and length of 30 mm. Fiber volumetric ratios that were tested were 0.5%, 1% and 1.5%. In order to define the shape effect, three different shapes were casted for the experiment. Tested specimens consisted of 100x200 mm cylinders, 100 mm cubes and 100x100x200 prisms.

Based on results it was concluded, that for vertically casted prisms and for cylinders, inclusion of fibers caused smaller initial tangent modulus while for horizontally casted prisms the fibers have practically no influence on the initial tangent modulus. Regarding the shape effect it was concluded that fiber volumetric ratio effect was found to be smaller for cylinders. Regarding compressive strength of the material it was concluded that vertically cast specimens are likely to exhibit higher strengths than those casted horizontally.

Proposed analytical model is following:

$$f_c = f'_c \frac{\beta\left(\frac{\varepsilon_{cf}}{\varepsilon'_c}\right)}{\beta - 1 + \left(\frac{\varepsilon_{cf}}{\varepsilon'_c}\right)^{\beta}} \qquad \text{for} \qquad 0 \leq \frac{\varepsilon_{cf}}{\varepsilon'_c} \leq 1 \tag{77}$$

$$f_c = f'_c \frac{k_1\beta\left(\frac{\varepsilon_{cf}}{\varepsilon'_c}\right)}{k_1\beta - 1 + \left(\frac{\varepsilon_{cf}}{\varepsilon'_c}\right)^{k_2\beta}} \qquad \text{for} \qquad 1 \leq \frac{\varepsilon_{cf}}{\varepsilon'_c} \tag{78}$$

$$k_1 = \left(\frac{50}{f'_c}\right)^3 [1 + 2.5(RI_v)^{2.5}] \tag{79}$$

$$k_2 = \left(\frac{50}{f'_c}\right)^{1.3} [1 - 0.11(RI_v)^{-1.1}] \tag{80}$$

$$E_c = (10300 - 400V_f)f'^{\frac{1}{3}}_c \tag{81}$$

$$\varepsilon_{c0} = (0.0005 + 00000072RI_v)f'^{\frac{1}{3}}_c \tag{82}$$

$$\beta = \frac{1}{[1 - (f'_c/\varepsilon_{c0}E_c)]} \tag{83}$$

Figure 3.23 shows that for given hypothetical specimen the analytical prediction of Mansur et al. (1999) agrees well with the model proposed by Popovics (1970) for the ascending branch. For the post-peak behavior, we can see that there is significant increase in stresses as it is expected due to presence of fibers.

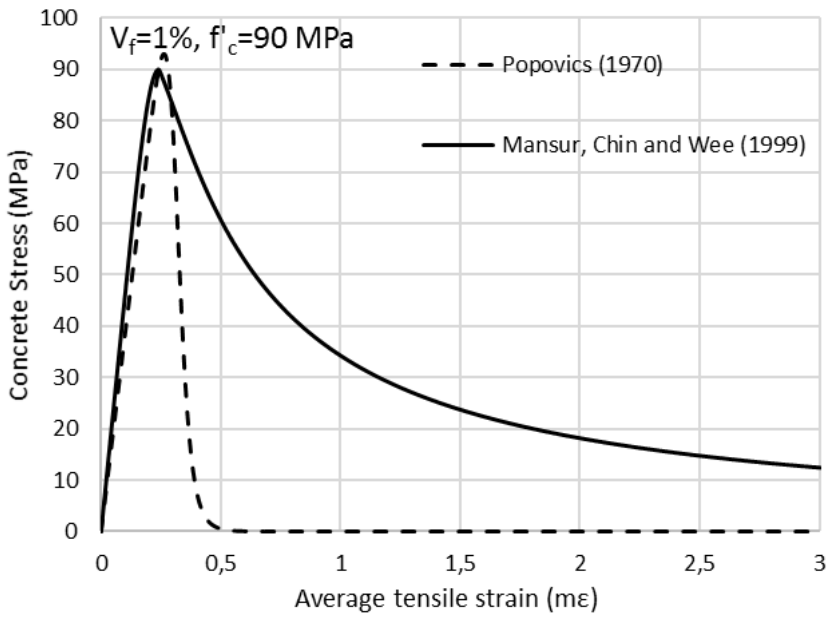

Figure 3.23 Analytical proposal of stress-strain compression for high-strength concrete by Mansur et al. (1999)

3.4.2.5 Conclusions

All of the previously mentioned models were compared and their limitations taken into account while selecting the most suitable stress-strain curve for the five-spring model. In the proposal by Barros and Figueiras (1999) the main problem was the limitation of the model to two specific fiber types and only one fiber aspect ratio, which does not provide accurate simulation of behavior of FRC for other fiber aspect ratios. It is also questionable whether the model estimates the behavior of the FRC after it reaches the peak stress correctly. The proposal by Lee et al. (2015) takes into account different fiber aspect ratios and is more conservative in the post-peak branch but if low amounts of fiber volumetric ratio are being considered, the resulting curve

does not capture the behavior correctly. Also, the curve by Lee et al. (2015) cannot be applied on the regular concrete without fiber inclusion.

Most suitable analytical method and method considered within the five-spring model is the proposal by Ou et al. (2012). This method takes into account different fiber aspect ratios and thus is not limited to one type of fibers, gives reasonable results for lower fiber volume ratios, can also be used for regular concrete without fiber inclusion, has a more conservative assumption for the post-peak behavior of the concrete than Barros and Figueiras (1999) and its pre-peak behavior agrees well with behavior described by Popovics (1970). However, one significant limitation has to be taken into account and that is the range of concrete strength considered within the method that only covers concrete strengths of 30 – 60 MPa and thus cannot be implemented for high-strength concretes.

In order to include high-strength concrete in the five-spring model, for concretes with strength higher than 50 MPa the method proposed by Mansur et al. (1999) was implemented. This method is suitable for different fiber aspect ratios and the assumption of post-peak behavior is as conservative as the model by Ou et al. (2012). The limitation in this case is that it cannot be used for regular concrete without fiber inclusion. In order to provide a solution for cases without fibers, Popovics (1970) curve was implemented in the five-spring model to describe the behavior of concrete under compression if no fibers are included.

3.4.3 Implementation of the Stress-Strain Curve into the Five-Spring Model

Adjusted stress-strain curve for FRC under uniaxial compression has been implemented in the five-spring model based on the given conclusions. For deep beams without fiber reinforcement and any concrete strength Popovics (1970) curve is used for the calculation of stress in the critical loading zone. For regular strength concretes with inclusion of fibers, the proposal by Ou et al. (2012) has been implemented and the definition of elastic modulus is taken according to Lee et al. (2015). For high-strength concrete the five-spring model uses the definition of stress-strain relationship by Mansur et al. (1999). The formulation of the methods used in the model is exactly as mentioned in the description of each analytical method.

After obtaining the stress-strain curve the area under the curve is computed as follows:

$$\Omega(\varepsilon) = \int_0^{\varepsilon} f_c \, d\varepsilon \approx \sum_i \frac{f_c(\varepsilon_i) + f_c(\varepsilon_{i-1})}{2(\varepsilon_i - \varepsilon_{i-1})} \tag{84}$$

Where the right-hand-side of the equation is the numerical integration of the integral using the trapezium rule. The strain axis is divided into small constant intervals $\Delta_\varepsilon = \varepsilon_i - \varepsilon_{i-1}$, and the area under the f_c curve within each interval is approximated as a trapezium.

Average diagonal compressive stress in the critical loading zone is computed:

$$\sigma_{avg} = -\frac{\Omega}{\varepsilon} \tag{85}$$

Where the ε represents the diagonal compressive strains in the CLZ which increase with increasing imposed shear distortion of the CLZ Δ_c. The code describing the calculation of the σ_{avg} within the five-spring model can be found in Appendix D. Obtaining σ_{avg} allows us to compute the shear carried in the critical loading zone:

$$V_{CLZ} = \sigma_{avg} b l_{b1e} \sin^2(\alpha) \tag{86}$$

Figure 3.24 and 3.25 highlight the modification introduced into the five-spring model using a stress-strain curve with consideration of fibers. Figure 2.24 illustrates the effect for given imposed displacement. The dotted lines represent values obtained using the original five-spring model and solid lines are values obtained from modified five-spring model. Thick blue line represents increased value of shear force provided by the critical loading zone. The only curve that is affected by the change of stress-strain response of FRC is the V_{CLZ}. The value remains constant, as it is not dependent on the strain in the bottom flexural reinforcement, however its value increases significantly due to the action of fibers.

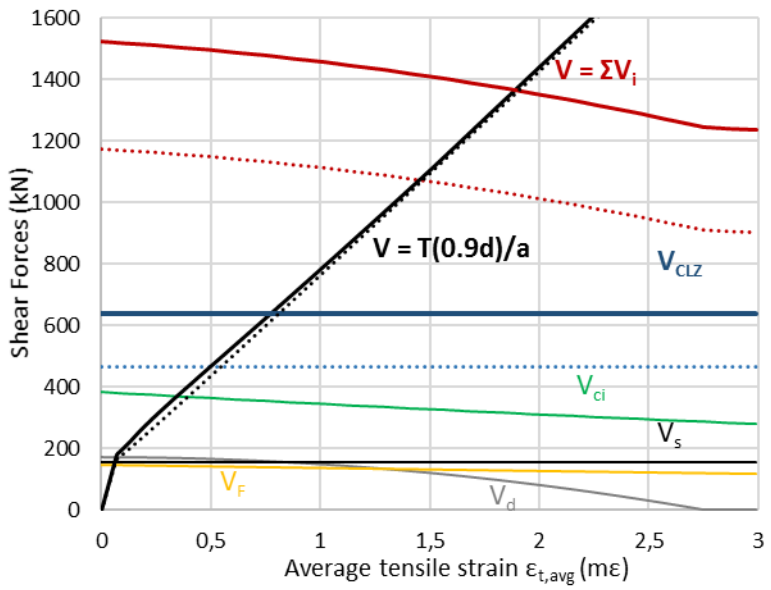

Figure 3.24 Equilibrium of forces in extended 5sm with adjusted stress-strain curve at Δ_c=5 mm

Figure 3.25 illustrates the influence of modification on the load-displacement curve. The only curve affected by the modification is the V_{CLZ} due to the shift of the curve representing shear force provided by V_{CLZ} showed in Figure 2.24. The original V_{CLZ} curve is depicted with blue dotted line while the modification with blue solid curve. As it is shown in the figure, adjusted stress-strain curve has mainly impact on the post-peak behavior of the beam. Overall, the inclusion of fibers results in less brittle behavior of the member in the post-peak branch of the curve.

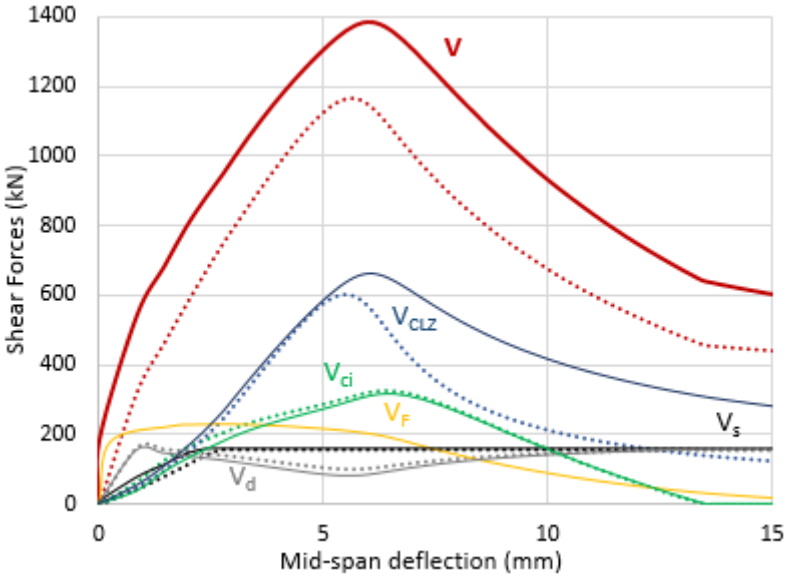

Figure 3.25 Predicted V-Δ response with modified stress-strain curve

3.5 DEFLECTIONS

3.5.1 Introduction

The original five-spring model only accounts for deflection in three-point loading where the deflection of the beam is equal to deflection under the loading point. In the extension of the model due to limited experimental results, it became one of the crucial points to take into account also deflection in four-point loading. Experimental results by Mansur and Ong (1991), which served for the validation of the extended five-spring model, tested all the members in four-point loading. In order to be able to compare the maximum deflection obtained from the five-spring model and the experiment, it was necessary to include the additional deflection in the original five-spring model. While in the three-point loading the calculated deflection under the loading point is equal to the midspan deflection in four-point loading an additional value that accounts for the difference in deflection under the loading point and the midspan needs to be introduced.

3.5.2 Definition of the Additional Deflection

Given the assumption that plane sections remain plane in bending, the value of the additional deflection can be taken as a sum of two deflections:

$$\Delta_1 = \Delta_{11} + \Delta_{12} \tag{87}$$

Where:

$$\Delta_{11} = \frac{\phi {l_s}^2}{8} \tag{88}$$

$$\Delta_{12} = \frac{\phi l_s}{2} a \tag{89}$$

Where l_s is the distance between the loading points, which in case of three-point loading is equal to zero and the curvature φ is described as:

$$\phi = \frac{Va}{E_c I_{cr}} \tag{90}$$

So the final formulation of the additional deflection is:

$$\Delta_1 = \frac{Va}{E_c I_{cr}} \left(\frac{{l_s}^2}{8} + \frac{l_s}{2} a \right) \tag{91}$$

Where the I_{cr} is the moment of inertia of cracked section and for cases without compression steel is calculated as follows:

$$I_{cr} = \frac{bk^3 d^3}{3} + nA_s (d - kd)^2 \tag{92}$$

And the coefficients are defined as follows:

$$n = \frac{E_s}{E_c} \tag{93}$$

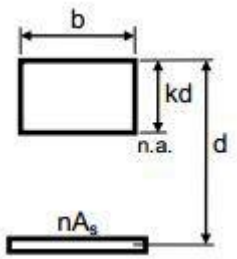

$$B = \frac{b}{nA_s} \tag{94}$$

$$I_g = \frac{bh^3}{12} \tag{95}$$

$$kd = \frac{\sqrt{2dB + 1} - 1}{B} \tag{96}$$

Where E_c is the tangent modulus of fiber-reinforced concrete and I_g is the moment of inertia of un-cracked section.

3.5.3 Implementation of the Additional Deflection into the Five-Spring Model

Within the extended five-spring model the additional deflection to account for four-point loading is added to the sum of the deflection of the shear span due to elongation of the bottom longitudinal reinforcement Δ_t and the shear distortion of critical loading zone Δ_c. Final formulation of the overall deflection at the midspan is defined as follows:

$$\Delta = \Delta_c + \Delta_t + \Delta_1 \tag{97}$$

Where Δ is the overall deflection when defining the shear strength and displacement capacity of deep beams under single curvature.

4 VALIDATION OF THE EXTENDED FIVE-SPRING MODEL

4.1 INTRODUCTION

Developed extended five-spring model as shown in Appendix E is validated against existing experimental results. Two experimental studies were considered for the validation, one being the study of FRC deep beams in shear by Mansur and Ong (1991) and another experimental study by Mansur and Alwist (1984) on FRC deep beams with web openings where one of the control specimens was considered without openings and thus relevant for the validation of the extended five-spring model.

Validation consists of comparisons of the experimental results with extended five-spring model and results obtained from a finite element model. Analyses of the effect of fiber volumetric ratio and effect of shear span over effective height ratio were carried out, where four different fiber volumetric ratios and five different *a/d* ratios were tested and compared within the experimental study.

In the end, results of the comparisons are discussed and a validation of the model is provided with corresponding figures. A verification for FRC beams with high shear reinforcement is performed and relevant issues that arise with high shear reinforcement ratios are discussed and explained.

4.2 SAMPLE SPECIMEN EVALUATION

In order to validate the extended five-spring model, one representative specimen was selected from the experimental study of Mansur and Ong (1991) and analyzed in detail. Out of ten specimen tested in the experimental study five had variety of shear span to depth ratios from 0.31 to 1.85. Four of the specimens were tested to analyze the effect of fiber volume ratio varying from 0% to 2%. From these specimens the most representative one was selected being the specimen B4 with 1% fiber volume ratio and *a/d* of 1.23.

Selected specimen is 500 mm high and has a width of 90 mm. Effective depth has been calculated based on provided drawings of the setup to 463 mm. Length of the specimen is 1590 mm which gives a shear length of 570 mm. Concrete strength of the specimen is 31.1 MPa with maximum aggregate size of 10 mm. Flexural reinforcement of the beam is provided by four reinforcing bars of 16 mm in diameter, yield strength 440 MPa and reinforcement area of 804 mm^2 which gives a reinforcement ratio of 1.93%. The beam has additional web reinforcement provided by bars with diameter 6 mm and yield strength 375 MPa with spacing in transversal direction of 110 mm and in longitudinal direction of 125 mm which gives a reinforcement ratio of 0.27% and 0.47%, respectively. Fibers used in this experimental study were 30 mm long straight fibers, slightly twisted and with square cross section and sides length of 0.5 mm. In order to get equivalent diameter of fiber that is used in the extended five-spring model, perimeter of the square was calculated from which the corresponding diameter was expressed as 0.564 mm. Longitudinal length of loading plates is 80 mm and is equal to the support plates.

The beam is loaded in four-point loading where distance between the loading plates is equal to 200 mm.

Mansur and Ong (1991) provide a detailed description of behavior of the beam throughout the experiment. According to Mansur and Ong (1991) in the early stages of loading the beam behaved in a truly elastic manner giving a linear load-deflection curve. Diagonal crack within the shear span was the first one to form and is described to appear approximately at mid-depth of the beam with extension towards both the support and the loading points. Further increase in load resulted in the propagation and widening of the existing cracks while simultaneously new diagonal cracks developed more or less parallel to the existing ones. Some of the cracks originated vertically, but later became inclined in a diagonal direction. Flexural cracks propagated within the constant moment region of the beam but only after formation of diagonal cracks and, according to Mansur and Ong (1991), they hardly reached the mid-depth of the beam. At load ranging from 80% - 90% of the ultimate load, one of the diagonal cracks began to grow excessively wide, finally leading to failure which for this particular beam was at load of 228 kN. At impending failure, some crushing of the concrete was observed between the loading points and the tip of the major inclined crack. The failure load of the beam and its cracking patterns can be observed in Figure 4.1.

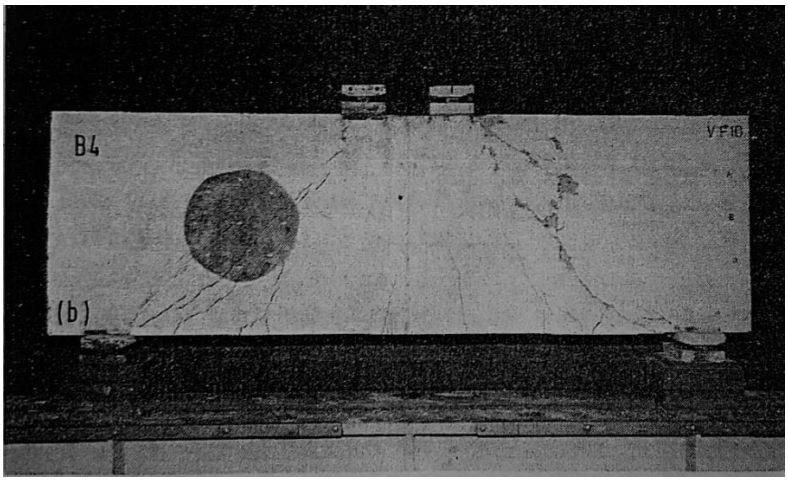

Figure 4.1 Cracking pattern and mode of failure of beam B4 by Mansur and Ong (1991)

All of the previously described properties of the beam were implemented into the extended five-spring model and a load-deformation curve was generated, the curve can be seen in Figure 4.2. Based on the detailed description of behavior of the beam throughout the experiment some general assumptions of the five-spring model theory can be validated against real life observations. One of the main assumptions of the five-spring theory is a formulation of a critical diagonal crack. In this case the crack propagated as expected and also was the reason of the failure of the beam as assumed in the model. Furthermore, the experiment description also mentions the presence of crushing of the concrete between the loading points and the tip of the major inclined crack which is in the five-spring model described as crushing of the critical loading zone.

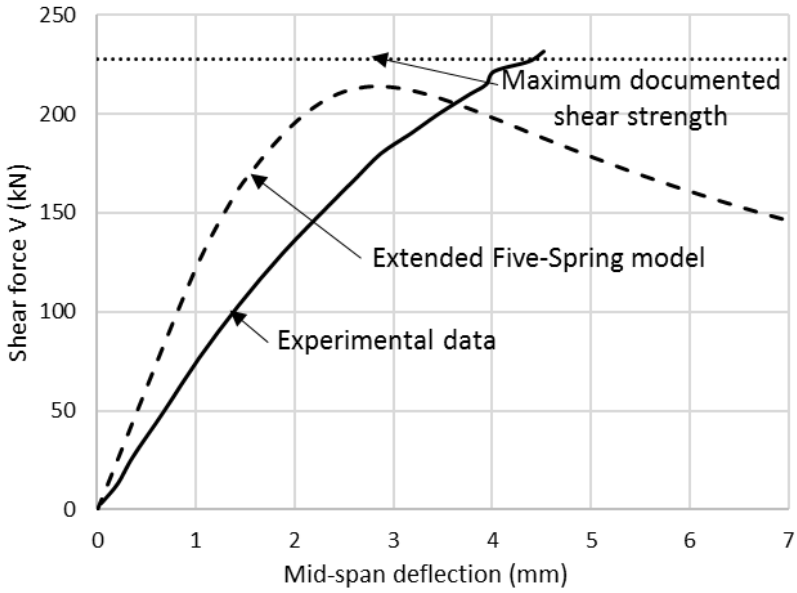

Figure 4.2 Comparison of load-deflection curves for beam B4 obtained from five-spring method and experimental results by Mansur and Ong (1991)

As it can be seen in Figure 4.2, ultimate shear strength obtained from the five-spring method is more conservative than the shear strength obtained in the test. Shear capacity obtained by the five-spring method is 214 kN, which gives ratio between experimental result and prediction of 1.06. As it can be observed from Figure 4.2, deformations of the experimental results are slightly higher than the five-spring predictions, which results in the deformation at a peak strength of 4.5 mm for the test and only 2.8 mm for the five-spring model. Such difference can be caused by the settlement of supports due to high compression forces applied to the beam during the loading.

In order to evaluate the effect of support settlement and to define its impact on the overall deflections of the beam, a finite element model (FEM) was created using a VecTor2 program for 2D static and dynamic analysis of reinforced concrete structures. The analysis was carried out by Jian Liu (2016) who provided the results for the comparisons. The sample specimen was modeled in the software using same properties as the five-spring model and specimen B4 in the experimental study. Force method using a load step of 2 kN was applied in order to define the shear strength of the member. Resulting curve can be seen in Figure 4.3 which also includes experimental and five-spring model results.

From Figure 4.3 we can observe that the shear resistance is slightly higher than the experimental result. For the finite element model the failure occurs at shear force of 238 kN which gives ratio of experimental shear resistance to FEM prediction of 0.96. For the FEM the shear failure occurs at 3 mm deflection which supports the theory of overestimated deformation in the experimental study and suggests that some settlement of supports, that might have not been accounted for, takes place in the experimental study.

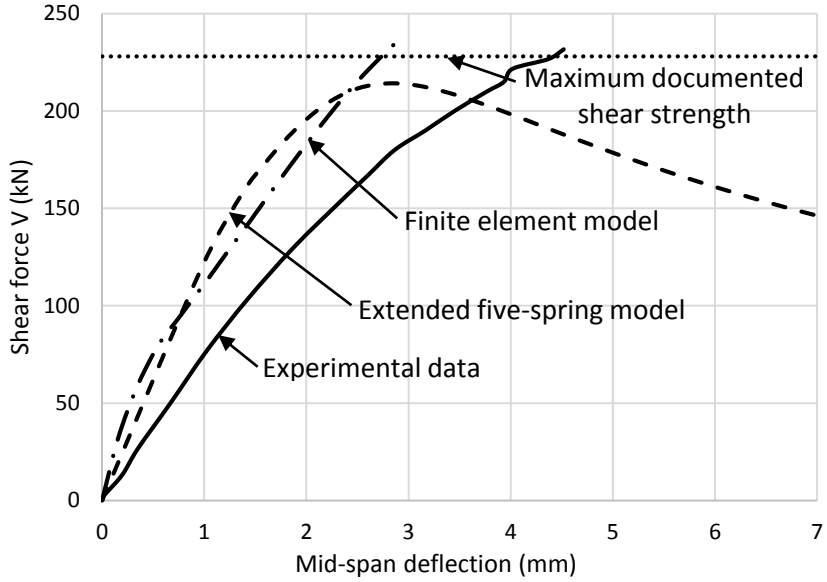

Figure 4.3 Comparison of load-deflection curves for beam B4 obtained from finite element model, five-spring method and experimental results by Mansur and Ong (1991)

Figure 4.4 pictures the cracking pattern of one half of the beam B4 right before the failure as predicted by the FE model. The formation of diagonal cracks corresponds to the formation of cracks as described in the experimental study, as well as the flexural cracks in the constant moment region which only propagated to the mid-depth of the beam at the moment of the failure. Additional cracking can be observed on the edge of the beam where horizontal cracks started forming, as well as cracking on top of the beam with some vertical cracks, these cracks do not copy the real cracking behavior of the beam as observed in the experimental study and are most likely caused by incorrect simulation of cracking by the FE model.

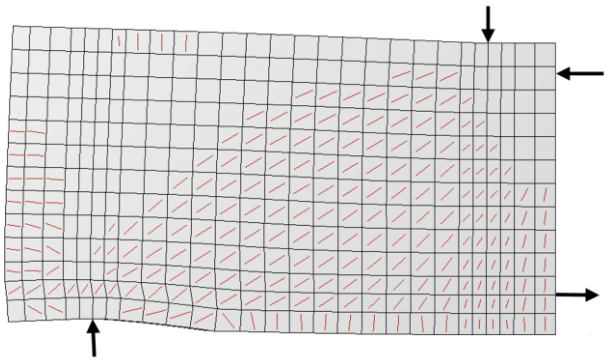

Figure 4.4 Cracking pattern of the beam B4 obtained by the FE analysis

4.3 EFFECT OF FIBER VOLUMETRIC RATIO

In the experimental study, Mansur and Ong (1991) have focused on two main parameters one of which was the effect of fiber volumetric ratio. Based on their study they concluded that adding fibers to the concrete mixture significantly influenced cracking behavior of the beams. The experiment showed that increase of fiber volume ratio decreased maximum crack width and also average crack width at all load levels. Higher fiber volume ratio also resulted in smaller concrete strains and smaller deflections at a particular load level. Increasing fiber content increased both the cracking and ultimate strengths of the beams.

The effect of fiber volume ratio on the ultimate shear strength is shown in Figure 4.5. Apart from the experimental results and VecTor2 results, Figure 4.5 shows also the effect of fiber volume ratio according to the extended five-spring model. Separate curves represent the shear strength provided by each of the springs of the five-spring model. The biggest shear resistance is provided by the critical loading zone and the stirrups. For the extended five-spring model an average compressive strength of 33.1 MPa was implemented to generate the average curve of the behavior of the specimen, and different fiber volume ratios with step of 0.1% were applied to generate resulting curve. Results show that the model created in VecTor2 overestimates the ultimate shear strength at lower fiber volumes, however the extended five-spring model copies the behavior of the beams quite accurately with comparison to the experimental results.

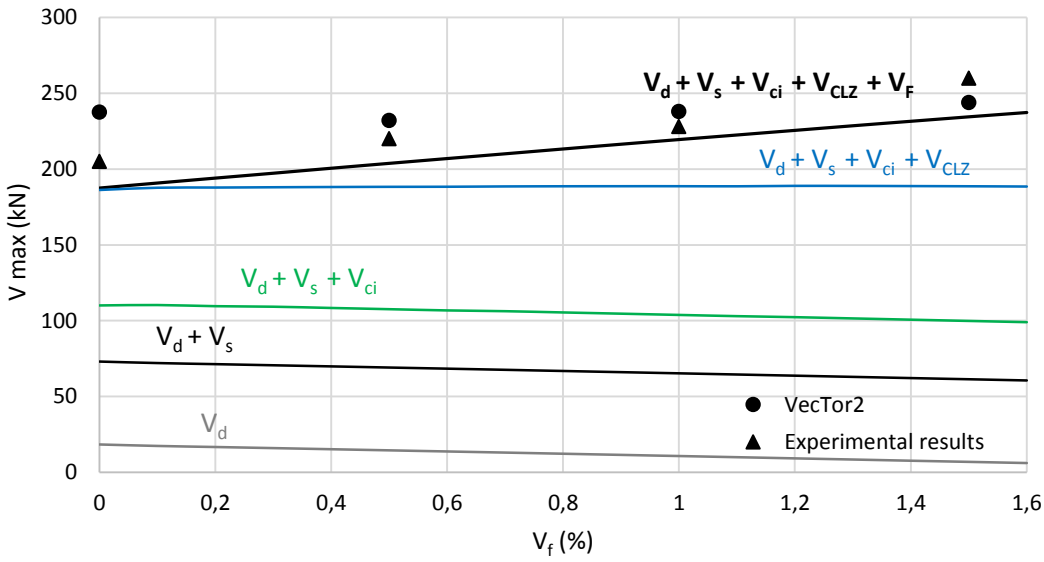

Figure 4.5 Effect of fiber volume ratio on ultimate shear strength

4.4 EFFECT OF *A/D* RATIO

Second parameter analyzed in the experimental study of Mansur and Ong (1991) was shear-span-to-depth (*a/d*) ratio. Five different *a/d* ratios were considered in the study of Mansur and Ong (1991), varying from 0.31 to 1.85. Shear length of the members varied from 740 mm to 2140 mm and the concrete cylinder strength varied from 31.1 MPa to 35.7 MPa. All of the

tested specimen had the same longitudinal and transversal reinforcement ratios of 1.93% and 0.27%, respectively and fiber volume ratio of 1%.

Conclusions of the experimental study state that shortening of shear span reduced the occurrence and extent of the flexural cracking. In the member with the highest *a/d* ratio of 1.85, flexural cracks appeared first followed by diagonal cracking. In the beam with *a/d* ratio of 1.23, both flexural and diagonal cracking occurred almost simultaneously and for the beam with *a/d* ratio of 0.93, diagonal cracks were the first ones to form. In tested beams with ratios 0.31 and 0.62 no flexural cracking was observed up to failure. It was also concluded that an increase in *a/d* ratio decreases the stiffness of the beam.

Within the extended five-spring model an average concrete cylinder strength of 33.9 MPa was implemented to obtain the corresponding behavior of the members and gradually increasing *a/d* value with step of 0.1 was implemented to generate the *a/d* ratio curve. Due to limited time, only one member with *a/d* ratio of 1.23 was analyzed in VecTor2 software and included in the comparison of the effect of *a/d* ratio, properties of the member were the same as the corresponding specimen used in the experimental study.

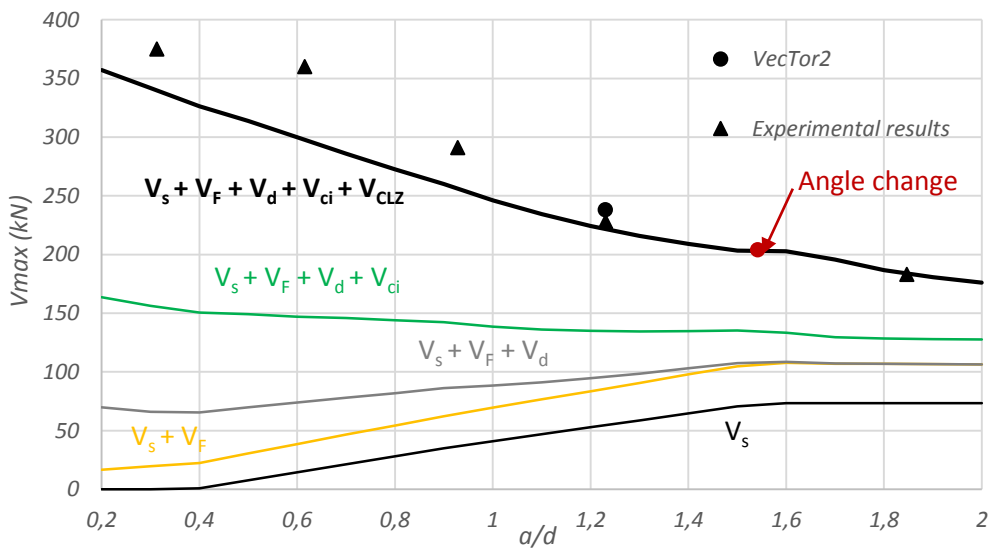

Figure 4.6 Effect *a/d* ratio on ultimate shear strength

Figure 4.6 shows results from the experimental study compared with one result from VecTor2 and curve generated using the extended five-spring model. Separate curves show the influence of each of the springs of the five-spring model. From the graph we can observe that for *a/d* ratio up to 1.6 the biggest contribution is caused by critical loading zone, while after *a/d* ratio of 1.6 the stirrups provide the most shear strength. Proposed analytical model copies the behavior of the member well, however a sudden change of the slope of the curve occurs around *a/d* of 1.6. The cause of such change is most likely the change of the angle of critical crack as defined in the model, which changes when the beam is transitioning from deep beam to slender beam. Highlighted on the curve is a point, where the angle of critical crack α_1 changes its value from

α to θ, determined using the extended five-spring method. α is the angle of line connecting inner end of support plate l_{b2} and outer end of the loading plate l_{b1} and is described as follows:

$$\alpha = \text{atan}\frac{h}{a_{eff}} \tag{98}$$

Where h is the height of the member and effective shear span a_{eff} is defined as:

$$a_{eff} = a_{c1} + l_{b1e} \tag{99}$$

$$a_{c1} = a - \frac{l_{b1}}{2} + \frac{l_{b2}}{2} \tag{100}$$

$$l_{b1e} = \max(\frac{V}{P} l_{b1}, 3a_g) \tag{101}$$

Where a_{c1} is the distance between the facing edges of the loading plate and support plate and l_{b1e} is the effective width of loading plate parallel to longitudinal axis of member which is defined as the maximum of either three times the size of aggregate or contribution of length of the loading plate defined by the ratio of shear force to applied point load. The value of angle θ, which is the angle of the shear cracks obtained from sectional shear models for slender beams, is in this case simplified to the value of 35°, however can be defined using level three approximation described in *fib* MC2010 (2013).

4.5 DISCUSSION

Finally, conclusions based on the results obtained from the performed analyses are made and a discussion about the results is carried out. In order to verify the results obtained using the extended five-spring theory, a load-displacement curve was plotted for four specimens from experimental study of Mansur and Ong (1991) along with the curve obtained in the experiment. Curve obtained using the extended five-spring model captures well the ultimate shear strength of the model, however the deflections are smaller at a particular load level and the stiffness of the model is overestimated. An explanation for such behavior could be the settlement of supports, caused by the high compression force applied on the beam. Since the material of the support plates and its stiffness was not defined in the article by Mansur and Ong (1991) and the settlement of the supports was not measured to provide another explanation, finite element analysis of the beams was performed.

Finite element analysis was performed by Jian Liu (2016) with the same properties as described in the experiment and the obtained load-displacement curves were compared with the experimental and analytical ones. Results obtained by using the finite element analysis captured well the ultimate shear strength of the specimen according to the experiments, however the deflections were again smaller at a particular load level and the stiffness of the model was overestimated. The finite element analysis showed good agreement with the analytical results and thus it can be concluded that the main reason for the difference in deflections and stiffness is the settlement of supports.

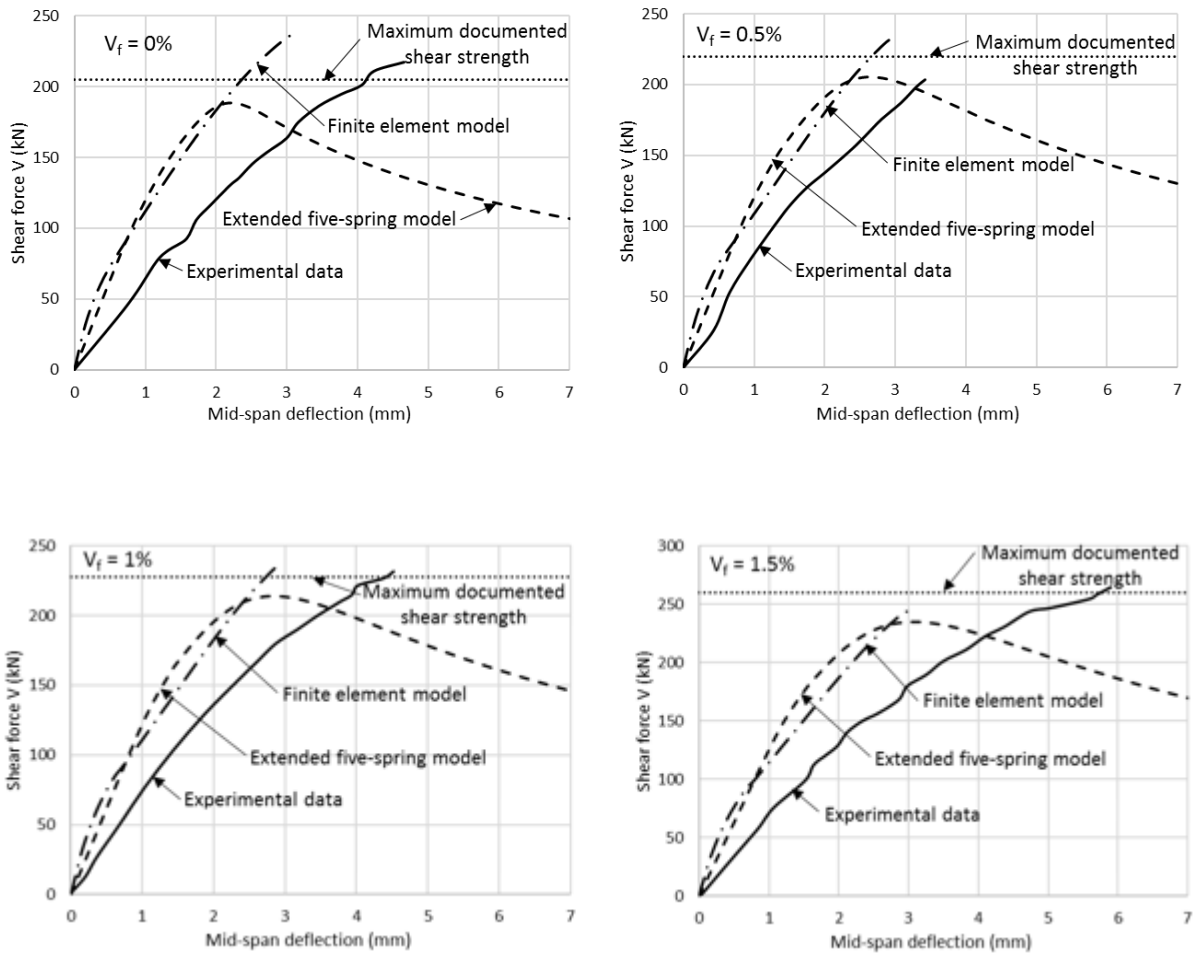

Figure 4.7 Comparison of results obtained by FEM and five-spring model for different fiber volumetric ratios

Figure 4.7 shows comparisons of results obtained from the experimental study performed by Mansur and Ong (1991), extended five spring model and VecTor2 analysis for four different specimens with varying fiber volume ratios, B4, B6, B7 and B8. The ocumented shear strength depicted in the graphs with dotted line is the ultimate shear strength of the member as defined by Mansur and Ong (1991).

Apart from the displayed comparisons, all the members from specimens from Mansur's experimental studies relevant for the extended five-spring model were analyzed and the ultimate shear strength for each member was predicted. Table 4.1 shows most important properties of each beam and ratio of experimental over predicted ultimate shear strength.

Table 4.1 Standard deviation and coefficient of variation of results obtained with extended five-spring model

Beam Name	a/d	d (mm)	V_f (%)	l_f (mm)	d_f (mm)	ρ_l (%)	f_c' (MPa)	ρ_v (%)	V_{exp} (kN)	V_{pred} (kN)	$\frac{V_{exp}}{V_{pred}}$
B1	0,36	463	1	30	0,56	1,93	35,7	0,42	375	350	1,07
B2	0,62	463	1	30	0,56	1,93	35,7	0,49	360	307	1,17
B3	0,93	463	1	30	0,56	1,93	35,5	0,48	291	262	1,11
B4	1,23	463	1	30	0,56	1,93	31,1	0,47	228	214	1,06
B5	1,85	463	1	30	0,56	1,93	31,5	0,49	183	177	1,04
B6	1,23	463	-	-	-	1,93	34,4	0,47	205	190	1,08
B7	1,23	463	0,5	30	0,56	1,93	33,8	0,47	220	205	1,07
B8	1,23	463	1,5	30	0,56	1,93	33,2	0,47	260	235	1,11
B9	1,51	463	1	30	0,56	1,93	29,5	0,48	224	195	1,15
B10	1,51	463	1	30	0,56	1,93	30,1	1,26	290	299	0,97
WO-1/1	0,58	624	1	30	0,40	0,81	40	0,43	345	355	0,97
										Average:	1,07
										Standard deviation:	0,064
										Coefficient of variation:	0,060

Given results from Table 4.1 it can be concluded that the shear strength obtained using the extended five-spring model shows good accuracy when compared to the experimental results. With coefficient of variation of 6% it can be concluded that the effect of fibers has been well represented within the extended five-spring model, and the five-spring model is now able to capture not only behavior of regular deep beams, but also fiber reinforced concrete deep beams.

5 PARAMETRIC STUDY

5.1 INTRODUCTION

To study the effects of several variables, a parametric study was carried out using the extended five-spring model. First a sample beam was created, properties of the beam were based on an experimental beam from tests by Mihaylov (2008). Properties of the sample beam as used in the study are described in Table 5.1. The beam is considered to be loaded in three-point loading and reinforced with straight fibers.

Table 5.1 Properties of a sample beam for parametric study

a/d	b (mm)	d (mm)	h (mm)	l (mm)	ρ_l (%)	A_s (mm^2)	$\varnothing_l$ (mm)	No. $bars_l$	f_y (MPa)
1,55	400	1095	1200	3900	0,70	3060	25	6	650

V_f (%)	l_f (mm)	d_f (mm)	l_{b1} (mm)	l_{b2} (mm)	a_g (mm)	f_c' (MPa)	f_{yv} (MPa)	ρ_v (%)	$\varnothing_v$ (mm)
1	30	0,5	300	150	20	40	490	0,1	10

Variables investigated in the parametric study were the effect of *a/d* ratio, effect of longitudinal reinforcement, shear reinforcement, fiber volume ratio and size effect. Each of the investigated variables was adjusted within each parametric study, with the rest of the properties remaining as described in the Table 5.1. Some of the parameters were evaluated for beams with no shear reinforcement, most of the studies were carried out for three different fiber volume ratios of 0%, 1% and 2%. The last study investigated the effectiveness of fiber and shear reinforcement. The impact of each parameter included within the study is evaluated and described in this chapter.

5.2 PARAMETRIC STUDY

5.2.1 *a/d* Ratio

First, the effect of the shear-span-to-depth ratio was evaluated. The range of the ratio taken into account varied from 0.5 to 2.5 *a/d*. The effect was investigated for fiber volume ratios of 0%, 1% and 2%. For each of the fiber volume ratios a curve was created by generating the shear capacity for given *a/d* ratio where the step of 0.1 was used. Sample beam with no shear reinforcement was considered in this part of study to focus on the effect of fibers.

The results of the study are shown in Figure 5.1. Horizontal axis describes the values of *a/d* ratio, and the vertical axis represents the shear strength of the beam for given *a/d* ratio. Three different lines represent three different fiber volume ratios. The black dots mark the point of change of the angle α_1 from α to θ as explained previously in Chapter 2.2. From the graph we

can observe gradual decrease of shear strength for increasing *a/d* ratios, where for the shortest considered ratio the shear resistance has the highest value. For the highest *a/d* ratio the shear strength of the beam shows to be the lowest. The shear strength resisted by the beam between the ratios 0.5 and 2.5 dropped by 78% for the beam with no fiber reinforcement, by 73% for 1% of fibers, and 69% for 2% of fiber volume ratio.

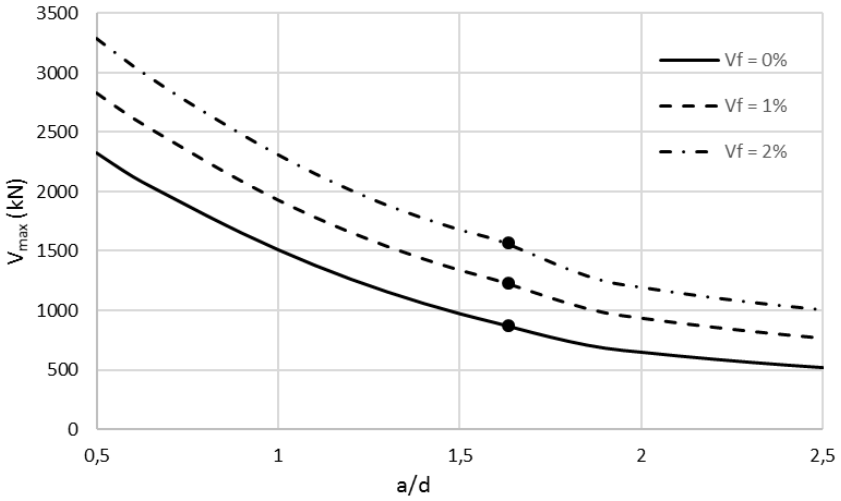

Figure 5.1 Effect of *a/d* ratio for different fiber volume ratios

The effect of fiber volume ratio on the shear strength was evaluated next. Comparison between the curves with different fiber volume ratios in Figure 5.1 shows a significant increase in shear strength for fiber volume ratio of 1% and 2% compared to the beam with no fibers included. The shear strength at 0.5 *a/d* ratio has increased by 21% for 1% fiber volume ratio compared to the beam with no fibers, and by almost 30% for 2% fiber volume ratio. However the difference between the shear resistance for *a/d* ratio of 2.5 is slightly more significant. The beam with 1% fiber volume ratio shows increase of 32% in the shear strength compared to deep beam with no fiber inclusion, and 2% fiber volume ratio shows and increase of 48% in the shear strength.

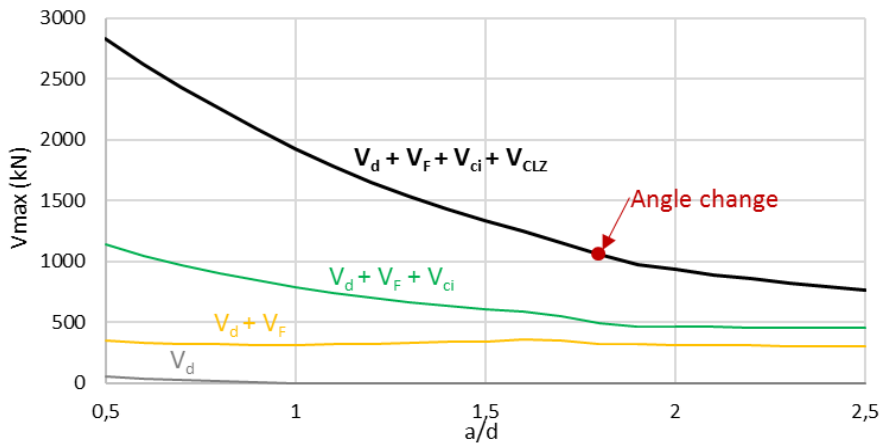

Figure 5.2 Breakdown of effect of a/d ratio for V_f = 1%

Figure 5.2 shows the breakdown of the forces contributing to the shear resistance for 1% fiber reinforcement ratio. The decreasing tendency of the curve is mainly dependent on the contribution from the critical loading zone, whose size decreases as the *a/d* ratio gets higher. The aggregate interlock also decreases with increasing *a/d* ratio, however not as significantly as the critical loading zone. The effect of fibers slightly reduces the decreasing tendency of the curve, where for higher *a/d* ratios the contribution of fibers is more significant than for lower ones.

In conclusion, the shear force resisted by the beam has desceding tendencies for increasing *a/d* ratios. The inclusion of fibers provides additional shear strength resistance, and the shear strength provided by fibers increases with higher fiber volume ratios.

5.2.2 Longitudinal Reinforcement

Next parameter investigated within the parametric study was the bottom longitudinal reinforcement and its effect on the shear strength of the beam. Reinforcement ratios taken into account in this case varied from 0.5% to 3%. The effect was investigated for three different fiber volume ratios of 0%, 1% and 2%. For each fiber volume ratio a curve was created by generating the shear strength resisted by the beam at a step of 0.1%. To focus on the effect of fibers no shear reinforcement was considered in this study.

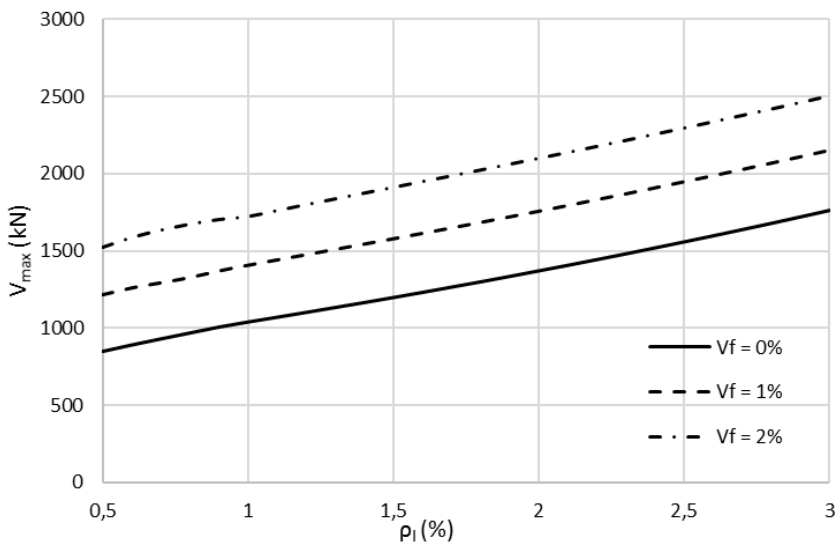

Figure 5.3 Effect of longitudinal reinforcement for different fiber volume ratios

Figure 5.3 shows results of the study. Horizontal axis describes different ratios of shear reinforcement taken into account. Vertical axis shows the shear strength achieved for each reinforcement ratio. Three different lines represent different fiber volume ratios. The tendency of the graph shows linear increase in shear strength resistance for increasing ratio of longitudinal reinforcement. The increase of shear strength between the ratios 0.5% and 3% for beam without fibers was by 107%, for 1% fiber volume ratio by 77% and for 2% fiber volume

ratio by 64%. Thus the results show that bottom longitudinal reinforcement contributes greatly to the resistance of the deep beams.

Inclusion of fibers shows again a significant increase in shear capacity. From Figure 5.3 we can observe that the contribution of fibers is a constant value added to the overall shear strength of the member. The increase in shear strength for beam with 1% of fiber volume ratio and longitudinal reinforcement ratio of 0.5% is by 42% compared to beam with no fiber reinforcement. The beam with fiber reinforcement of 2% has shear strength higher by 78% than beam with no fiber reinforcement. For higher longitudinal reinforcement the percentage of increase in overall shear strength decreases and for 1% fiber volume ratio is only 22% higher. For fiber volume ratio of 2% the shear strength increases by 42%.

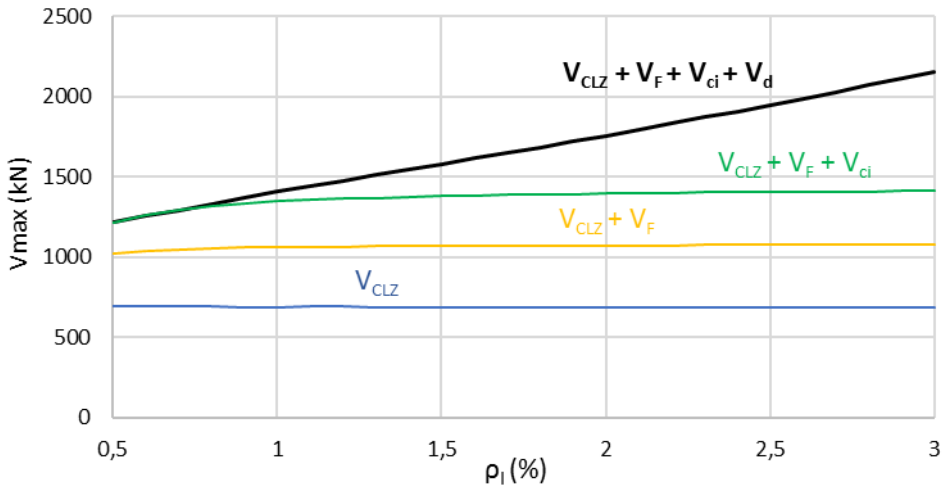

Figure 5.4 Breakdown of effect of longitudinal reinforcement for V_f = 1%

Figure 5.4 shows the breakdown of the forces contributing to the shear resistance of the beam for 1% fiber reinforcement ratio. As it can be seen in the figure the contribution of fibers and the critical loading zone is constant. Biggest contribution to the shear resistance comes from the critical loading zone, and depending on the reinforcement ratio also from the dowel action for higher ratios. The main reason for the increase in the shear strength is the contribution from the dowel action which increases with increasing reinforcement ratio.

It can be concluded, that higher longitudinal reinforcement ratios provide higher shear resistance of the beam. The inclusion of fibers increases the shear resistance of the beam, where the contribution of fibers highly depends on the fiber volume ratio.

5.2.3 Fiber Volumetric Ratio

The effect of fiber volumetric ratio was investigated in each of the parametric studies. However, a separate analysis focused on the effect of fibers was also carried out. The shear resistance of the beam was evaluated for fiber volumes varying from 0% to 2.5%. Three curves were generated for three different shear reinforcement ratios of 0%, 0.5% and 1% and curves were created by generating the shear strength at a step of fiber volume ratio of 0.1%. The rest of the properties were as proposed for the sample beam in the introduction of this chapter.

Figure 5.5 shows the results of the study, where the horizontal axis represents different fiber volume ratios, and vertical axis the variation in the shear strength of the beam. Each of the three different lines represents one shear reinforcement ratio. As it was previously observed in the parametric studies for *a/d* ratio and longitudinal reinforcement, the inclusion of fibers increases the capacity. The resistance of the beam linearly increases with increasing fiber volume ratio. For beams with no shear or fiber reinforcement the increase of shear resistance compared to the beam with 2.5% volume of fibers is by 91%. For 1% volume of fibers the shear resistance increases by 38% compared to the beam with no fibers. When shear reinforcement is 0.5% the resistance of the beam with 1% fiber volume ratio increases by 46%, and for 1% shear and fiber reinforcement by 29% compared to no fiber reinforcement.

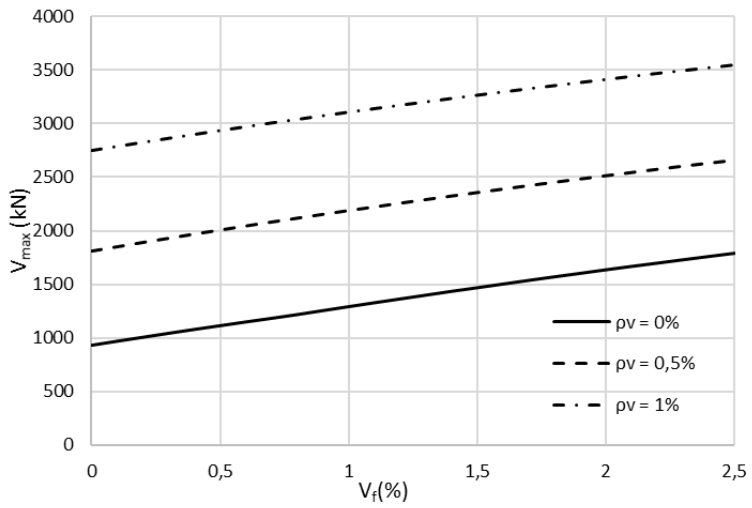

Figure 5.5 Effect of fiber volumetric ratio for different shear reinforcement ratios

The impact of shear reinforcement was also evaluated within the study. Increase in shear reinforcement caused significant increase in shear resistance of the beam. Increase in shear resistance for 0.5% shear reinforcement and 1% fiber volume is almost by 70%. For 1% shear reinforcement and 1% fiber volume ratio the increase in shear strength is by 140%.

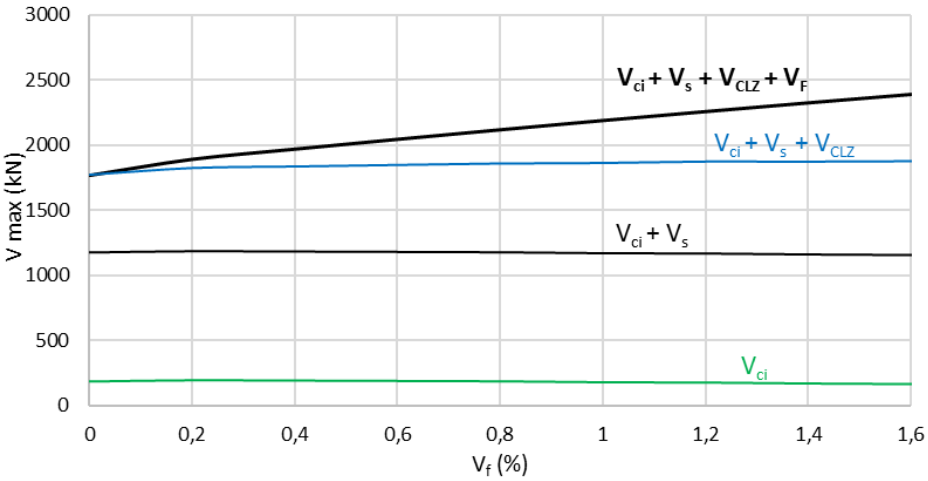

Figure 5.6 Breakdown of effect of fiber volumetric ratio for ρ_v = 0.5%

Figure 5.6 shows the breakdown of forces contributing to the shear strength for 0.5% shear reinforcement. As it can be seen in the figure the main contribution is caused the shear reinforcement. The effect of fibers increases with increasing fiber volumetric ratio.

In conclusion, the inclusion of fibers provides significant increase in shear resistance for deep beams. However, shear reinforcement such as stirrups seems to contribute to the overall strength more than the fibers.

5.2.4 Shear Reinforcement

Next study focused on the effect of shear reinforcement on the shear strength of the beam. Shear reinforcement ratio considered in the study varied from 0% to 0.7%. As in the previous studies, the effect was evaluated for three different fiber volume ratios of 0%, 1% and 2%. The curves were created by generating the shear strength at a step of 0.1%. The rest of the properties of the beam remained as mentioned in the introduction of this chapter.

Figure 5.7 represents the outcome of the study. Horizontal axis consists of different shear reinforcement ratios, and vertical axis describes the shear strength achieved. Three different curves represent three different fiber volume ratios. The study shows that for increasing shear reinforcement ratio the shear strength linearly increases. The increase in the shear strength is most significant for case with no fiber reinforcement where the difference between the shear strength with 0% shear reinforcement and 0.7% is by 134%. The increase in shear strength for 1% fiber reinforcement is 98% and for 2% fiber reinforcement ratio is 76%.

The inclusion of fibers provides additional shear strength to the beam. A constant value of shear force is added to the original shear strength depending on the amount of fibers added. Beams with no shear reinforcement to 1% fiber reinforcement increased in the shear strength by 39% and with 2% of fiber reinforcement ratio by 75%. For members with 0.7% shear reinforcement

ratio the shear strength increased less significantly by 11% for 1% fiber volume ratio and by 20% for 2% fiber volume ratio.

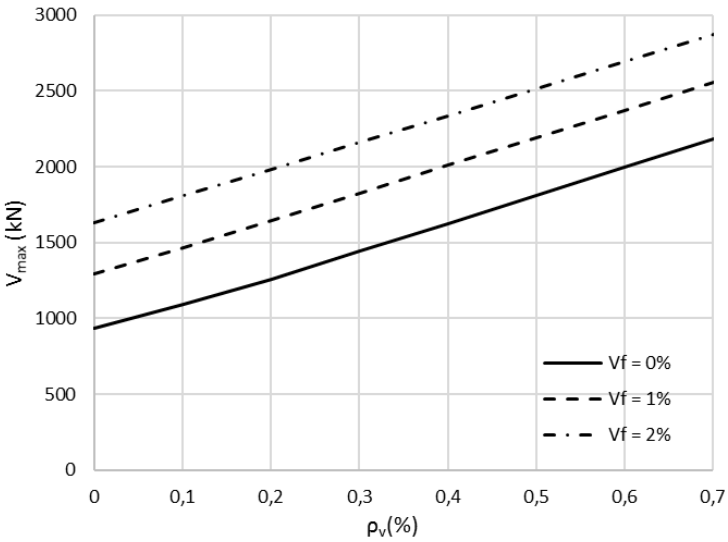

Figure 5.7 Effect of shear reinforcement for different fiber volume ratios

Figure 5.8 shows the breakdown of the effect of shear reinforcement. As shown in the figure, the biggest contribution to the shear resistance comes from the critical loading zone or shear reinforcement depending on the reinforcement ratio. The force due to the shear reinforcement linearly increases as the ratio of reinforcement increases.

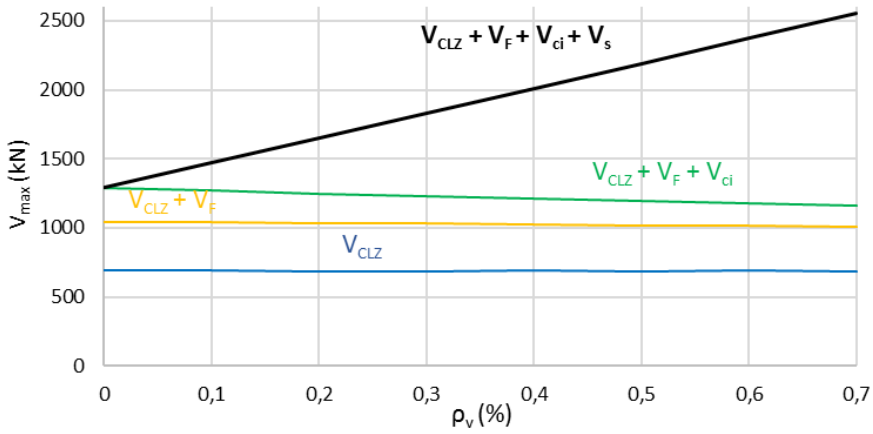

Figure 5.8 Breakdown of effect of shear reinforcement for V_f = 1%

5.2.4.1 FRC with High Shear Reinforcement

While generating results to obtain the ultimate shear strength using the extended five-spring model, it was observed that in some cases the resulting curve started at a nonzero deformation value as shown on Figure 5.9. Such phenomenon was observed for example in specimen B10 from the experimental study of Mansur and Ong (1991) where the beam B10 was included in

the program to study effects of shear reinforcement on the ultimate shear strength. Unlike other beams that contained shear reinforcement around 0.47%, beam B10 had percentage of shear reinforcement of 1.26% along with fiber reinforcement ratio of 1%. Such high reinforcement ratio resulted in the phenomenon depicted in Figure 5.9 where the resistance provided by the stirrups is so high that the model is not able to capture the behavior of the curve from the beginning but rather from a certain value of deflection.

When provided with large amount of flexural reinforcement, the beams start to propagate flexural deformations before the shear deformations. In this particular case, the transverse displacement of critical loading zone does not start propagating only after the deflection of the shear span due to elongation of bottom reinforcement has reached 2.9 mm. Due to the high shear resistance of the beam the deflection due to transverse displacement is restrained by action of stirrups and fibers in the beam and thus only flexural deflections of the shear span propagate at the beginning of the loading of the beam.

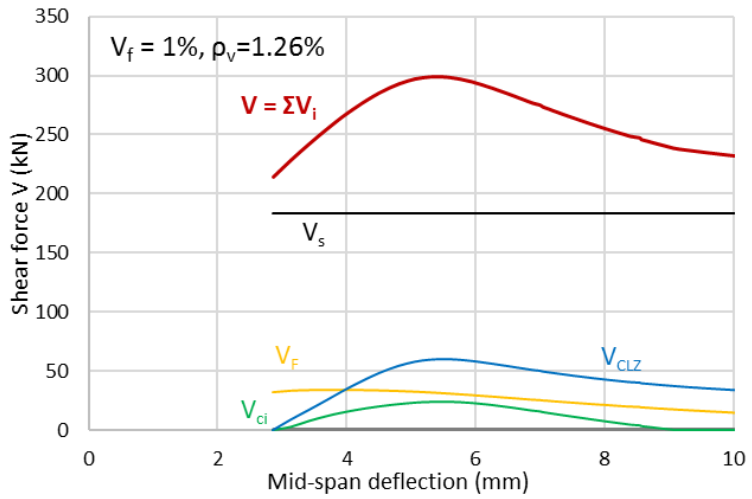

Figure 5.9 Results for B10 obtained with the extended five-spring model

Figure 5.10 shows the average tensile strength to shear force at deflection of the beam equal to zero for two different shear force reinforcement ratios of 0.47% and 1.26%, respectively. As shown in the figures, resulting shear force curve intersects the flexural spring force curve only once for 0.47% shear reinforcement ratio. However, due to significant increase in shear force provided by stirrups the curve representing the sum of forces, consisting of 1% fiber reinforcement ratio and 1.26% shear reinforcement ratio, intersects the flexural spring curve three times.

Five-spring model defines the equilibrium of forces using a bisectional method where it searches for a value of the intersection iteratively. Only one correct solution is assumed to exist by the model and thus causing the phenomenon showed in Figure 5.9 for beams with high shear reinforcement. In highly reinforced members, for fixed Δ equal to zero, the multiple intersection of the flexural spring force is causing the model to define the equilibrium at an intersection

point with the highest shear force instead of zero where the equilibrium is found for members with regular shear reinforcement as shown in Figure 5.10.

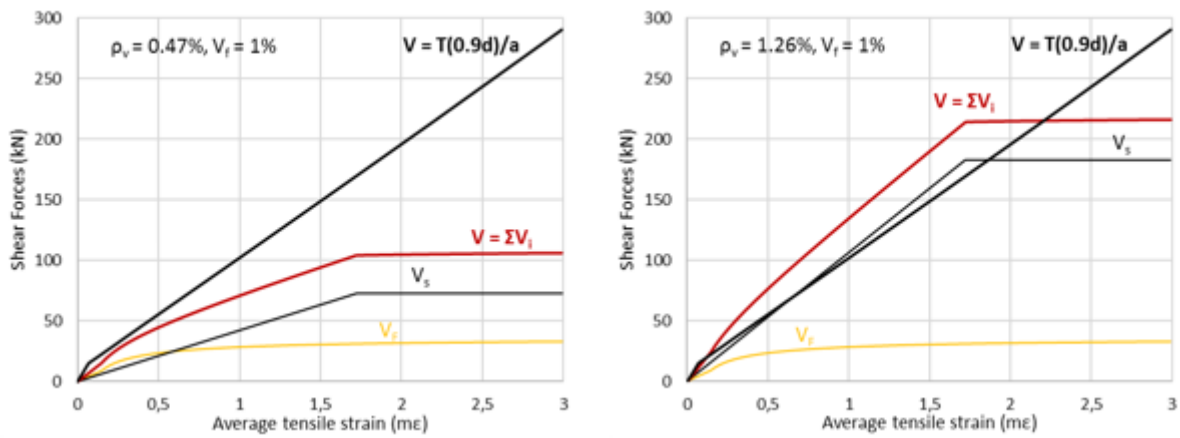

Figure 5.10 Average tensile strain at deflection equal to zero for different shear reinforcement ratios

With the provided explanation an assumption can be made regarding the missing part of the plot for a given load-deflection curve. A linear growth of the curves can be assumed to model the behavior of the beam before the propagation of transverse displacement of the critical loading zone as shown in Figure 5.11. However, the assumption is only a rough prediction of the behavior of the curve and does not necessarily represent the real behavior of the specimen.

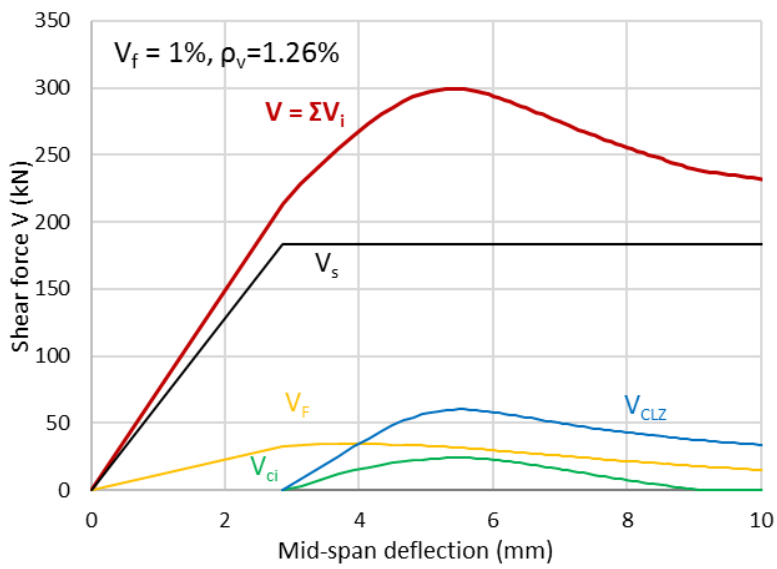

Figure 5.11 Results for B10 obtained with the extended five-spring model with completed curve

5.2.5 Comparison of Effectiveness of Fibers vs. Shear Reinforcement

Previously, the effects of fiber volume ratio and shear reinforcement were separately evaluated. It was concluded that both of the parameters contribute significantly to the shear strength of the

beam. However, another parametric study was carried out to determine which of the two reinforcements is more efficient. Firstly, the shear strength was obtained considering shear reinforcement ratio of 0.2% and no fiber reinforcement for different *a/d* ratios. Then, for each step of *a/d* ratio a fiber volume ratio was specified to match the shear strength obtained using 0.2% of shear reinforcement. For this case a beam with no shear reinforcement was considered. The results then show the amount of fibers necessary to match the shear strength achieved with 0.2% shear reinforcement for different *a/d* ratios.

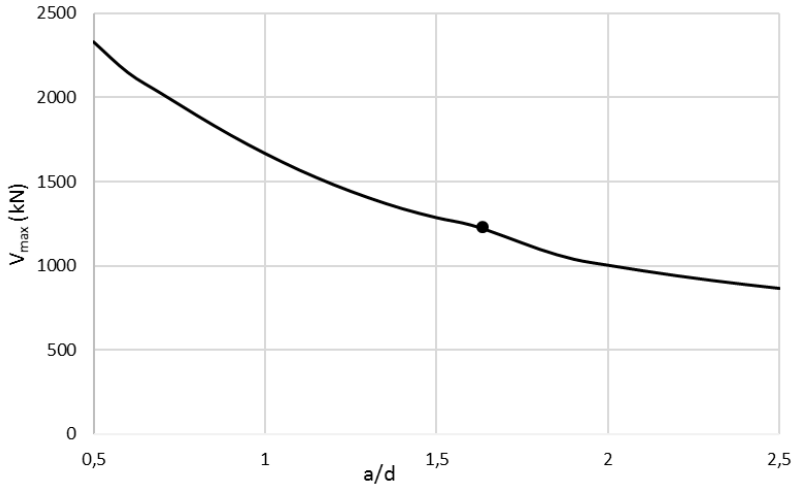

Figure 5.12 Variation of V_{max} for different *a/d* ratios with ρ_v = 0.2%

Figure 5.12 illustrates the shear strength for different *a/d* ratios for beam with 0.2% of shear reinforcement. The curve was created by generating the shear strength for different *a/d* ratios at a step of 0.1. The black dot represents the angle change as previously explained in Chapter 5.2.1. The same curve was then generated for beam with certain ratio of fiber reinforcement and 0% shear reinforcement. However, to generate such curve, fiber volume ratio that provides the beam with equal shear strength as 0.2% shear reinforcement had to be found.

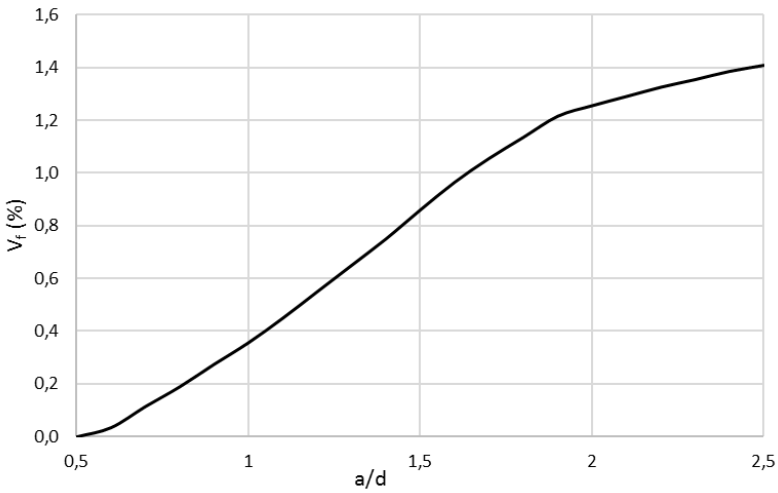

Figure 5.13 Fiber volume ratio equivalent to 0.2% shear reinforcement ratio

Figure 5.13 shows the fiber volume ratio equivalent to the shear strength obtained by using 0.2% shear reinforcement for different *a/d* ratios. Horizontal axis shows the range of *a/d* ratios taken into consideration, vertical axis describes the fiber volume ratio equivalent to 0.2% of shear reinforcement.

The outcome of the study shows, that the fiber reinforcement is more effective than shear reinforcement only for *a/d* ratios under 0.8. This is due to the effective length of shear span considered within the equation that defines the contribution of shear strength provided by stirrups. To obtain the effective shear length, the lengths l_0 and $1.5l_{b1e}$ are subtracted from expression $dcot\alpha_1$to neglect the stirrups too close to the edges of the shear span. Unfortunately, for smaller shear spans such subtraction greatly reduces the amount of stirrups contributing to the shear strength. Such reduction does not apply to the contribution of fibers and thus the fibers are able to provide more shear resistance than the shear reinforcement in these cases. For higher *a/d* ratios than 0.8 however, the shear reinforcement shows to be more efficient than fibers.

5.2.6 Size Effect

Last parameter investigated within the parametric study was the size effect. The size effect was examined for effective depth ranging from 700 mm to 2700 mm. For the study a member with only fiber reinforcement and without additional shear reinforcement was considered. Three different fiber volume ratios of 0%, 1% and 2% were considered. Figure 5.14 shows the results of the study. Horizontal axis shows different effective depths and vertical axis describes the shear strength divided by the effective cross section of the beam. Three different lines represent three different fiber volume ratios.

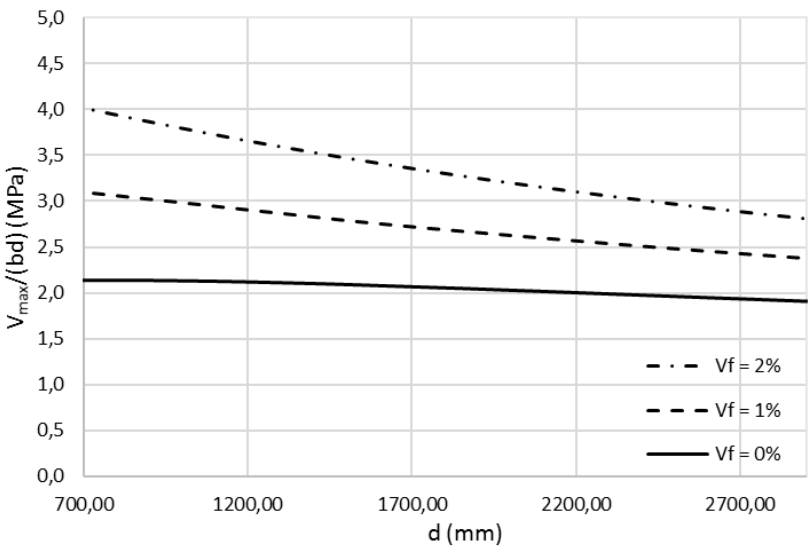

Figure 5.14 Size effect for different fiber volume ratios

From the Figure 5.14 it can be observed that for beams with no fiber reinforcement the size effect is very small. The decrease in stress resisted by the cross section is only 10% between the and minimum effective depth considered. For 1% fiber reinforcement ratio the effect becomes more significant, the size effect decreases by 24%, and for 2% fiber volumetric ratio by 31%. Thus it can be concluded, that the size effect gets bigger for members with higher fiber reinforcement ratio.

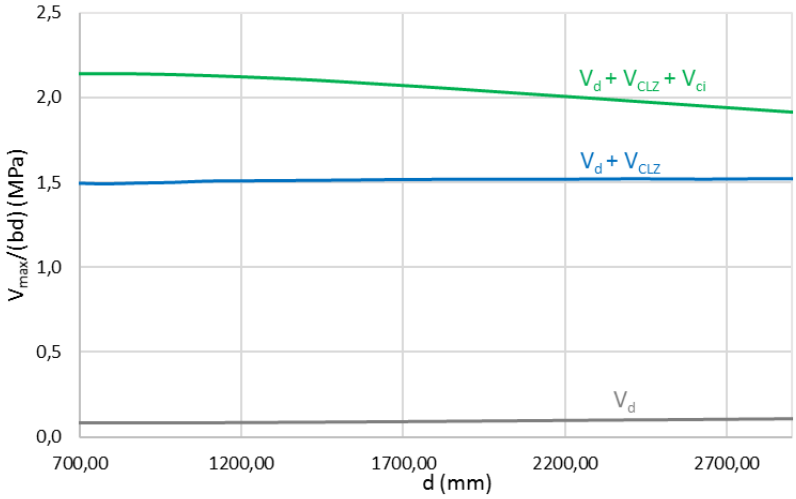

Figure 5.15 Size effect breakdown for 0% fiber volume ratio

Figure 5.15 represents a breakdown of the size effect for members with 0% fiber reinforcement ratio. The figure shows a breakdown of the size effect to contribution of separate shear forces. Because in this case no additional shear reinforcement was considered, the graph only consists of three shear forces contributing to the stress resisted by the cross section. As it is shown in the figure, the dowel action and the effect of the critical loading zone have almost no impact on the size effect. However, the aggregate interlock contribution is influenced by the size of the member the most.

Figure 5.16 shows the breakdown of size effect for member with 2% fiber volume ratio. Just as for the breakdown of member with 0% fiber volume ratio, this member does not include any shear reinforcement. Figure 5.16 shows four different forces contributing to the stress resisted by the cross section. The dowel action in this case does not contribute much to the size effect. The effect of aggregate interlock decreases with increasing effective height. However, the effect of the critical loading zone is more significant than the one of aggregate interlock. Biggest contribution to the size effect is provided by the fibers, which is depicted in the figure with yellow line. The difference between the contribution to the size effect by the critical loading zone for beam with 0% fibers and one with 2% is caused by the redefined stress-strain curve. The stress-strain curve definition used in the Figure 5.16 is affected by inclusion fibers, while the one in Figure 5.15 is not.

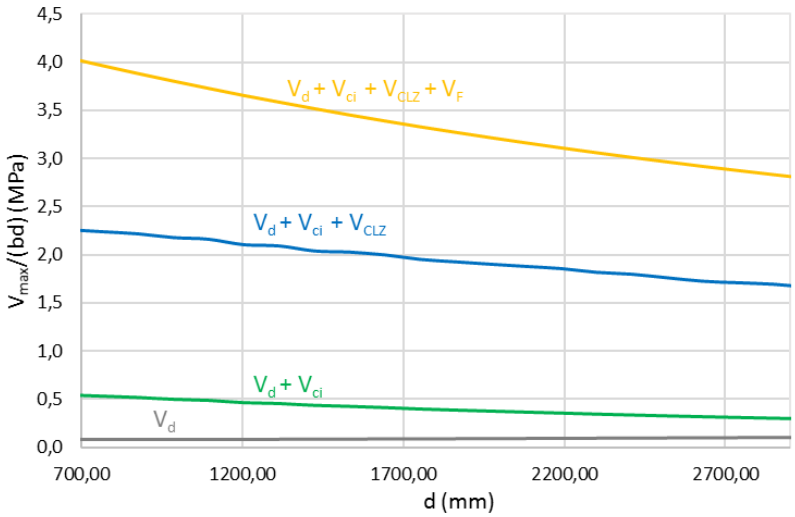

Figure 5.16 Size effect breakdown for 2% fiber volume ratio

It can be concluded, that the size effect mainly depends on the fiber volume ratio. While for beams with no fiber reinforcement the size effect is insignificant, for beams with increasing fiber volume ratios the effect becomes bigger and more significant.

5.3 DISCUSSION

Based on the results of the parametric study several conclusions can be made. Regarding the effect of *a/d* ratio, the study has shown that for increasing *a/d* the shear strength becomes smaller. This is caused mainly by the reduction of the size of the critical loading zone which has shown to have significant impact on the shear resistance of the beam. The effect of bottom longitudinal reinforcement has shown to improve the shear strength of the beam with increasing reinforcement ratio. Higher ratio of flexural reinforcement increases the resistance of the beam, and with addition of fibers the tension stiffening effect increases the resistance even more.

Shear reinforcement such as stirrups and its impact on the shear strength was investigated in three of the studies. Firstly, shear reinforcement and its effect on the shear strength was evaluated as a separate parameter. In this study, a linear increase of shear resistance was observed for increasing shear reinforcement ratios. The effect of shear reinforcement was also included in the study of fiber reinforcement ratio as well as its impact on the maxim shear strength of the beam. Again, a significant contribution of the shear reinforcement to the shear strength was observed. Lastly, the efficiency of shear reinforcement was compared with the efficiency of the fiber reinforcement. It was concluded, that for beams with *a/d* ratio higher than 0.8 the shear reinforcement is more effective than fiber reinforcement. For lower *a/d* ratios, the effect of stirrups was lower due to the limitations of the definition of effective area for shear reinforcement considered to contribute to the shear resistance.

Fiber volume ratio and its effect on the shear resistance was evaluated separately and then also in each of the studies. It can be concluded, that fibers provide additional shear strength to the beam and with increasing amount of fibers the contribution becomes more significant. However, based on the study of comparing the effectiveness of fiber and shear reinforcement, fibers have shown to provide less shear strength to the beam.

Last parameter investigated was the size effect. It was concluded that while for beams with no fiber or shear reinforcement the size in effect is not significant, the addition of fibers notably affects the size effect. It was observed that for increasing fiber reinforcement ratios, the size effect becomes more significant than for beams with no fiber reinforcement.

6 SUMMARY AND CONCLUSIONS

First, all data available on tests performed on fiber reinforced concrete deep beams was collected. Based on a literature review, several experimental studies were found. However, only the study by Mansur and Ong (1991) and Mansur and Alwist (1984) were summarized and placed in a test database due to limitations such as missing data or unsuitable experimental setup in other studies. All the tests showed that the addition of fibers increases the shear resistance of deep beams. The effects of fiber volumetric ratio, *a/d* ratio, shear and additional longitudinal reinforcement ratios were evaluated in the experimental study by Mansur and Ong (1991), where for increasing fiber volume ratio a higher shear resistance was observed. For increasing *a/d* ratio, the shear strength showed a significant decrease. The shear reinforcement enhances the shear strength significantly, while the additional longitudinal reinforcement shows to have a negligible effect on the shear resistance.

The main goal of the thesis was to propose an extension to an existing five-spring model (5sm) for the shear behavior of deep beams (Mihaylov, 2015) to include the effects of steel fibers in such members. A two-parameter kinematic theory proposed by Mihaylov et al. (2013), on which the five-spring model is based, was analyzed in detail and explained before an extension of the model was implemented.

The extension of the five-spring model accounts for three effects caused by steel fibers in the concrete. To represent the shear resistance provided by the fibers across the critical shear crack, the SDEM model proposed by Lee et al. (2013) was selected. The SDEM model is a simplified version of DEM model introduced by Lee et al. (2011), and can be used for straight or hooked-end fibers. To model the tension-stiffening effect of the fibers around the bottom longitudinal reinforcement, a tension-stiffening model by Lee et al. (2013) was used. The model takes into account the tension resistance of the bottom longitudinal reinforcing bar, the effect of fibers and tension-stiffening or softening effect whichever is higher. The last adjustment introduced into the model regarding the effect of fibers was the stress-strain curve to represent the compressive behavior of the critical loading zones in deep beams. The original code considered Popovics (1970) stress-strain curve for the behavior of concrete under uniaxial compression. However, extensive research on stress-strain behavior of FRC has shown that, while the inclusion of fibers does not significantly affect the pre-peak part of the stress-strain response, it greatly enhances the post-peak response compared to regular concrete. A model proposed by Ou et al (2012) was used to describe the stress-strain response of regular strength concrete, while for high-strength FRC the approach by Mansur et al. (1999) was used. Finally, an extension of the Matlab code of the five-spring model was introduced to account for deflections in members under four-point loading.

The proposed extended five-spring model was validated against the collected experimental data. The model showed good agreement regarding the shear strength of the test specimens. Yet the deflections at the maximum predicted shear force (displacement capacity) were only about 50% of the deflections measured in the tests. A possible explanation of such difference was

considered to be the settlement of the supports that was possibly unaccounted for in the experimental study. To confirm this assumption, four of the beams from the experimental study of Mansur and Ong (1991) were analyzed by Liu (2016) using non-linear finite element models, and the load-deflection curves obtained from the models were compared with the experimental and analytical results. The results of the analyses supported the assumption of support settlements, and it was concluded that they were the main cause of the difference in deflections. Finally, the measured shear strength of the FRC deep beams from the database was compared with the predictions of the extended 5sm. With an average experimental-to-predicted ratio of 1.07 and a coefficient of variation of 6%, the proposed model was shown to predict the shear strength of FRC deep beams with adequate accuracy.

With the validated model, a parametric study was carried out to study the effect of *a/d* ratio, shear and longitudinal reinforcement ratio, fiber volumetric ratio, and the size effect in shear. As it was previously concluded by Mansur and Ong (1991), the 5sm shows that the shear strength decreases with increasing *a/d* ratio. For the fiber volumetric ratio and shear reinforcement, the same conclusion was reached as by Mansur and Ong (1991) that for increasing fiber volumetric ratio and shear reinforcement ratio the shear resistance of the beam increases. A comparison of both types of shear reinforcement was carried out for different *a/d* ratios where the stirrups showed to be more efficient than equal amounts of fiber reinforcement for *a/d* ratios higher than 0.8. The effect of bottom longitudinal reinforcement was also evaluated where it was concluded that higher reinforcement ratios provide higher shear strength to the member. The last parameter evaluated was the size of the member (size effect in shear). Three different fiber volumetric ratios were considered in the size effect series. For beams without fibers, the size effect was negligible, while for increasing fiber volume ratios the effect became more significant.

Finally, there are several limitations of the proposed extended 5sm model for FRC deep beams that should be considered for future research. It should be taken into account that the SDEM does not account for fiber rupture, and therefore when using hooked-ended fibers with low strength, the model can overestimate the shear strength. Second, the lack of experimental data did not allow an extensive validation of the model. The database created for the validation should be extended as new tests become available to validate the model against more experimental results. Also, the impact of fibers on the post-peak behavior was not evaluated due to the lack of tests in which the post-peak response was measured.

REFERENCES

ACI Committee 544, [1993]. "Guide for Specifying, Proportioning, Mixing, Placing, and Finishing Steel Fiber Reinforced Concrete," *ACI Materials Journal*, Vol. 90, No. 1, pp. 94-101.

ACI Committee 544, [2008]. "State-of-the-Art Report on Fiber Reinforced Concrete - ACI 544.1R-96 (Reapproved 2002)," *ACI Manual of Concrete Practice*, Part 6, pp. ACI544.1R-7 - ACI544.1R-24.

Barros, J. A. O., Figueiras, J. A., [1999] "Flexural behavior of SFRC: Testing and modeling," *Journal of Materials in Civil Engineering*, ASCE, Vol. 11, No.4, pp. 331–339.

Bentz, E. C., [2005] "Explaining the Riddle of Tension Stiffening Models for Shear Panel Experiments," *Journal of Structural Engineering*, ASCE, Vol. 131, No. 9, pp. 1422-1425.

Bischoff, P. H., [2003] "Tension Stiffening and Cracking of Steel Fiber-Reinforced Concrete," *Journal of Materials in Civil Engineering*, ASCE, Vol. 15, No. 2, pp. 174-182.

Campione, G., [2012] "Flexural Behavior of Steel Fibrous Reinforced Concrete Deep Beams," *Journal of Materials in Civil Engineering*, ASCE, Vol. 138, No. 2, pp. 235 - 246.

Carreira, D. J., and Chu, K. H., [1985] "Stress-Strain Relationship for Plain Concrete in Compression," *ACI Structural Journal*, Vol. 82, No. 6, pp. 797-804.

CSA A23.3-04, [2004] "Design of Concrete Structures," *Canadian Standards Association*, Mississauga, ON, Canada, 214 p.

Deluce, J. R., [2011] "Cracking Behavior of Steel Fiber Reinforced Concrete Containing Conventional Steel Reinforcement," *Master Thesis*, Department of Civil Engineering, University of Toronto, Toronto, ON, Canada, 308 p.

Deluce, J. R., Vecchio, F. J., [2013] "Cracking of SFRC Members Containing Conventional Reinforcement," *ACI Structural Journal*, Vol. 110, No. 3, pp. 481-490.

Di Prisco, M., Colombo, M., Dozio., D., [2013] "Fiber-reinforced concrete in fib Model Code 2010: principles, models and test validation," *Structural Concrete*, Vol. 14, No. 4, pp. 342-361.

European Committee for Standardization, CEN, EN 1992-1-1 [2004] *Eurocode 2: Design of Concrete Structures- Part 1-1: General Rules and Rules for Buildings*, Brussels, Belgium, 225 pp.

Ezeldin, A. S., and Balaguru, P. N., [1992] "Normal- and High-Strength Fiber-Reinforced Concrete under Compression," *Journal of Materials in Civil Engineering*, ASCE, Vol. 4, No. 4, pp. 415–429.

fib – International Federation for Structural Concrete, [2013] "*fib* Model Code for Concrete structures 2010," *Berlin: Verlag Ernst & Sohn*.

Hooke, R., [1678] "Lectures de Potentia Restitutiva (Spring Explaining the Power of Springing Bodies)," printed for John Martyn Printer to The Royal Society, at the Bell in St. Paul's Church-Yard, 24 p.

Hsu, L.S., Hsu, C.T.T., [1994] "Stress-strain Behavior of Steel-Fiber High-Strength Concrete under Compression," *ACI Structural Journal*, Vol. 91, No. 4, pp. 448-457.

Johnston, C. D., [2001]. "Fiber-Reinforced Cements and Concretes", *Gordon and Breach Science Publishers*, Ottawa, Canada, 372 p.

Lee, S.-C., Cho, J.-Y., Vecchio, F. J., [2011] "Diverse Embedment Model for Steel Fiber-Reinforced Concrete in Tension: Model Verification," *ACI Materials Journal*, Vol. 108, No. 5, pp. 526-535.

Lee, S.-C., Cho, J.-Y., Vecchio, F. J., [2011] "Diverse Embedment Model for Steel Fiber-Reinforced Concrete in Tension: Model Development," *ACI Materials Journal*, Vol. 108, No. 5, pp. 516-525.

Lee, S.-C., Cho, J.-Y., Vecchio, F. J., [2013] "Simplified Diverse Embedment Model for Steel Fiber-Reinforced Concrete Elements in Tension," *ACI Structural Journal*, Vol. 110, No. 4, pp. 403-412.

Lee, S.-C., Cho, J.-Y., Vecchio, F. J., [2013] "Tension-Stiffening Model for Steel Fiber-Reinforced Concrete Containing Conventional Reinforcement," *ACI Structural Journal*, Vol. 110, No. 4, pp. 639-648.

Lee, S.-C., Cho, J.-Y., Vecchio, F. J., [2016] "Analysis of Steel Fiber-Reinforced Concrete Elements Subjected to Shear," *ACI Structural Journal*, Vol. 113, No. 2, pp. 275-285.

Lee, S.-C., Oh, J.-H., and Cho, J.-Y., [2015] "Compressive Behavior of Fiber-Reinforced Concrete with End-Hooked Steel Fibers," *Materials*, Vol. 8, pp. 1442-1458.

Li, B., Maekawa, K., Okamura, H., [1989] "Contact Density Model for Stress Transfer Across Cracks in Concrete," *Journal of the faculty of engineering*, University of Tokyo (B), Vol. 40, No. 1, pp. 9–52.

Lim, T. Y., Paramasivam, P., Lee, S. L., [1987] "Analytical Model for Tensile Behavior of Steel-Fiber Concrete," *ACI Materials Journal*, Vol. 84, No. 4, pp. 286-298.

Liu, J., [2016] "Personal communication," November 21st 2016.

Mansur, M. A., Alwist, W. A. M., [1984] "Reinforced Fiber Concrete Deep Beams with Web Openings," *The International Journal of Cement Composites and Lightweight Concrete*, Vol. 6, No. 4, pp. 263-271.

Mansur, M. A., Chin, M. S., Wee, T. H., [1999] "Stress-Strain Relationship of High-Strength Fiber Concrete in Compression," *Journal of Materials in Civil Engineering*, ASCE, Vol. 11, No. 1, pp. 21–29.

Mansur, M. A., Ong, K. C. G., [1991] "Behavior of Reinforced Fiber Concrete Deep Beams in Shear," *ACI Structural Journal*, Vol. 88, No. 1, pp. 98-105.

Mihaylov, B. I., [2008] "Behavior of Deep Reinforced Concrete Beams under Monotonic and Reversed Cyclic Load," *doctoral thesis*, European School for Advanced Studies in Reduction of Seismic Risk, Pavia, Italy, 2008, 379 pp.

Mihaylov, B. I., [2015] "Five-Spring Model for Complete Shear Behavior of Deep Beams, "*Structural Concrete*, Vol. 16, No.1, pp. 71-83.

Mihaylov, B. I., Bentz, E. C., Collins, M. P., [2013] "Two-Parameter Kinematic Theory for Shear Behavior of Deep Beams," *ACI Structural Journal*, Vol. 110, No. 3, pp. 447-455.

Naaman, A. E., and Najm, H., [1991] "Bond-Slip Mechanisms of Steel Fibers in Concrete," *ACI Materials Journal*, Vol. 88, No. 2, pp. 135-145.

Narayan, R., Darwish., I. Y. S., [1988] "Fiber Concrete Deep Beams in Shear," *ACI Structural Journal*, Vol. 85, No. 2, pp. 141 - 149.

Newman, J., Choo, B. S., [2013] "Advanced Concrete Technology 3: Processes," *Elsevier Ltd.*, Oxford, Great Britain, 704 p.

Ou, Y.-C., Tsai, M.-S., Liu, K.-Y., Chang, K.-C., [2012] "Compressive Behavior of Steel-Fiber-Reinforced Concrete with a High Reinforcing Index," *Journal of Materials in Civil Engineering*, ASCE, Vol. 24, No. 2, pp. 207-215.

Popovics, S., [1970] "A Review of Stress-Strain Relationships for Concrete," *ACI Journal*, Vol. 67, No. 3, pp. 243-248.

Ramaswamy, A., Barzegar, F., Voyiadjis, G. Z., [1994] "Post-cracking Formulation for Analysis of RC Structures Based on Secant Stiffness," *Journal of Engineering Mechanics*, ASCE, Vol. 120, No. 12, pp. 2621-2640.

Shah, D. U., Schubel, P. J., Licence, P., Clifford, M. J., [2012] "Determining the Minimum, Critical and Maximum Fiber Content for Twisted Yarn Reinforced Plant Fiber Composites," *Composites Science and Technology*, Vol. 72, No. 15, pp. 1909-1917.

Susetyo, J., [2009] "Fiber Reinforcement for Shrinkage Crack Control in Pre-stressed, Precast Segmental Bridges," *Doctoral Thesis*, Department of Civil Engineering, University of Toronto, Toronto, ON, Canada, 307 p.

Voo, J. Y. L., Foster, S. J., [2003] "Variable Engagement Model for Fiber-Reinforced Concrete in Tension," *Uniciv Report No. R-420*, University of New South Wales, School of Civil and Environmental Engineering, 86 p.

Zollo, R. F., [1997] "Fiber-reinforced Concrete: An Overview after 30 Years of Development," *Cement and Concrete Composites*, Vol. 19, pp. 107-122.

APPENDIX A: TEST DATABASE

Ref. No 1 – Mansur and Ong (1991)
Ref. No 2 – Mansur and Alwist (1984)

No.	Ref. No.	Beam Name	a/d	b (mm)	d (mm)	h (mm)	l (mm)	a:M/V (mm)	V_f (%)	l_f (mm)	l_i (mm)	d_f (mm)	Fiber type	l_{b1} (mm)
1	1	B1	0,31	90	463	500	740	145	1	30	-	0,564	S	80
2	1	B2	0,62	90	463	500	1020	285	1	30	-	0,564	S	80
3	1	B3	0,93	90	463	500	1310	430	1	30	-	0,564	S	80
4	1	B4	1,23	90	463	500	1590	570	1	30	-	0,564	S	80
5	1	B5	1,85	90	463	500	2160	855	1	30	-	0,564	S	80
6	1	B6	1,85	90	463	500	1590	570	0	0	-	-	-	80
7	1	B7	1,23	90	463	500	1590	570	0,5	30	-	0,564	S	80
8	1	B8	1,23	90	463	500	1590	570	1,5	30	-	0,564	S	80
9	1	B9	1,51	90	463	500	1850	700	1	30	-	0,564	S	80
10	1	B10	1,51	90	463	500	1850	700	1	30	-	0,564	S	80
11	2	WO-1/1	0,58	80	624	650	1550	360	1	30	22	0,4	EH	100

No.	l_{b2} (mm)	V/P	l_s (mm)	ρ_l (%)	A_s (mm^2)	$\varnothing_l$ (mm)	No. $bars_l$	f_y (MPa)	a_g (mm)	f_c' (MPa)	f_{yh} (MPa)	ρ_h (%)	$\varnothing_h$ (mm)	No. $bars_h$	f_{yv} (MPa)	ρ_v (%)	$\varnothing_{bv}$ (mm)	No. $bars_v$	V_u (kN)
1	80	1	200	1,93	804,25	16	4	440	10	35,7	375	0,54	6	4	375	0,42	6	5	375
2	80	1	200	1,93	804,25	16	4	440	10	35,7	375	0,54	6	4	375	0,49	6	8	360
3	80	1	200	1,93	804,25	16	4	440	10	35,5	375	0,54	6	4	375	0,48	6	10	291
4	80	1	200	1,93	804,25	16	4	440	10	31,1	375	0,54	6	4	375	0,47	6	12	228
5	80	1	200	1,93	804,25	16	4	440	10	31,5	375	0,54	6	4	375	0,49	6	17	183
6	80	1	200	1,93	804,25	16	4	440	10	34,4	375	0,54	6	4	375	0,47	6	12	205
7	80	1	200	1,93	804,25	16	4	440	10	33,8	375	0,54	6	4	375	0,47	6	12	220
8	80	1	200	1,93	804,25	16	4	440	10	33,2	375	0,54	6	4	375	0,47	6	12	260
9	80	1	200	1,93	804,25	16	4	440	10	29,5	375	1,22	6	9	375	0,48	6	14	224
10	80	1	200	1,93	804,25	16	4	440	10	30,1	375	0,54	6	4	375	1,26	6	37	290
11	100	1	580	0,81	402,12	16	2	418	10	40	304	0,206	3,3	12	304	0,43	3,3	31	345

APPENDIX B: SDEM - MATLAB CODE

```
function [ff]=SDEM(wcr,fc,Vf,lf,lh,li,df)

taufmax = 0.396*sqrt(fc);
tauehmax = 0.429*sqrt(fc);

betaf = 0.67;
betaeh = 0.76;

sf = 0.01;
seh = 0.1;
Kehi      =      1+(1+(7*betaeh/15-1)*sqrt(seh/(lf-li/2))-(2*(sqrt(lf-li/2))-
sqrt(seh))^2)/(lf-li);

    if wcr < sf
        Kst = betaf*wcr/3/sf;
    else
        Kst = 1-sqrt(sf/wcr)+betaf/3*sqrt(sf/wcr);
    end

    if wcr < seh
        Keh = betaeh*(2*wcr/3/seh-1/5*(wcr/seh)^2);
    elseif seh <= wcr < lf-li/2
        Keh         =         1+(7*betaeh/15-1)*sqrt(seh/wcr)-(2*(sqrt(wcr)-
sqrt(seh))^2)/(lf-li);
    elseif lf-li/2 <= wcr < li/2
        Keh = (li-2*wcr/(2*li-lf))^2*Kehi;
    else
        Keh = 0;
    end

alphaf = 0.5;

fst = alphaf*Vf.*Kst.*taufmax.*lf./df.*(1-2.*wcr./lf).^2;
if lh >= 1
    feh = alphaf*Vf.*Keh.*tauehmax.*2.*(li-2.*wcr)/df;
else
    feh = 0;
end

ff = feh+fst;

return
```

APPENDIX C: TENSION-STIFFENING - MATLAB CODE

```
function [N]=TS_R_FRC_S(Aceff,Ec,e,ag,Vf,lf,df,db,sb,fc,nb,lh,li,Er,As)

rs=As/Aceff;
c=1.5*ag;
k1=0.4;
k2=0.25;
k3=1-(min(Vf,0.015)/0.015)*(1-min(50/(lf/df),1));
smi=rs/db+0.5*Vf/df*(max((lf/df)/50,1));
scr=2*(c+sb/10)*k3+k1*k2/smi;
fcr=0.33*sqrt(fc);
M=Aceff/(nb*db*pi);

  if lh<=0
      cf=0.6+1/0.058*(lf/df)^0.9*((100*Vf)/M^0.8);
  else
      cf=0.6+1/0.034*(lf/df)*((100*Vf)^1.5/M^0.8);
  end

wcri=scr*e;
[ff]=SDEM(wcri,fc,Vf,lf,lh,li,df);
fcsofti=fcr*exp(-15*wcri);
fcTSi=fcr/(1+(3.6*cf*M*e)^0.5);
fctj=min(Ec*e,max(fcsofti,fcTSi));

freb=min(Er*As*e);
ffib=min(ff*Aceff);
fcon=fctj*Aceff;
N=(freb+ffib+fcon);
return
```

APPENDIX D: AVERAGE DIAGONAL STRESS IN THE CRITICAL LOADING ZONE - MATLAB CODE

```
function [favg,Ec,Dcenv]=FAVG(Vf,lf,df,fc,alfa,lb1e)

e=-(0:0.0001:1.0001)'*0.3;
RIv=Vf*lf/df;
if Vf<=0;
    n=0.8+fc/17;
    kk=0.67+fc/62;
    if fc<=41
        Ec=4730*fc^0.5;
    else
        Ec=(3320*fc^0.5+6900);
    end
    ec=-fc/Ec*n/(n-1);
     for i=1:length(e)
        f(i,1)=fc*n*e(i)/ec./(n-1+(e(i)/ec).^(n*kk));
     end
else
    if fc<=60
        Ec=(-367*Vf*lf/df+5520)*fc^(0.41);
        fcf=fc+2.35*RIv;
        eco=0.002;
        ecf=-(eco+0.0007*RIv);
        beta=0.71*RIv^2-2*RIv+3.05;
      for i=1:length(e)
        f(i,1)=fcf*beta*(e(i)/ecf)/(beta-1+(e(i)/ecf)^beta);
      end
    else
    eo=-((0.0005+0.00000072*RIv)*fc^0.35);
    Ec=(10300-400*Vf)*fc^(1/3);
    beta=1/(1-(fc/(-eo*Ec)));
    k1=(50/fc)^3*(1+2.5*RIv^2.5);
    k2=(50/fc)^1.3*(1-0.11*RIv^(-1.1));
    for i=1:length(e)
        if e(i)/eo <= 1
            f(i,1)=fc*beta*(e(i)/eo)/(beta-1+(e(i)/eo)^beta);
        else
            f(i,1)=fc*k1*beta*(e(i)/eo)/(k1*beta-1+(e(i)/eo)^(k2*beta));
        end
    end
    end
end
Om(1,1)=0;
for i=2:10002
    Om(i,1)=Om(i-1)-(f(i)+f(i-1))/2*(e(i)-e(i-1));
end
Dcenv=-3*lb1e*e/tan(alfa);
favg=-Om./e;
end
```

APPENDIX E: EXTENDED FIVE-SPRING MODEL - MATLAB CODE

```
%% Input
kci=0.18;
[fc, h, d, a, b, As, rs, sb, fy, Er, ls, Vf, lf, lh, li, df, fyf, nb, ag,
rv, fyv, Ev, lb1, lb2, VoP, Id, Vexp]=BeamData('B1');

PDexp1=B1;

Dc=(0:0.1:15)';

%% Geometry
lb1e=max(VoP*lb1,3*ag);
acl=a-lb1/2-lb2/2;
acalc=a-lb1/2+lb1e/2;
aeff=acl+lb1e;
alfa=atan(h/aeff);
alfa1=max(alfa,35/180*pi);

db=(As/nb*4/pi)^0.5;
rl=100*As/b/d;
scr=0.28*db*2.5*(h-d)/(rl/100)/d;
l0=max(scr,1.5*(h-d)/tan(alfa1));
l0=min(l0,d/tan(alfa1)/2);
lk=l0+min(l0,d*(1/tan(alfa)-1/tan(alfa1)));
lt=d/tan(alfa1)+(lk-l0);

Av=max(min(rv/100,0.15*fc/fyv)*b*(d/tan(alfa1)-l0-1.5*lb1e),0);

Aceff=b*min(2.5*(h-d),h/2);

z=0.9*d;

%% CLZ
[favg,Ec,Dcenv]=FAVG(Vf,lf,df,fc,alfa,lb1e);
favg(1)=0;
Vclzenv=favg*b*lb1e*sin(alfa)^2;
[Vclzmax, row]=max(Vclzenv);
Dcmax=Dcenv(row);
Kclz0=Vclzenv(2)/Dcenv(2);

%% Bottom reinforcement
kt=1;

%% Solution
LS=size(Dc,1);

for i=1:LS
    etl=0;
    etr=20/100;

    for j=1:100
        etj=(etl+etr)/2;
        etminj=kt*etj;
        etmaxj=(etj*lt-etminj*lk)/(lt-lk);
```

```
        Dtj=etj*lt/d*a;

        % CLZ
        Vclzj=interp1(Dcenv,Vclzenv,Dc(i),'linear');

        % Stirrups
        evj=(Dc(i)+0.25*etj*d/(tan(alfa1))^2)/(0.5*z);
        fvj=min(Ev*evj,fyv);
        Vsj=Av*fvj;

        % Shear derived from moment equilibrium

       [N]=TS_R_FRC_S(Aceff,Ec,etmaxj,ag,Vf,lf,df,db,sb,fc,nb,lh,li,Er,As);
        Vtj=N*z/acalc;

        etminj=N/Er/As;

        % Dowel action
        fyej=fy*max((1-(Er*etminj/fy)^2),0);
        Vdj=min(12*Er*Id/lk^3*Dc(i),nb*fyej*db^3/3/lk);

        % Aggregate interlock
        sj=Dc(i)*sin(alfa1);
        wj=Dc(i)*cos(alfa1)+0.5*etminj*lk/sin(alfa1);
        [ncij,vcij]=CDMfunc(fc,ag,sj,wj);
        Vcij=kci*vcij*b*d;

        % Fiber action
        [ff]=SDEM(wj,fc,Vf,lf,lh,li,df);
        beta=0;
        VFj=ff*b*d/sin(alfa1);

        % Shear resistance across diagonal crack
        Vccj=Vclzj+Vcij+Vsj+Vdj+VFj;

        % Error in equilibrium condition Vtj=Vccj
        erj=100*abs((Vtj-Vccj)/Vccj);
        if erj<0.01
            break
        end

        % Additional deformation to account for four-point loading
        n=Er/Ec;
        B=b/(n*As);
        Ig=b*h^3/12;
        kd=(sqrt(2*d*B+1)-1)/B;
        Icr=b*kd^3/3+n*As*(d-kd)^2;
        D11ij=(Vtj*a)/(Ec*Icr)*((ls^2/8)+(ls/2*a));

        % Adjustment of boundaries for bisection method
        if Vtj<Vccj
            etl=etj;
        else
            etr=etj;
        end
    end

    er(i,1)=erj;
```

```
        V(i,1)=Vtj/1000;
        Vclz(i,1)=Vclzj/1000;
        VF(i,1)=VFj/1000;
        Vci(i,1)=Vcij/1000;
        Vs(i,1)=Vsj/1000;
        Vd(i,1)=Vdj/1000;
        Dt(i,1)=Dtj;
         Vcc(i,1)=Vccj;

        if Vtj<0;
            LS=i;
            break
        end

    end
    etmax=et*(lt-kt*lk)/(lt-lk);
    Dc=Dc(1:i);

    D=Dt+Dc+D11;
    [Vmax, rvmax]=max(V);
    VFmax=VF(rvmax);
    Vcimax=Vci(rvmax);
    Vclzmax=Vclz(rvmax);
    Vsmax=Vs(rvmax);
    Vdmax=Vd(rvmax);
    Dcu=Dc(rvmax);

    % max error
    max(abs(er))
```